UNCLASSIFIED

AD 404 176

Reproduced
by the

DEFENSE DOCUMENTATION CENTER

FOR

SCIENTIFIC AND TECHNICAL INFORMATION

CAMERON STATION, ALEXANDRIA, VIRGINIA

UNCLASSIFIED

NOTICE: When government or other drawings, specifications or other data are used for any purpose other than in connection with a definitely related government procurement operation, the U. S. Government thereby incurs no responsibility, nor any obligation whatsoever; and the fact that the Government may have formulated, furnished, or in any way supplied the said drawings, specifications, or other data is not to be regarded by implication or otherwise as in any manner licensing the holder or any other person or corporation, or conveying any rights or permission to manufacture, use or sell any patented invention that may in any way be related thereto.

404 176
CATALOGED BY ASTIA AS AD No.
404176

63-3-4

AEDC-TDR-63-91

SOLAR RADIATION SIMULATION STUDIES, PART 2

By

W. A. Jaatinen, D. L. Rothacker, and C. D. Fitz

Vitro Laboratories
Division of Vitro Corporation of America
West Orange, N. J.

and

R. H. Bull, M. A. Dachs, and M. Shenker

Farrand Optical Company, Inc.
New York, N. Y.

TECHNICAL DOCUMENTARY REPORT NO. AEDC-TDR-63-91

May 1963

AFSC Program Area 850E, Project 7778, Task 777801

(Prepared under Contract No. AF 40(600)-951 by Vitro Laboratories, Vitro Corporation of America, West Orange, N.J. (Prime Contractor) and Farrand Optical Company, Inc., New York, N.Y. (Subcontractor).

ARNOLD ENGINEERING DEVELOPMENT CENTER

AIR FORCE SYSTEMS COMMAND

UNITED STATES AIR FORCE

NOTICES

Qualified requesters may obtain copies of this report from ASTIA. Orders will be expedited if placed through the librarian or other staff member designated to request and receive documents from ASTIA.

When Government drawings, specifications or other data are used for any purpose other than in connection with a definitely related Government procurement operation, the United States Government thereby incurs no responsibility nor any obligation whatsoever; and the fact that the Government may have formulated, furnished, or in any way supplied the said drawings, specifications, or other data, is not to be regarded by implication or otherwise as in any manner licensing the holder or any other person or corporation, or conveying any rights or permission to manufacture, use, or sell any patented invention that may in any way be related thereto.

SOLAR RADIATION SIMULATION STUDIES,

PART 2

By

W. A. Jaatinen, D. L. Rothacker, and C. D. Fitz
Vitro Laboratories
Division of Vitro Corporation of America
West Orange, N. J.
and
R. H. Bull, M. A. Dachs, and M. Shenker
Farrand Optical Company, Inc.
New York, N. Y.

(The reproducibles used in the reproduction of this report were supplied by the authors.)

May 1963

AF - AEDC
Arnold AFS Tenn

FOREWORD

This Technical Documentary Report summarizes the research on solar radiation simulation for a large Aerospace Environmental Chamber from November 1961 to January 1962 under Contract AF 40(600)-951.

The research was conducted by Vitro Laboratories, Division of Vitro Corporation of America, West Orange, N. J. as Prime Contractor, and the Farrand Optical Company, Inc., New York, N. Y., as Subcontractor.

Vitro Laboratories personnel who participated in the research and in the preparation of the report are C. D. Fitz, Head, Physics and Space Science Dept., W. A. Jaatinen, and D. L. Rothacker. Farrand Optical Company personnel were R. H. Bull, M. A. Dachs, and M. Shenker.

This report has been assigned Vitro Laboratories Report No. VL-2244-6-0. It represents a continuation of work described in Technical Note No. 1, VL-2244-3-0.

ABSTRACT

Studies and tests performed to establish the feasibility of solar simulation systems for an environmental chamber are reported. Performance objectives for the chamber and other solar simulator systems have been delineated and compared.

The earlier survey of radiation sources had shown that short-arc lamps have sufficient feasibility for this application to warrant further critical testing. Tests were initiated on several sources of this type including the 10-kw xenon lamp, the 2.5-kw xenon-mercury lamp and the fluid-transpiration arc source. The spectral energy distribution, radiant efficiency, polar diagram, intensity and uniformity as well as size and shape of the radiating medium under several conditions for each radiant source are being examined. More energy in line spectra was detected than had previously been reported. The 10-kw lamp had excessive radiant energy relative to the solar spectrum in the near infrared range. This energy must be reduced by filters. A deficiency of energy also relative to the solar requirement was noted in the range below 0.6 microns. The influence of quartz envelope adsorption, envelope blackening, optical system reflectivities, detector fatigue, and standard source calibration on this deficiency is under evaluation.

A reference module optical system concept based upon three and one half on-axis reflectors is examined. Ray tracing techniques are applied to determine the collimation and uniformity obtainable with an ideal short-arc source, and optical efficiencies of the several components are examined. After determination of the module efficiency, the number of molecules required to illuminate the chosen test area and the amount of power required for operation can be simply determined. Preliminary studies of the stability of simulator materials in the nuclear radiation environment of the chamber are also reported. In addition, the multiple source concept supplying a single collimator and the problems associated with refracting vs reflecting elements are analyzed.

PUBLICATION REVIEW

This report has been reviewed and publication is approved.

G. M. Arnold
Chief, Engineering Division
Space Systems Office

Donald D. Carlson
Lt Col, USAF
Chief, Space Systems Office

TABLE OF CONTENTS

TABLE OF CONTENTS - (CONT'D)

LIST OF ILLUSTRATIONS

LIST OF ILLUSTRATIONS - (CONT'D.)

LIST OF ILLUSTRATIONS - (CONT'D.)

LIST OF TABLES

I. INTRODUCTION

The research described in this report has been performed on Contract No. AF 40(600)-951 by Vitro Laboratories and Farrand Optical Company, Inc. The purpose of this investigation is to determine the feasibility of Solar Simulation techniques for the space-environmental facility under construction by the Arnold Engineering Development Center.

Technical Note No. 1 issued November 10, 1961 discussed the initial research on this project. The current report, Technical Note No. 2, details the procedures and results of subsequent tests made by Vitro Laboratories on various radiation sources for solar simulation. It also covers the optical system feasibility studies conducted by the subcontractor, Farrand Optical Company, Inc.

A. SOLAR SIMULATION

In the region of space in the vicinity of the earth, but still outside the earth's atmosphere, the characteristics of solar radiation are considered to be as follows:

1. Intensity of the solar constant has been evaluated by Johnson* as 1396 watts/meter^2. This quantity varies by ±3.4% due to the ellipticity of the earth around the sun.

2. In the infrared, visible, and ultraviolet range down to 2500 A, the spectral distribution of the solar radiation closely approximates the radiation from a 6000°K black-body. In the ultraviolet range from 2500 A down to 1300 A the solar radiation may be better approximated by that of a 5000°K black-body. Although the energy present in the spectral range below 2500 A is only a small portion of the total energy, it may have particularly deleterious effects on spacecraft material.

---

* Handbook of Geophysics, Rev. Ed., United States Air Force, New York: MacMillan, 1960, p. 16-18.
Johnson, F.S., "The Solar Constant", Journal Meteorology, 11:431, 1954

3. Collimation of the solar flux specifies the parallelism of the rays of emitted radiation. The collimation angle or the angle subtended by the sun at the earth, is 32 minutes.

4. Uniformity—there is of course no variation of the actual solar radiation over an extended area.

B. DESIGN GOALS

Exact simulation of all the solar characteristics for long periods of time over a large area cannot be considered technically or economically feasible. Some variations or tolerances must be allowed in order to bring the design and construction of the solar simulator within the projected technical state of the art and within allowable costs. For the anticipated applications of the projected environmental facility the following design goals were selected:

1. Beam Size and Orientation

A beam of artificial sunlight covering the selected area is to be displayed vertically upon the maneuver sphere. The radiation intensity is to be uniform with respect to depth inside the test volume.

2. Intensity

A tolerance of ±3% is to be allowed on the solar constant of 1396 watts/meter^2.

3. Spectral Distribution

Allowable tolerances on the quality of the energy intensity within the solar spectral range are indicated in Table I.

TABLE I

SPECTRAL RANGE TOLERANCES FOR SOLAR SIMULATION

Spectral Range	Bandwidth	Tolerance
2,000 - 30,000 A	200 A	±20%
2,000 - 8,000 A	2,000 A	± 8%
8,000 - 20,000 A	3,000 A	± 8%
20,000 - 30,000 A	5,000 A	± 8%

4. Collimation

The collimation angle is to be held as close to the 32 minute angle as can be technically and economically provided.

5. Uniformity

Incident radiation on any 4-inch diameter area should not vary by more than ±5% from any other similar area in the beam.

6. Unattended Operating Time

Since nuclear equipment will probably be tested in the environmental chamber at a later date, the solar simulation should be capable of operating for at least 116 hours without attention, source replacement, or optical adjustment. If this design goal proves too restrictive, it may be necessary to relax the unattended operating time at least for the earlier period of the simulator's use.

7. Energy Economy

The size of the irradiated region and the problems related to energy removal require conservation of radiant energy and close attention to the efficiency of the radiant source and components of the optical system.

8. Other Chamber Conditions

The design of the solar simulator is also influenced by the requirements placed on the other environment characteristics. These include:

a. Vacuum

Down to 10^{-9} Torr with brief overpressures to 37.5 psig during which no radiation collimation is required. A guard vacuum is to be maintained at all points between chamber walls, therefore all windows must be in pairs.

b. Temperature

From 80°K to 500°K.

c. Nuclear Radiation

Gamma flux of 1.5×10^{14} Mev/cm^2/sec. Fast neutron flux of 7×10^{12} $_0n^1$/cm^2/sec.

Tables II and III present the gamma leakage and neutron leakage flux which may be expected in a hypothetical 3 Mw reactor under test in the chamber. Table IV provides a comparison of the performance objectives of the environmental facility with the performance objectives of other facilities.

C. OBJECTIVES OF CURRENT STUDIES

As a first phase of these research studies Vitro Laboratories and Farrand Optical Company, Inc., were to accomplish the following:

1. Conduct a literature search on methods to produce a high degree approximation of intensity, uniformity and collimation of fluxes from radiation sources having spectrum characteristics similar to solar radiation.

2. Survey the characteristics of available radiation sources and new concepts of sources suitable for producing the required radiation, conduct studies and perform computations to establish feasibility of simulation and applicability of considered sources to a space environment simulation chamber.

3. Perform laboratory tests on promising sources as determined by the previous studies. Objective of these tests was to be the determination of spectral distribution and brilliance within the spectral range of interest as functions of angular position, power input, and operation time. Also to be determined were the stability and energy conversion efficiency at different power levels and after different operation periods.

4. Conduct analytical studies and computations on intensity distribution patterns to be obtained from flux superpositions or combinations, from patterned filtering and/or from other concepts. Establish parameters which determine the degree of intensity, uniformity, and collimation of the combined total flux. Determine the relative importance of the effects of parameters like distances, spread angles, array patterns of sources, filters, Fresnel panes, mirrors, etc., number of sources per unit area, directional intensity characteristic of the source-reflector units which produce one dimensionally collimated fluxes (tubular light bulbs in parabolic cylinder reflectors), etc. Study possible required corrections on the border area of the radiated field in order to maintain highly constant intensity up to the boundary of the useful portion of the flux and minimize the unused portion which bypasses the test article.

TABLE II

GAMMA LEAKAGE FLUX FROM HYPOTHETICAL 3-MW REACTOR

Energy (Mev)	Flux at Chamber Wall (Photons/cm^2-sec)
(a) Epithermal	
10	5.7×10^6
8	1.4×10^7
5.5	2.7×10^7
3.5	7.3×10^8
(b) Fast	
4.7	5.6×10^7
2.9	1.5×10^8
1.75	3.3×10^8
1.0	2.1×10^8
0.35	1.6×10^8
(c) 4.7	2.8×10^7
2.9	7.5×10^7
1.75	1.6×10^8
1.0	1.1×10^8
0.35	8.0×10^7

TABLE III

NEUTRON LEAKAGE FLUX FROM HYPOTHETICAL 3-MW REACTOR

	Flux at Chamber Wall (n/cm^2-sec)		
Energy	Epithermal	Fast	Advanced Fast
3 - 10 Mev	4.0×10^7	7.9×10^7	3.9×10^7
1.4 - 3 Mev	1.3×10^8	2.3×10^8	1.4×10^8
.9 - 1.4 Mev	6.8×10^7	9.3×10^7	5.0×10^7
.4 - .9 Mev	9.9×10^7	1.9×10^8	1.1×10^8
.1 - .4 Mev	1.2×10^8	2.4×10^8	1.8×10^8
17 - 100 Kev	9.1×10^7	1.4×10^8	1.6×10^8
3 - 17 Kev	7.3×10^7	5.7×10^7	9.5×10^7
.55 - 3 Kev	5.9×10^7	2.2×10^7	5.6×10^7
100 - 550 Ev	5.1×10^7	8.1×10^6	3.1×10^7
30 - 100 Ev	3.2×10^7	2.5×10^6	1.3×10^7
10 - 30 Ev	2.8×10^7	1.0×10^6	7.9×10^6
3 - 10 Ev	2.8×10^7	5.1×10^5	5.2×10^6
1 - 3 Ev	2.3×10^7	2.2×10^5	3.0×10^6
.4 - 1 Ev	1.8×10^7	9.4×10^4	1.7×10^6
.1 - .4 Ev	2.3×10^7	5.2×10^4	1.4×10^6
0 - .1 Ev	6.5×10^7	4.2×10^4	1.9×10^6

TABLE IV

PERFORMANCE OBJECTIVES

Characteristic	AEDC Chamber	AEDC[1] Mark I	G. E.[2]	J. P. L.[3]
Uniform intensity to be provided over depth from entrance windows, (feet)				
Min.		3-1/2		
Max.		36-1/2		25
Area to be irradiated, (Sq. Feet)		181	314	176
Dimensions, (Feet)		5-1/2 x 33	20 Dia.	15 Dia.
Nuclear Radiation in chamber	See Tables II and III			
Distance from tank wall to source of Nuclear Radiation, (Feet)	40			
Chamber Pressure, Min. (Torrs)	10^{-9}			
Max. (Psia)	37.5			
Chamber Temperature, Min.	80°K			
Max.	500°K			
Continuous Operating Time, (Hours),				
System Unattended, Min.	116			
Per Lamp, Attended, Min.		24		
System Attended, Max.	4400			
Collimation, entire energy	±16'	±1°	±2°	±4.5°
50% of energy				±2.25°
Total energy incident on	4 in. dia.	3 cm dia.		1 sq. ft.
shall not vary by more than from total energy on any other similar area within irradiated area specified	5%	5%	5%	10%
Total integrated energy between				
A min.	2,000	2,000	2,000	
A max.	30,000	35,000	30,000	
shall be within	±3%	±5%	±5.4%	
of Solar energy (watts sq. ft.)	127.17	130	130	

(1) Construction Specification for Aerospace Simulator Mark I, USAF Specification 6B-1 15 March 1961; revised 9 October 1961.

(2) "Design Solution for a Space Environment Simulator" Gelhard, John C. and Meyer, S. Wayland, General Electric Company, I.E.S. Proceedings, 1961, pp. 335 - 347.

(3) Conference at Jet Propulsion Laboratory on 16 October 1961.

TABLE IV - (CONT'D.)

Characteristic	AEDC Chamber	AEDC Mark I	G.E.	J.P.L.
Total integrated energy in any band of listed A width, between listed A limits, shall equal energy in corresponding solar band within listed tolerances:				
Bandwidth	200	500	500	None
Limit Min.	2,000	2,000	2,000	
Limit Max.	30,000	4,000	2,500	
Tolerance	±20%	±10%	±15%	
Bandwidth	2,000	1000	800	
Limit Min.	2,000	4,000	2,500	
Limit Max.	8,000	12,000	3,300	
Tolerance	± 8%	±5%	±10%	
Bandwidth	3,000	2,000	700	
Limit Min.	8,000	12,000	3,300	
Limit Max.	20,000	35,000	4,000	
Tolerance	±8%	±10%	±10%	
Bandwidth	5,000		1,000	
Limit Min.	20,000		4,000	
Limit Max.	30,000		5,000	
Tolerance	±8%		±10%	
Bandwidth			2,000	
Limit Min.			5,000	
Limit Max.			7,000	
Tolerance			±10%	
Bandwidth			1,000	
Limit Min.			7,000	
Limit Max.			8,000	
Tolerance			±10%	
Bandwidth			1,000	
Limit Min.			8,000	
Limit Max.			9,000	
Tolerance			±10%	
Bandwidth			2,000	
Limit Min.			9,000	
Limit Max.			11,000	
Tolerance			±10%	
Bandwidth			4,000	
Limit Min.			11,000	
Limit Max.			15,000	
Tolerance			±15%	
Bandwidth			10,000	
Limit Min.			20,000	
Limit Max.			30,000	
Tolerance			±15%	
Radiation to be projected	Vert.	Horiz.	Vert.	Vert.

D. SCOPE OF REPORT

The literature search has resulted in a comprehensive bibliography of published literature and reports pertinent to radiation sources and associated optical design. This bibliography was presented in Technical Note No. 1.

The results of the survey of available radiation sources, sources under development, and concepts for new sources were also reported in Technical Note No. 1. Certain additional information is presented in this report.

As indicated in the previous technical note, short-arcs were selected as most appropriate for further investigation and testing. The primary purposes of Technical Note No. 2 is to describe: (1) the laboratory tests being made to determine to what extent these areas meet the requirements of the chamber solar simulator (Section II), and (2) the associated preliminary design of optical equipment (Section II).

II. RADIATION SOURCE INVESTIGATION

As indicated in Technical Note No. 1, a preliminary survey of sources revealed that for the complex requirements of the of the facility, short-arc type lamps exhibited sufficient feasibility to warrant further critical evaluation. Furthermore, sources of this type have been developed and used as prime sources of intense light. They are currently available in sizes up to 10 kw, and with various gas environments (primarily xenon and xenon-mercury). Scale-up to 20-kw power levels is expected within the next 12 months. In addition, development work is in progress to increase the operational life of these lamps by decreasing the electrode deposition on the envelopes. However, aside from photometric characteristics, very little reliable information was available on these lamps. In order to characterize these sources more extensively and to determine their applicability to solar radiation simulation, several of the lamps were tested.

The source tests were divided into two groups. The first group include tests of the source properties which determine directly the performance of any optical system incorporating the source, as well as tests of source characteristics important to the optical design. The spectral distribution, total radiant energy output, intensity and uniformity of the radiation, size and shape of the source, and the spatial radiation distribution are characteristics pertinent to the nature and geometry of the source.

In the second group of source tests are tests of the operating properties. These operating properties eventually determine the reliability, cost, and operational complexity of the system. Characteristics related to the operation of the source include stability or flickering, time to stabilize the source after startup, diminution of radiant output with running time, cooling requirements, variation of source size during operation, and variation of spectral output with time. This latter group of tests has not as yet been completed.

A. TEST PROCEDURES

1. Spectral Energy Distribution

A double beam recording spectrophotometer was used to obtain the spectral energy distribution of various sources. This instrument can be operated on either a single or double beam. Both methods of operation were considered and tested. It was found that the double beam method was more convenient, since calibration of the energy detectors as required in the single beam method could be eliminated. Figure 1 shows the major items of test equipment. The operation and theory of the double beam spectrophotometer is described in Appendix A.

2. Total Radiated Power

The total power radiated by a source is measured with a thermopile. The thermopile measures, F, the power radiated to a square cm of area at a fixed distance from the test source. Figure 2 shows the test source in a spherical coordinate system. The axis of the source is placed along the z axis. The thermopile is placed at a constant value of the radius r, and readings are taken at various values of θ. The source is assumed to have ϕ symmetry. The total power radiated by the source for a compact short arc under these conditions can be obtained from the following equations:

$$\text{Total Power} = \int_0^{2\pi}\int_0^{\pi} F(r,\theta)\, r^2 \sin\theta\, d\theta\, d\phi \quad (r = \text{constant})$$

$$\text{Total Power} = 2\pi \int_{-\frac{\pi}{2}}^{\frac{\pi}{2}} F(r,\theta)\, r^2 \sin\theta\, d\theta \quad (r = \text{constant})$$

For example, with a fluid-transpiration arc source placed with the anode face in the x-y plane and with the direction of the fluid jet pointing in the positive z direction, the total power (assuming ϕ symmetry) is calculated as:

Fig. 1 Apparatus for Measuring Spectral Energy Distribution

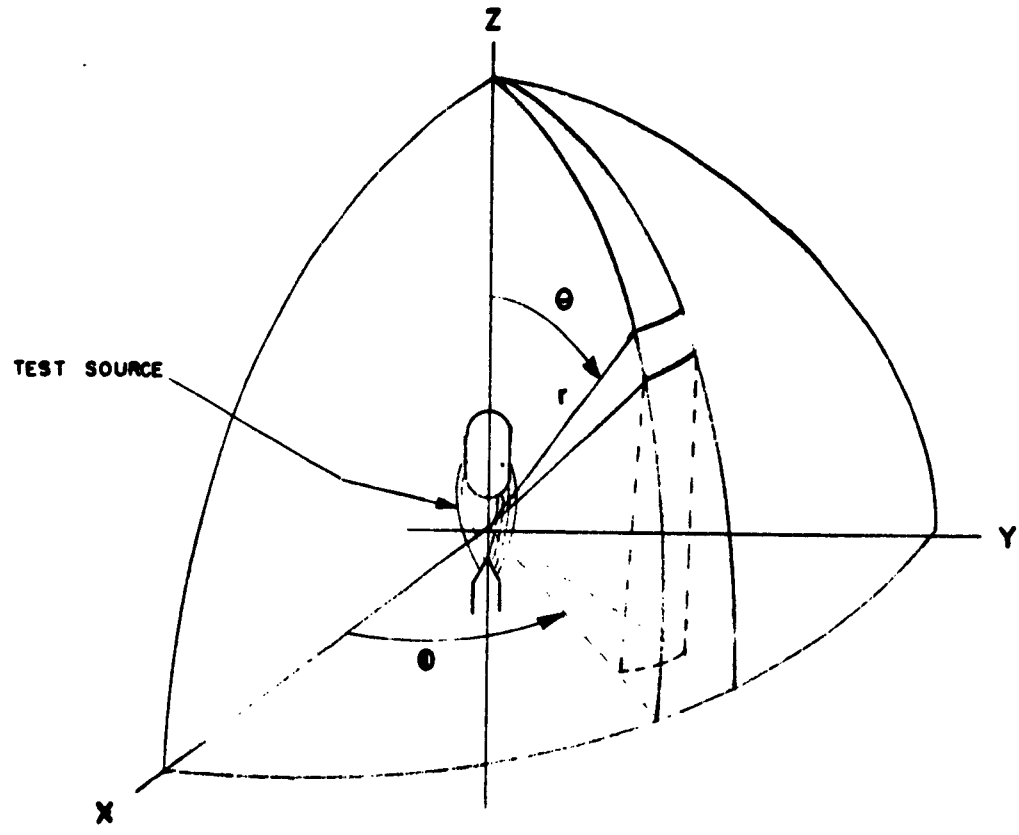

Fig. 2 Coordinate System for Thermopile Measurements

$$\text{Total Power} = 2\int_0^{2\pi} \int_0^{\frac{\pi}{2}} F(r,\theta)\, r^2 \sin\theta d\,\theta d\phi$$

$$\text{Total Power} = 4\pi \int_0^{\pi} F(r,\theta)\, r^2 \sin\theta d\theta$$

A crosscheck of thermopile and spectrophotometer measurements can be made by (1) evaluating the integral $\int B_s\, A_s\, d\lambda$, from the spectrophotometer measurements which yields the total power radiated per unit solid angle for some given value of θ, and (2) calculating the power radiated per unit solid angle for the same value of θ from the thermopile measurements. In the latter case

$$\frac{\text{total power}}{\text{solid angle}} = \frac{F(\text{milliwatts/cm}^2)}{\Omega_t}$$

where:

$$\Omega_t = \frac{1\ \text{cm}^2}{r^2\ (\text{cm})}$$

is the solid angle intercepted by the thermopile. Both of these measurements should give the same value of the power radiated per solid angle.

3. Uniformity and Intensity of Source

The absolute intensity and the uniformity of intensity in the radiating source are important to the design of any optical system. To a large extent, the ultimate performance obtainable from a system is controlled by the departure of the source from a theoretical uniform point source.

A good estimate of the intensity and variation of intensity in a source may be obtained from photometric measurements of brightness and corresponding brightness contour maps. Although these photometric values are measured in terms of candle power and are restricted to the visible portion of the spectrum, it may be assumed that any variation of photometric brightness in a source also implies a similar variation of absolute intensity. However, the

two quantities, photometric brightness and absolute intensity, are not directly comparable unless the source is a black or gray body.

Brightness values are obtained by measuring the light density in candles per square millimeter actually emitted by the source surface. As shown in Figure 3, a magnified image of the source is displayed on a convenient plotting board, and sections of the image are scanned with a photocell. For a particular optical system, the brightness of the source is related by the usual formula:

$$B = \frac{4ES^2}{T\pi R^2}$$

where:

B = source brightness candles/mm^2,

S = image distance in feet,

T = transmission of the optics in the system,

R = radius of the aperture in millimeters,

E = illumination in foot-candles.

4. Size and Shape of Source

The size and shape of the 10-kw xenon lamp, 2.5-kw xenon-mercury lamp, and the argon fluid-transpiration-arc sources were obtained by photographing them while in operation. The cross-sectional area and shape were then obtained from the photographs by a planimeter.

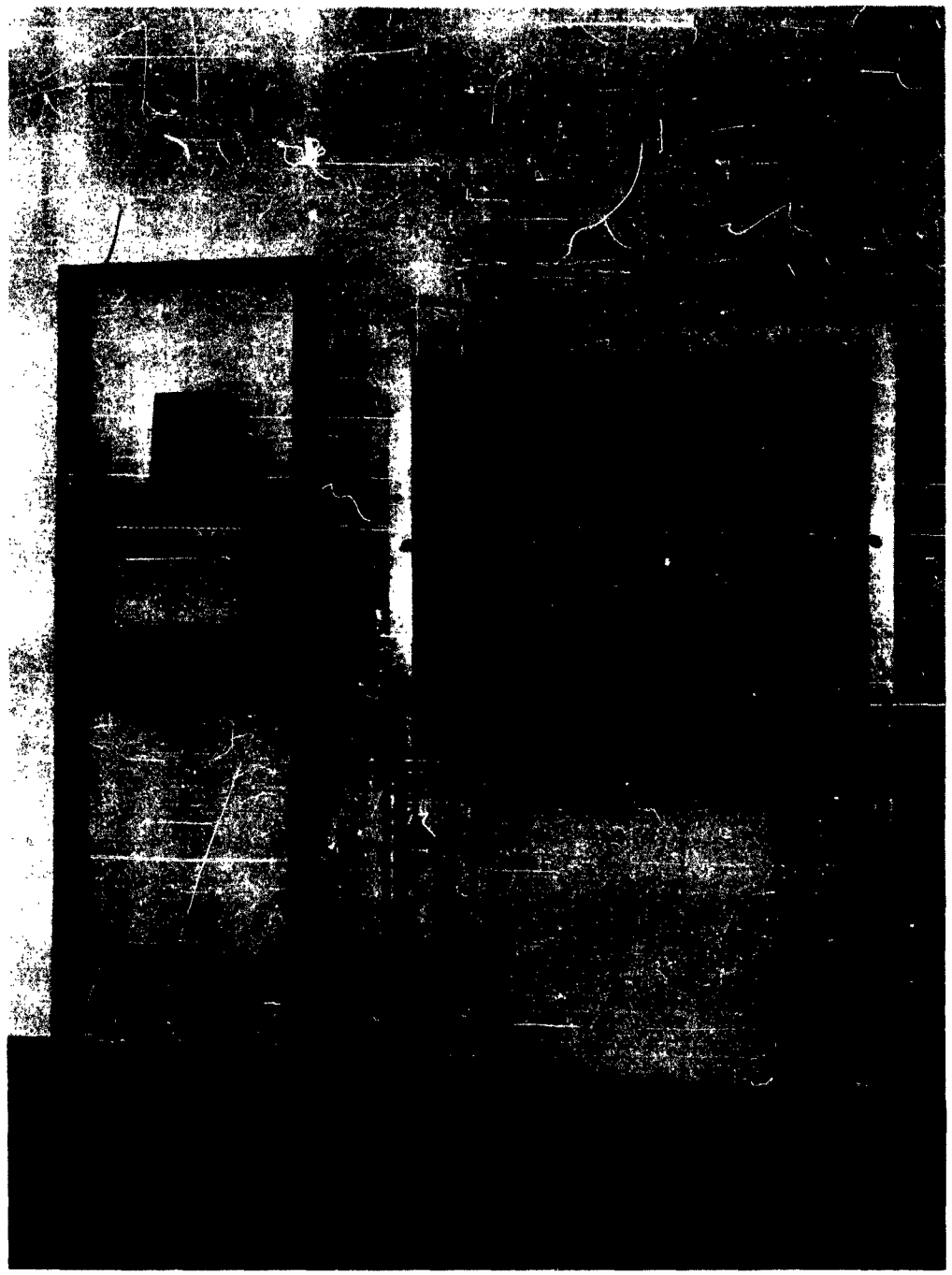

Fig. 3 Brightness Scanning System with Controller

B. TEST RESULTS

Preliminary test results have been obtained for three short arc sources: the 10-kw xenon lamp, the 2.5-kw xenon-mercury lamp and the fluid-transpiration short-arc source. Preliminary comparisons and matches to the solar energy distribution were also made.

1. 10-kw Xenon Short-Arc Lamp

The 10-kw xenon short-arc lamp* used for these tests is shown in Figure 4. This lamp was tested at three power inputs, 7.5, 10, and 12.5 kw respectively, in order to determine and delineate the change, if any, in its characteristics as the power was increased. These tests also served to simulate the actual operating conditions under which this type of lamp would be required to maintain constant output over extended periods of time. Figure 5 illustrates the size and shape of the radiation source and indicates the effects of increased input power.

a. Spectral Energy Output

The techniques described in the previous section were used to obtain the spectral energy measurements of the 10-kw xenon short-arc lamp at the three input power levels. These spectra are plotted as a function of wavelength in Figures 6, 7, and 8. The solar spectral energy curve has also been plotted on these curves by matching the energy represented by the solar curve to the energy represented by the Xenon curve at the three power levels. The spectrophotometer detector bandwidths, in microns, are superimposed on the spectral charts to indicate the sensitivity of the measurement at any particular wavelength.

The detector bandwidth varies through the whole spectral range from 0.2 to 3.0μ. The narrowest bandwidth is in the UV region from 0.25μ to 0.6μ and is of the order of 5 A. Between the spectral range 0.6 to 0.8μ, the bandwidth increases from 5 A to 80 A and in the IR from 0.8 to 2.5μ, the bandwidth remains at approximately 90 A. Beyond 2.5μ, the bandwidth increases rapidly to approximately 600 A at 3.0μ. Generally, the bandwidth remains small enough to trace out the majority of important spectral lines to allow a critical comparison with the solar spectral curve. However, even at the smallest bandwidth of 5 A, the profiles of individual spectral lines (usually 1 to 2 A wide) cannot be traced.

* Duro-Test Corp., North Bergen, New Jersey.

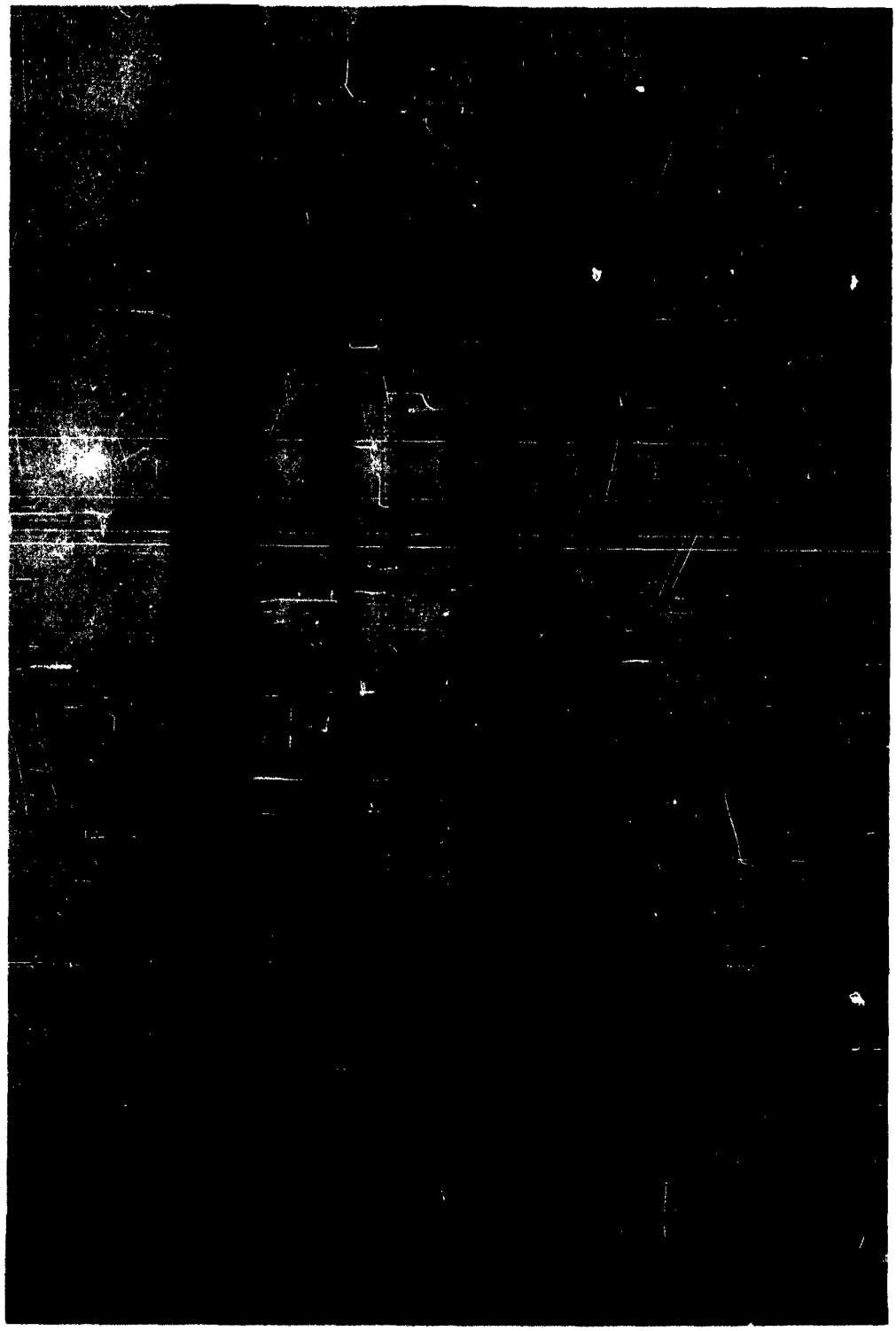

Fig. 4 10-KW Xenon Short-Arc Lamp

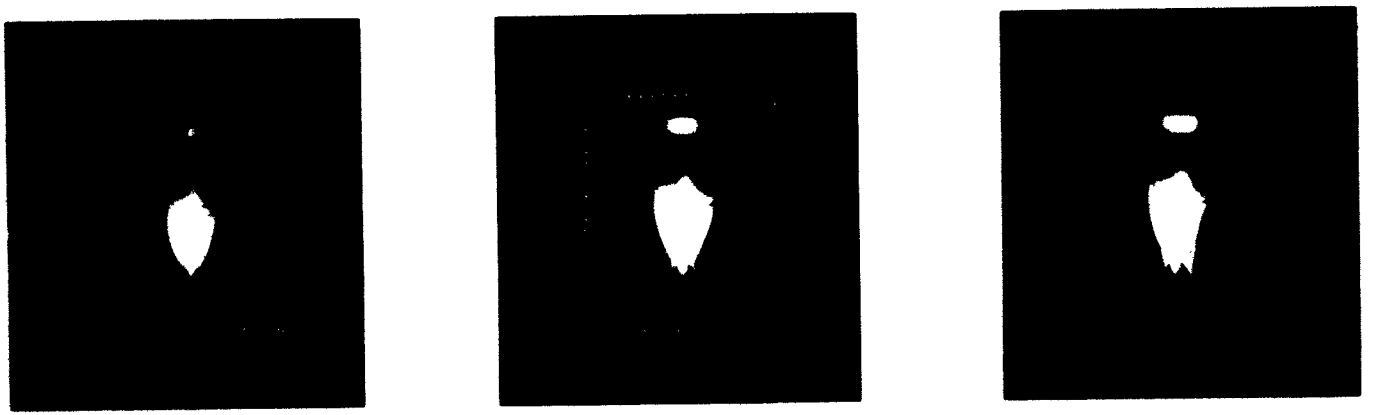

Fig. 5 10-KW Xenon Short-Arc in Operation at Various Power Input Levels

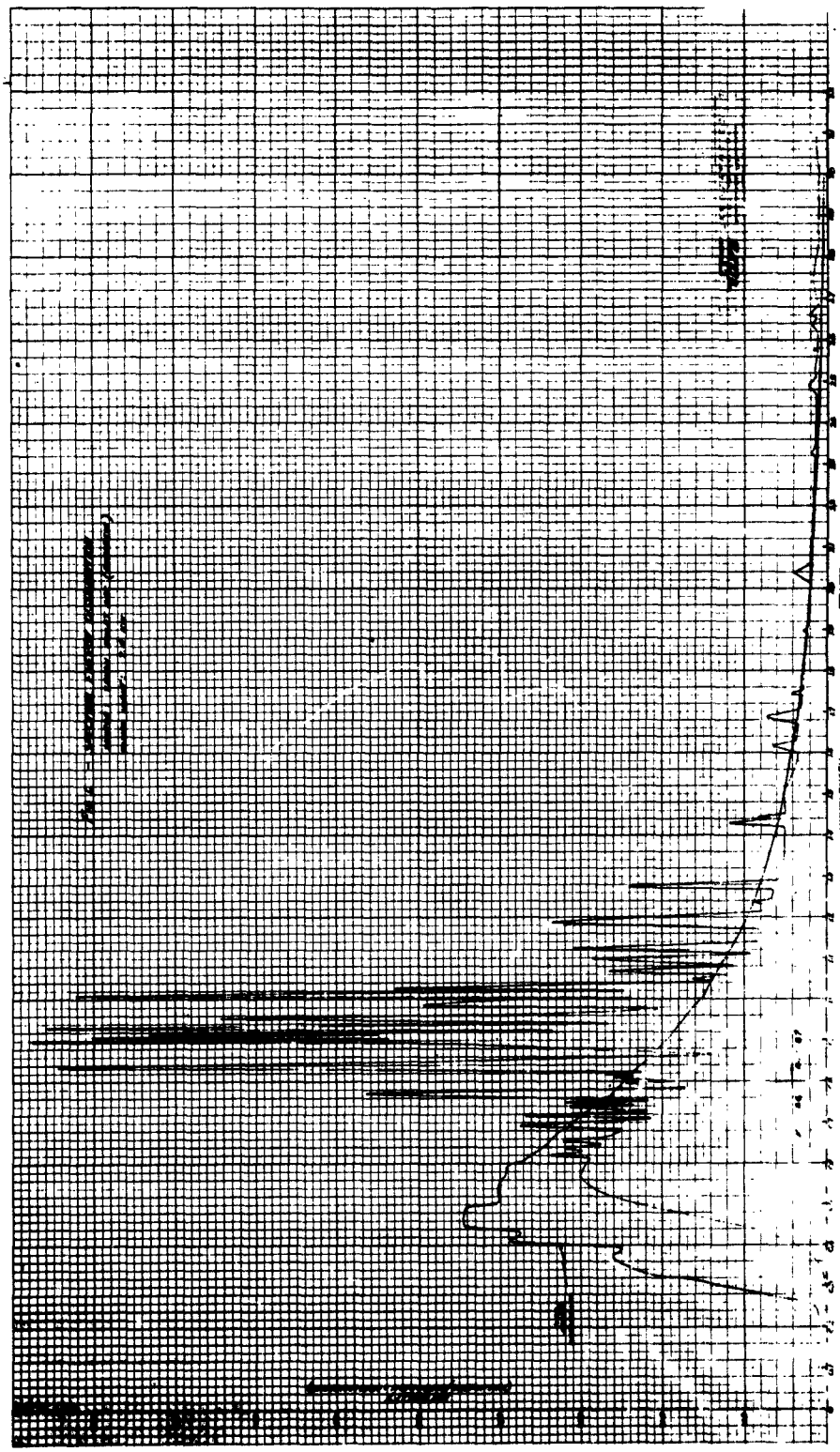

Fig. 6 Spectral Energy Distribution – Xenon Source at 7.4-KW Input Level

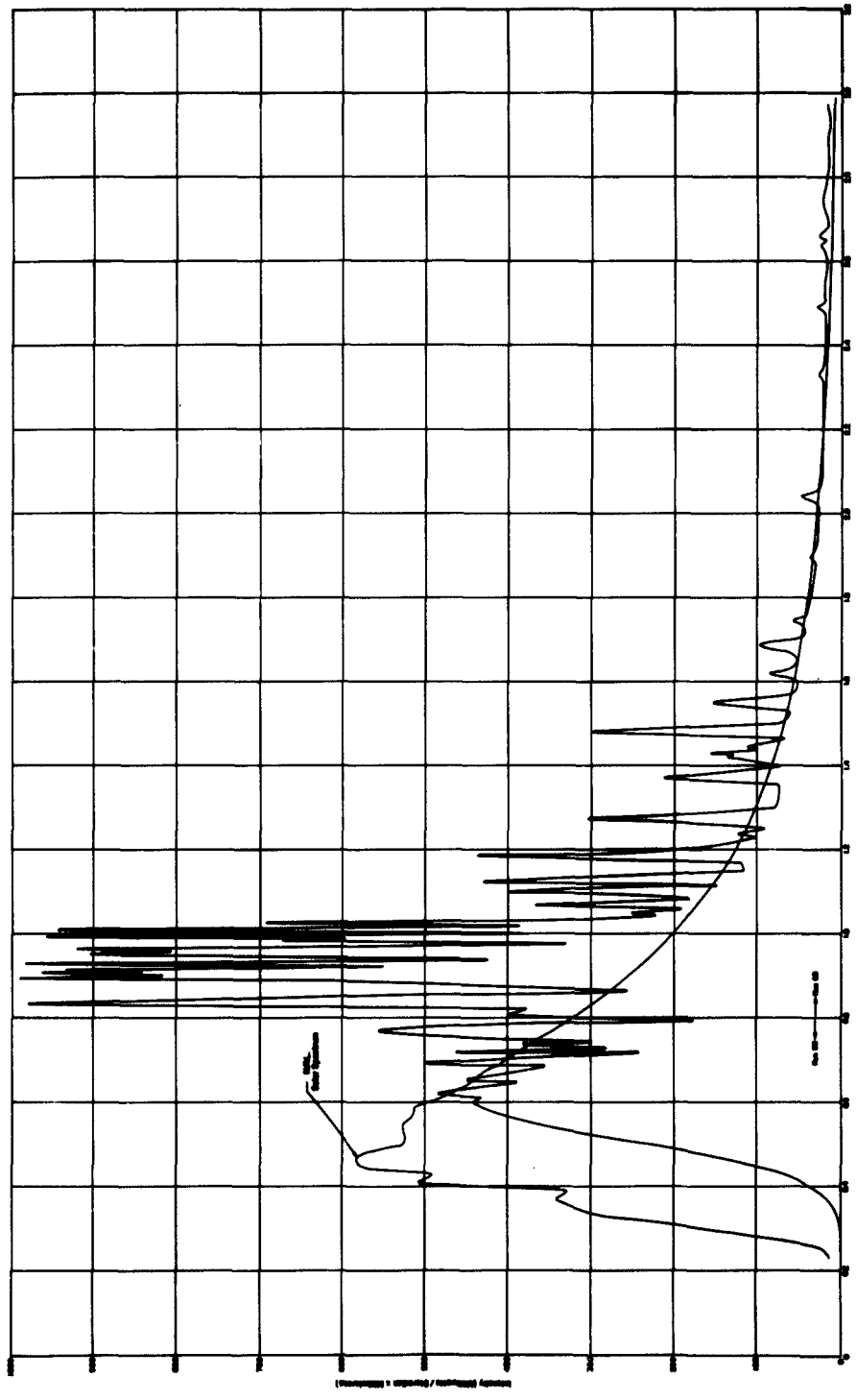

Fig. 7 Sectral Energy Distribution – Xenon Source at 10.1-KW Input Level

Fig. 8 Spectral Energy Distribution – Xenon Source at 12.5-KW Input Level

It will be noted that considerably more line spectra are present than has been reported in manufacturer's data. A rapid attenuation of intensity below 0.6μ is also noted. Similar attenuation is also noted for the other short-arc sources tested. Data in the spectral range 0.25 to 0.4μ for a low-powered xenon short-arc lamp (500w), obtained by Baum and Dunkelmann* indicate a UV continuum with considerably more intensity. The measured values are being re-examined to determine the extent of quartz absorption, envelope blackening, mirror systems reflectivity and standard source calibration in the UV.

b. Spectral Match

The match of the spectral energies obtained for the 10-kw xenon lamp operating at three power levels is shown in Figures 9, 10, and 11. The percent deviation from the maximum or minimum allowable tolerance within the indicated successive bandwidths is shown in Table V.

TABLE V

ACTUAL VS ALLOWABLE SPECTRAL DEVIATIONS FOR XENON LAMP AT 10.1-KW POWER LEVEL

Spectral Bandwidth	Allowable Tolerance	Actual Deviation from Allowable Tolerance
0.20 - 0.4μ	±8%	-96.5%
0.4 - 0.6μ	"	-52.8%
0.6 - 0.8μ	"	within tolerance
0.8 - 1.1μ	"	+99.5%
1.1 - 1.4μ	"	+24%
1.4 - 1.7μ	"	+30.8%
1.7 - 2.0μ	"	within tolerance
2.0 - 2.5μ	"	within tolerance
2.5 - 3.0μ	"	+57%

* Baum, W. A. and Dunkelman, L., "Ultraviolet Radiation of High Pressure Xenon Lamps and Arcs," Optical Society of America Journal, 40, No. 11, 782-86 (November, 1950).

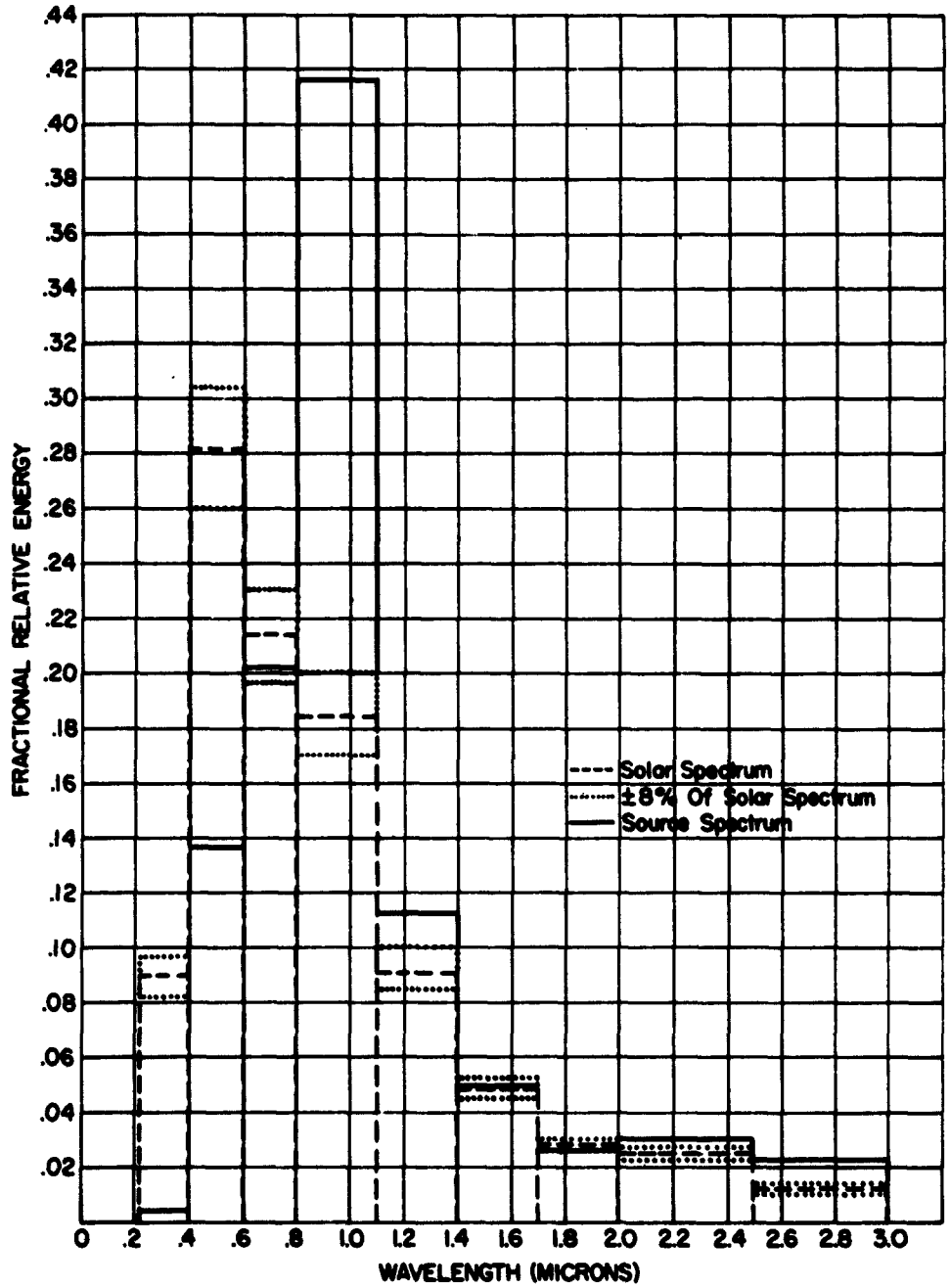

Fig. 9 Xenon Source Spectrum at 7.4-KW Input Power as Compared to Solar Spectrum

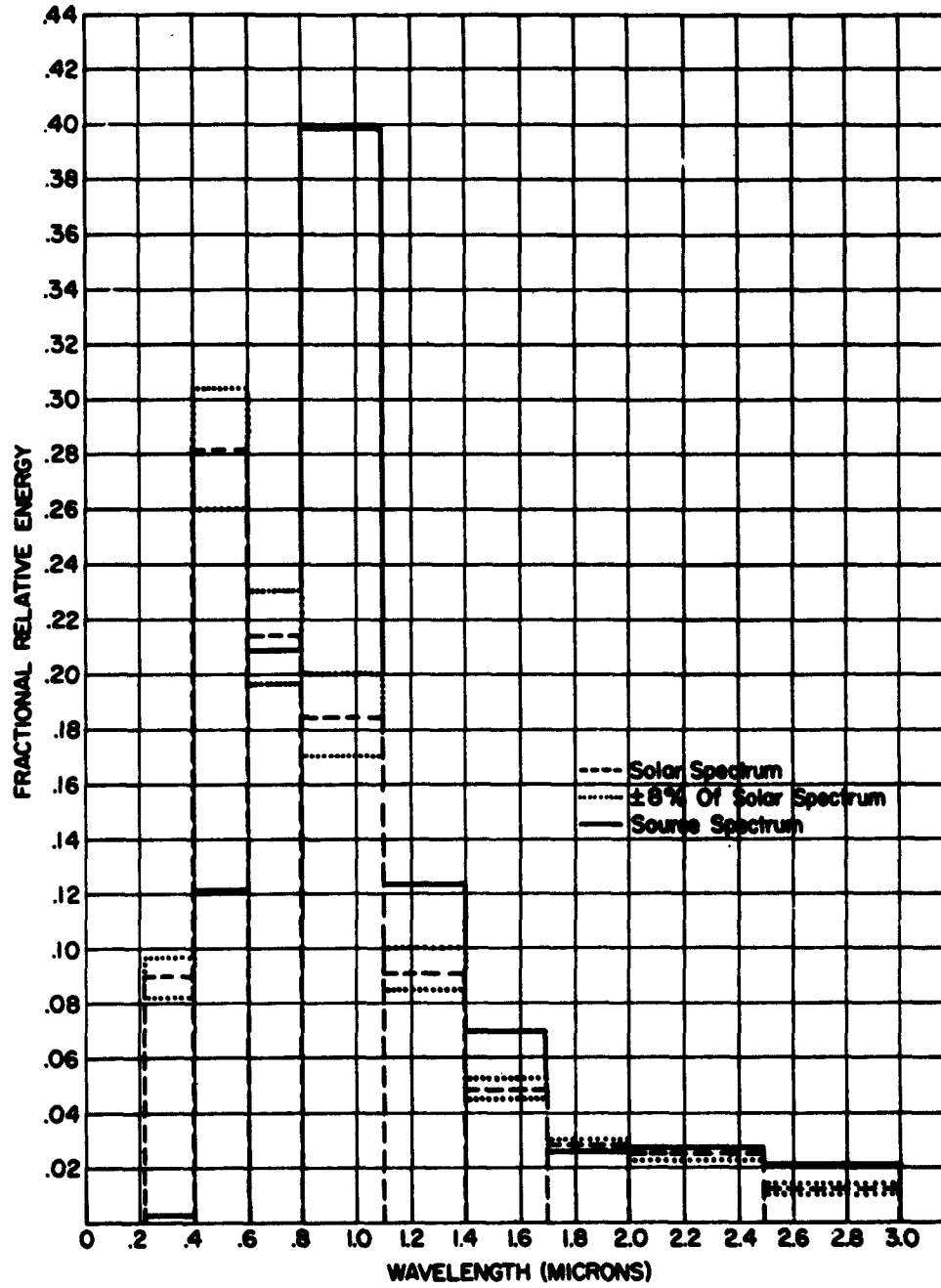

Fig. 10 Xenon-Source Spectrum at 10.1-KW Input Power as Compared to Solar Spectrum

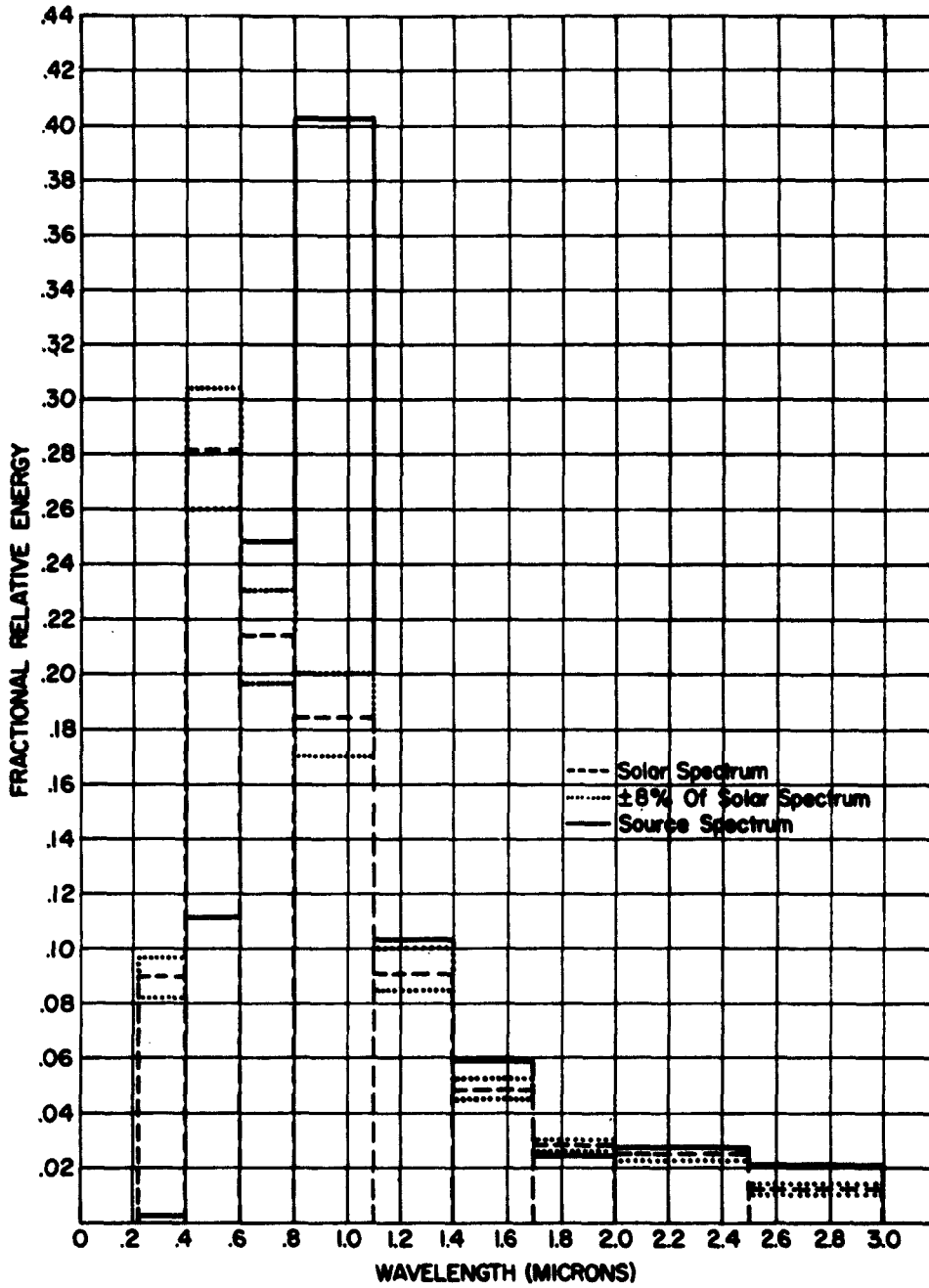

Fig. 11 Xenon-Source Spectrum at 12.5-KW Input Power as Compared to Solar Spectrum

Above 0.6μ the deviations from the allowable tolerances are all positive and will require filtering. The negative deficiencies below 0.6μ are due to the UV attenuation mentioned previously and will be reexamined.

Deviations within 200A bandwidths and deviations for runs at 7.4 kw and 12.5 kw have not been completed. However, the spectral energy distribution varied only slightly with the change in power input from 7.5 kw to 12.5 kw.

c. Brightness, Uniformity, Size and Shape of Source

The brightness profiles for the 10-kw xenon lamp obtained by the manufacturer (Duro-Test) using a technique similar to that described above are shown in Figure 12. Examination of the brightness variation indicated a variation of approximately 14 to 1 in axial direction over an 8.25 mm gap not counting the peak brightness of 7600 cal/mm^2.

2. 2.5 kw Mercury-Xenon Short-Arc Lamp

The mercury-xenon lamp* tested and the source in operation at 12.5 kw input power are shown in Figures 13 and 14 respectively.

a. Spectral Energy Output

Spectral energy measurements for this lamp made by the techniques described previously, are plotted as a function of wavelength in Figure 15. The solar spectral energy curve has been superimposed on the measured Xe-Hg curve for comparison. The total energies represented by the two curves are equal. Attenuation of UV energy in the range below 0.6μ, similar to that noted in measurements with the 10-kw xenon lamp is evident and will be re-examined.

b. Spectral Match

In Figure 16 the spectral energy of the 2.5 kw xenon-mercury source is compared to the solar spectral energy in the specified bandwidths. In the range 1.1 to 2.5μ, the spectral energy from the lamp is approximately twice that required to match the solar energy in this range. An approximate match is obtained in the range 2.5 to 3μ and approximately 50% excess energy is

* Hanovia Lamp Division, Engelhard Hanovia, Inc., Newark, New Jersey

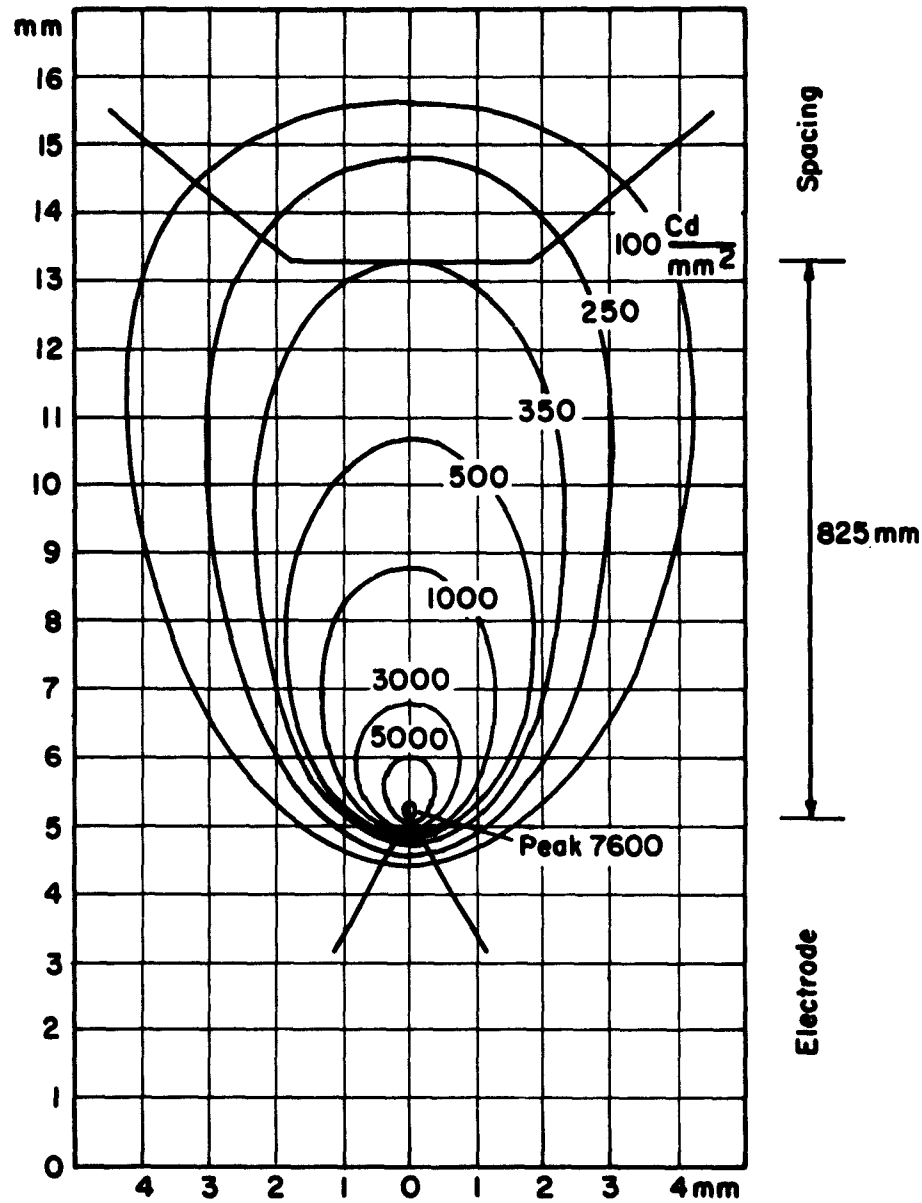

Fig. 12 Brightness Profile for 10-KW Xenon Lamp

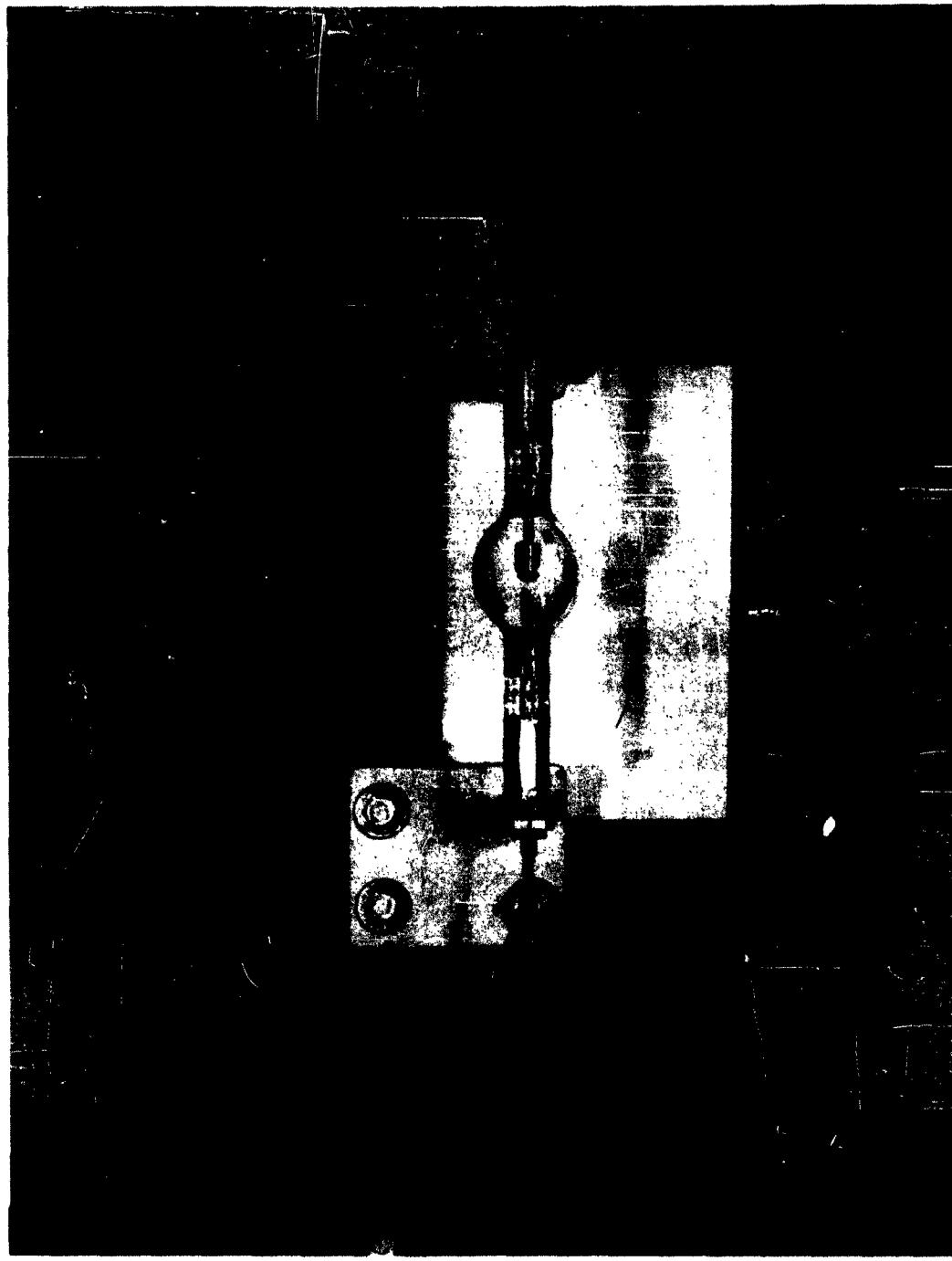

Fig. 13 2.5-KW Xenon-Mercury Short-Arc Lamp

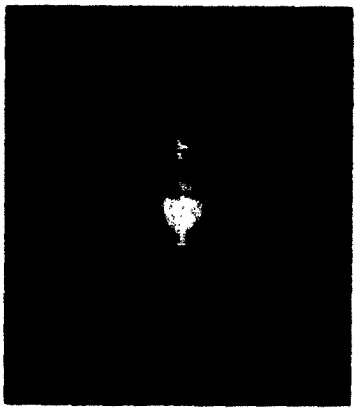

Fig. 14 2.5-KW Xenon-Mercury Short-Arc in Operation

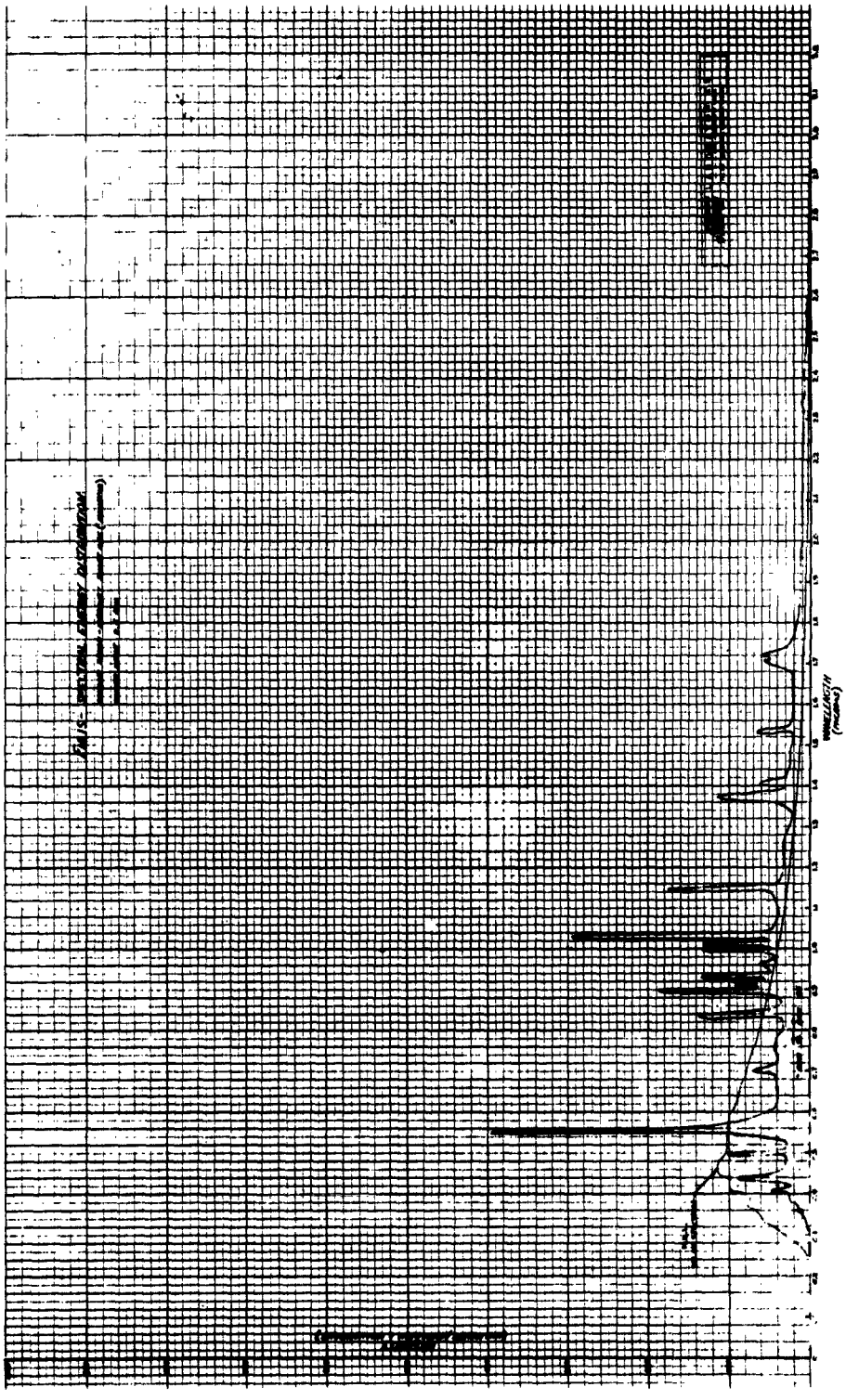

Fig. 15 Spectral Energy Distribution – Xenon Mercury Source

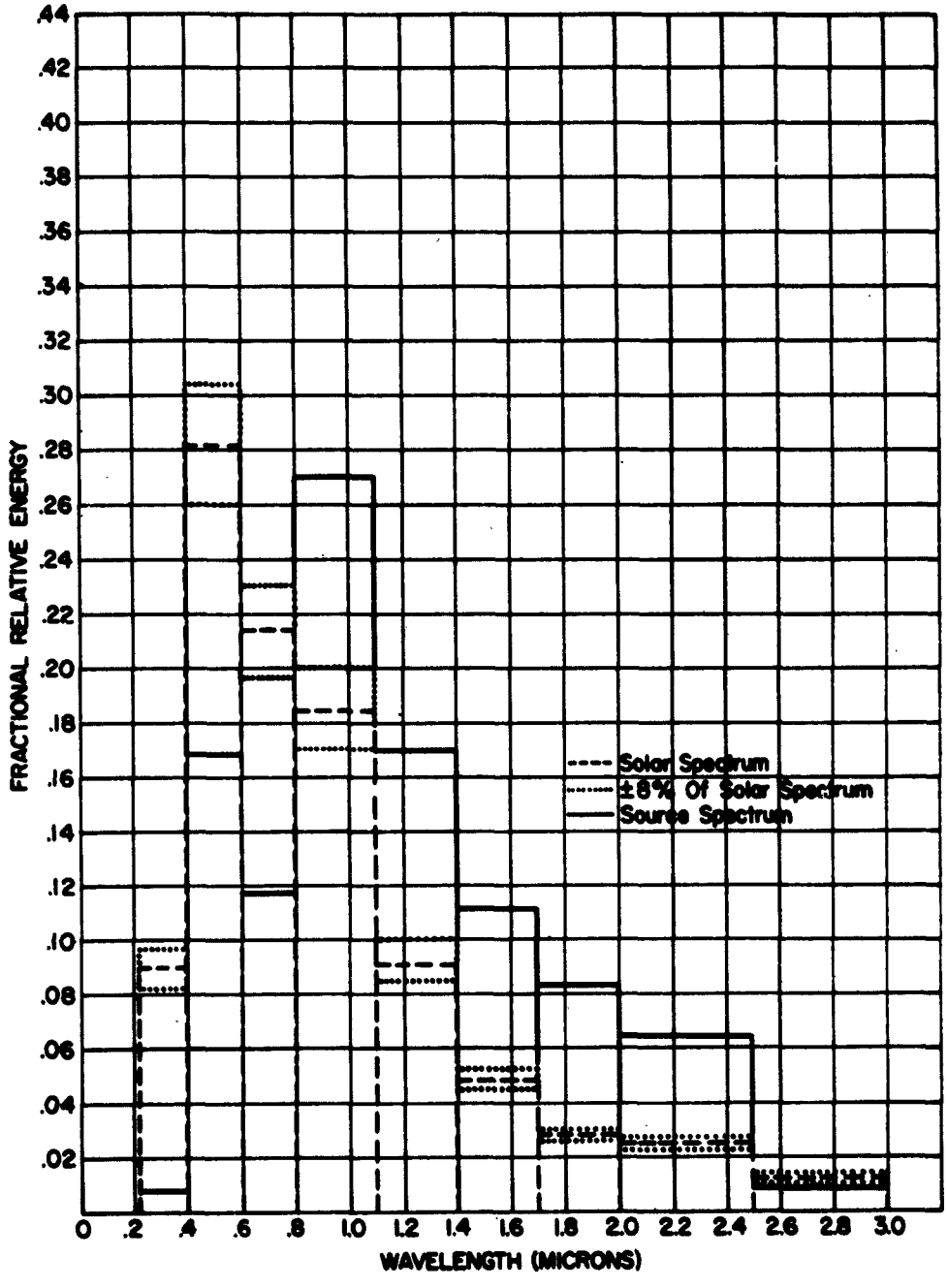

Fig. 16 Xenon-Mercury Source Spectrum Compared to Solar Spectrum

centered in the band 0.8 to 1.1μ. Again UV attenuation is evident in the bands below 0.8μ. Measurements of radiant energy output and of the intensity and uniformity of the output are in process.

3. Fluid-Transpiration Short-Arc Source

The fluid-transpiration arc equipment used in these tests is shown in Figure 17 while the arc in operation with argon transpiration at 75 gm/min. and 5.0 kw input power is illustrated in Figure 18.

a. Spectral Energy Output

The spectral intensity as a function of wavelength for the argon fluid-transpiration arc at 90 and 165 psia pressure are shown in Figures 19 and 20. A solar spectral distribution curve has been superimposed on each. Practically no change in the spectral distribution or broadening of lines is noted for the change in pressure from 90 psia to 165 psia. Again a sharp drop-off in intensity is noted in the region from 0.6 to 0.25 microns. The above spectral diagrams were taken through a one-inch-thick quartz window (Suprasil grade #2). This thickness will cause slightly more attenuation in the UV and infrared than the 1/4-inch thick quartz envelope used for testing the short arc lamp.

b. Spectral Match

The match of the spectral energy for the argon fluid-transpiration arc to the solar spectral energy in the specified bandwidths is shown in Figures 21 and 22.

The energy in the band 2.5 to 3.0 microns is only about 10% of that required. Possibly this is due to absorption in the 1-inch-thick quartz window especially in the 2.6 to 2.7 micron region. Between 1.7 to 2.4 and 0.6 to 0.8 microns an approximate match is obtained. From 0.8 to 1.7 microns there is about 50% excess energy. Again in the region below 0.6 microns the energy is far less than that required.

c. Total Radiant Energy Output

The total power radiated per solid angle as a function of the polar angle θ, is shown in Figure 23 for the argon fluid-transpiration arc at 100 psia. A complete polar diagram could only be made at atmospheric pressure since the polar angle measurements necessitated the removal of the present cast iron chamber housing around the arc.

Fig. 17 Fluid-Transpiration Arc Equipment

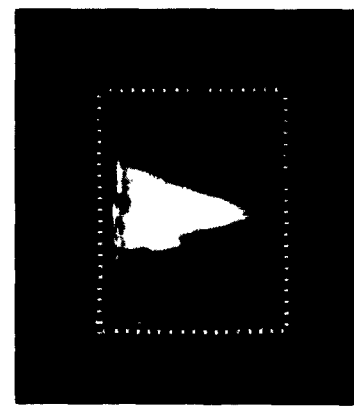

Fig. 18 Argon Fluid-Transpiration Arc in Operation at 50 psig

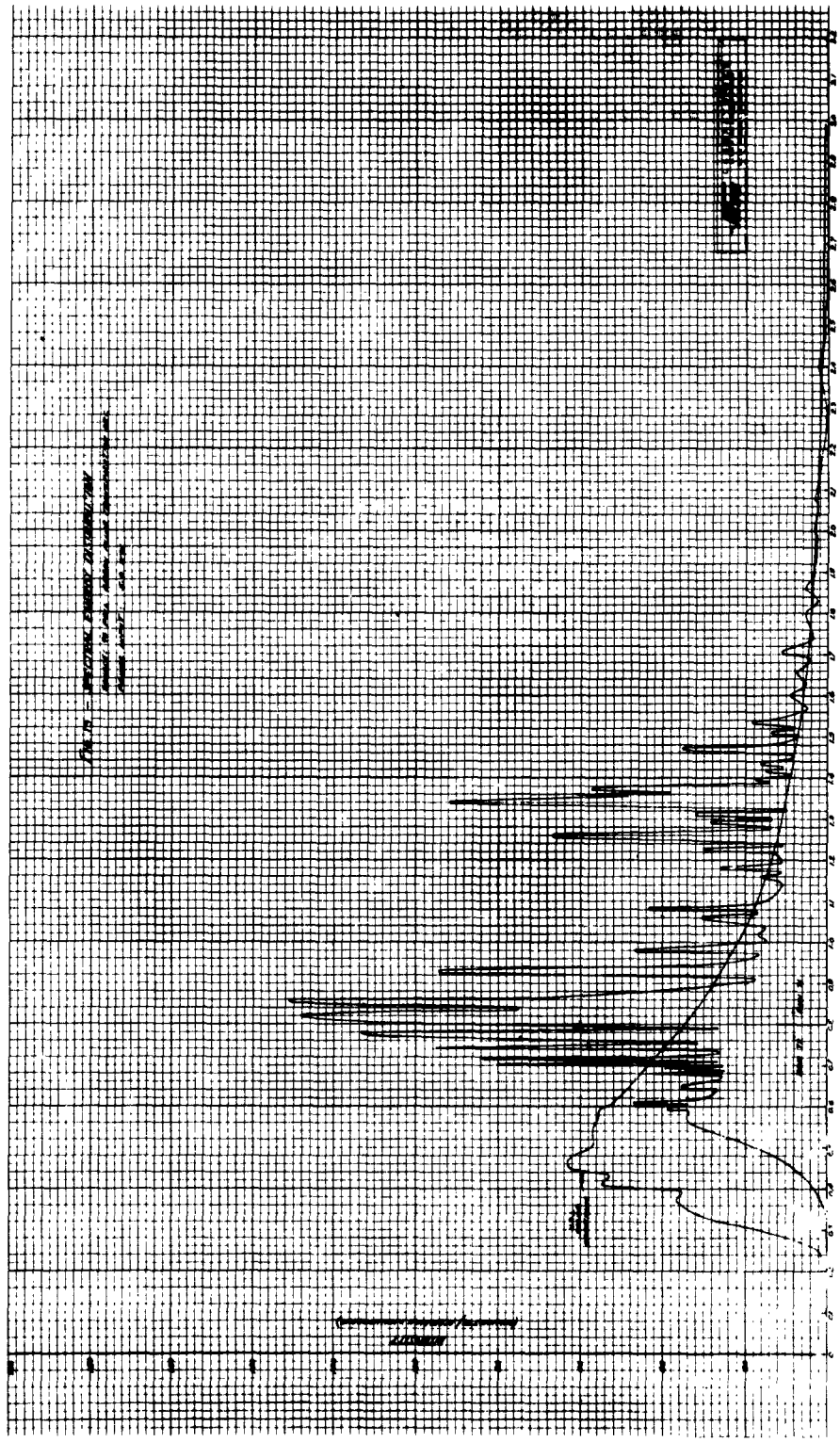

Fig. 19 Spectral Energy Distribution – Fluid - Transpiration Arc at 90 psia

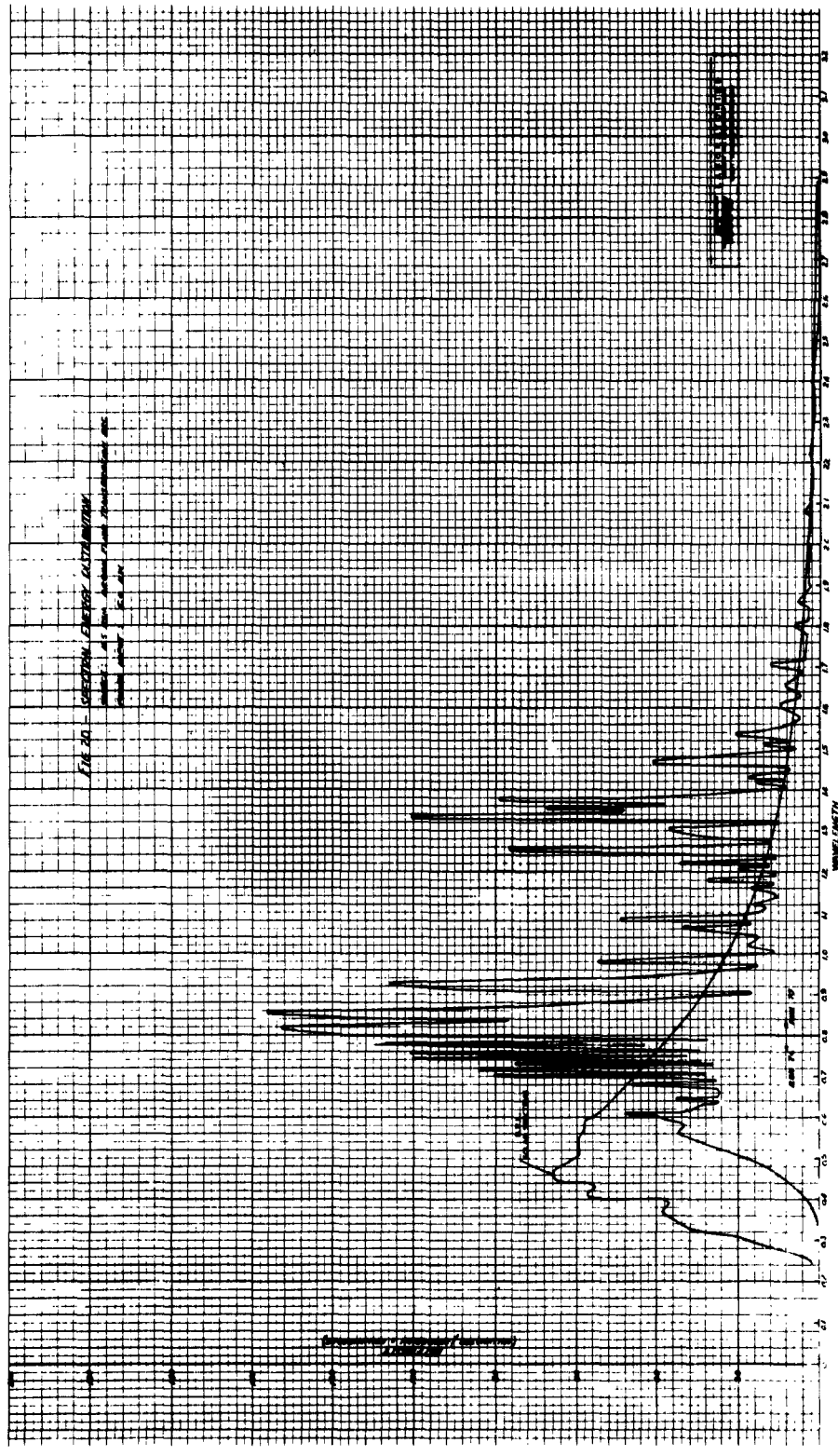

Fig. 20 Spectral Energy Distribution – Fluid -Transpiration Arc at 165 psia

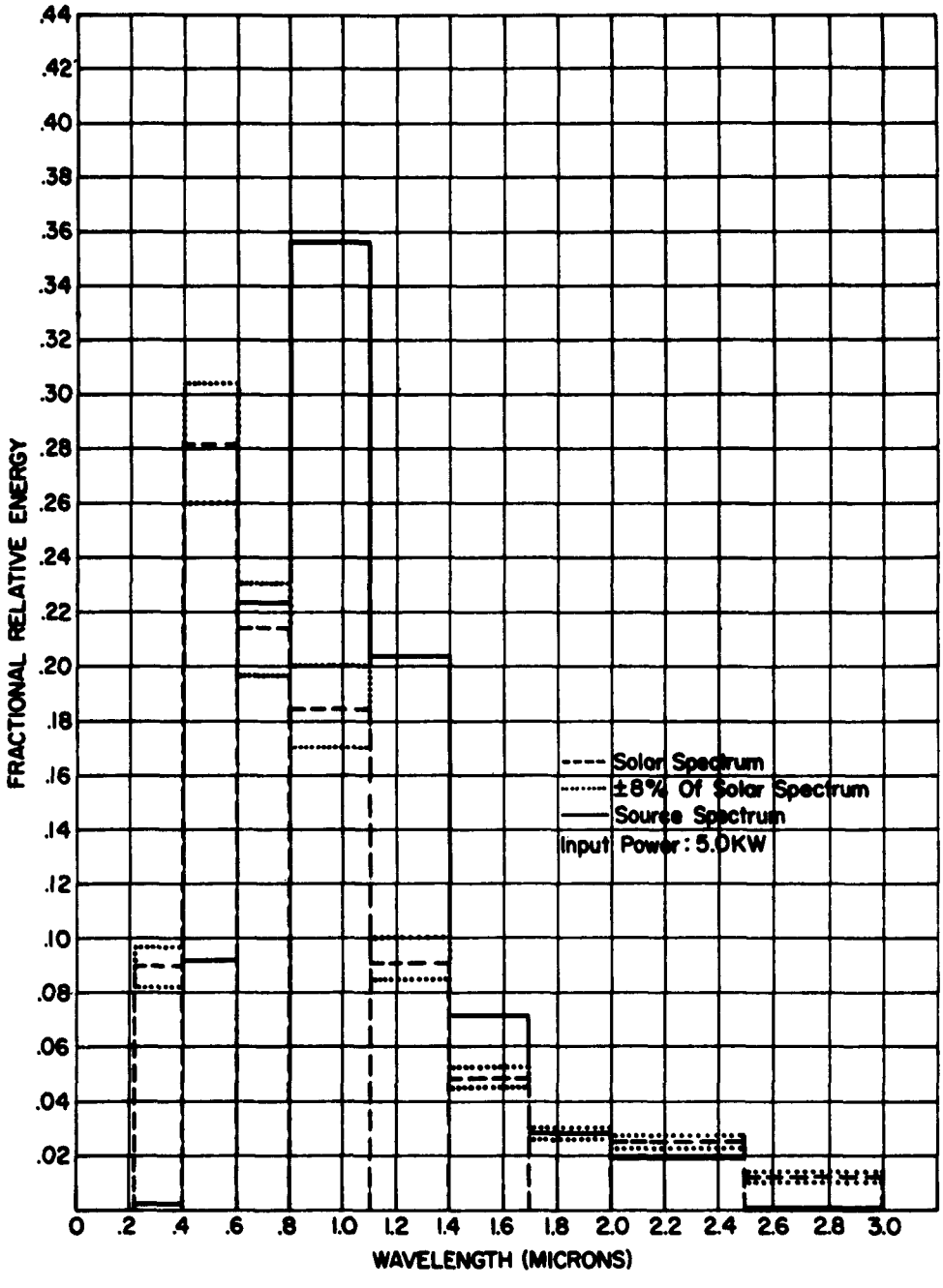

Fig. 21 Argon Fluid-Transpiration Arc Spectrum at 90 psia Compared to Solar Spectrum

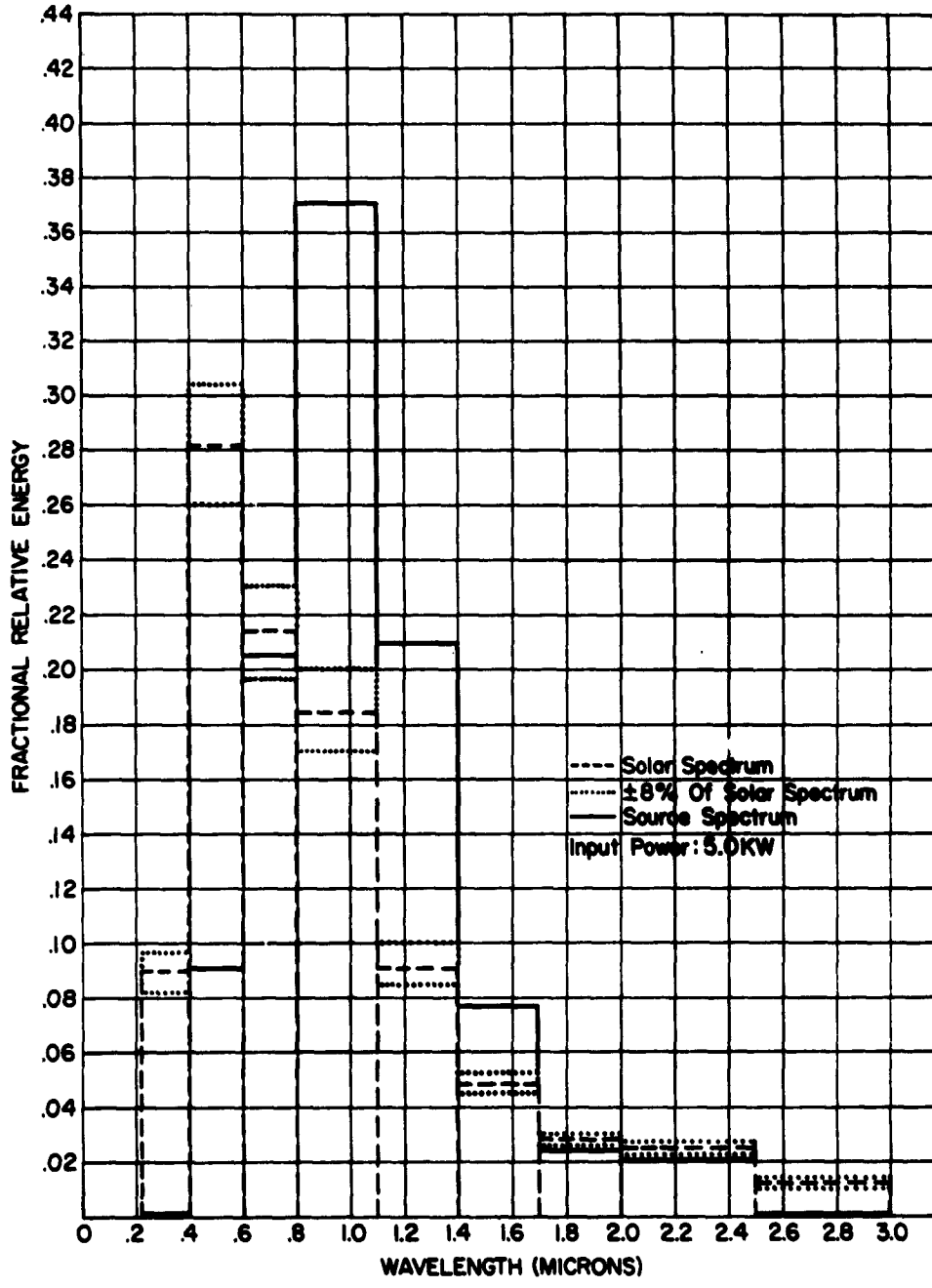

Fig. 22 Argon Fluid-Transpiration Arc Spectrum at 165 psia Compared to Solar Spectrum

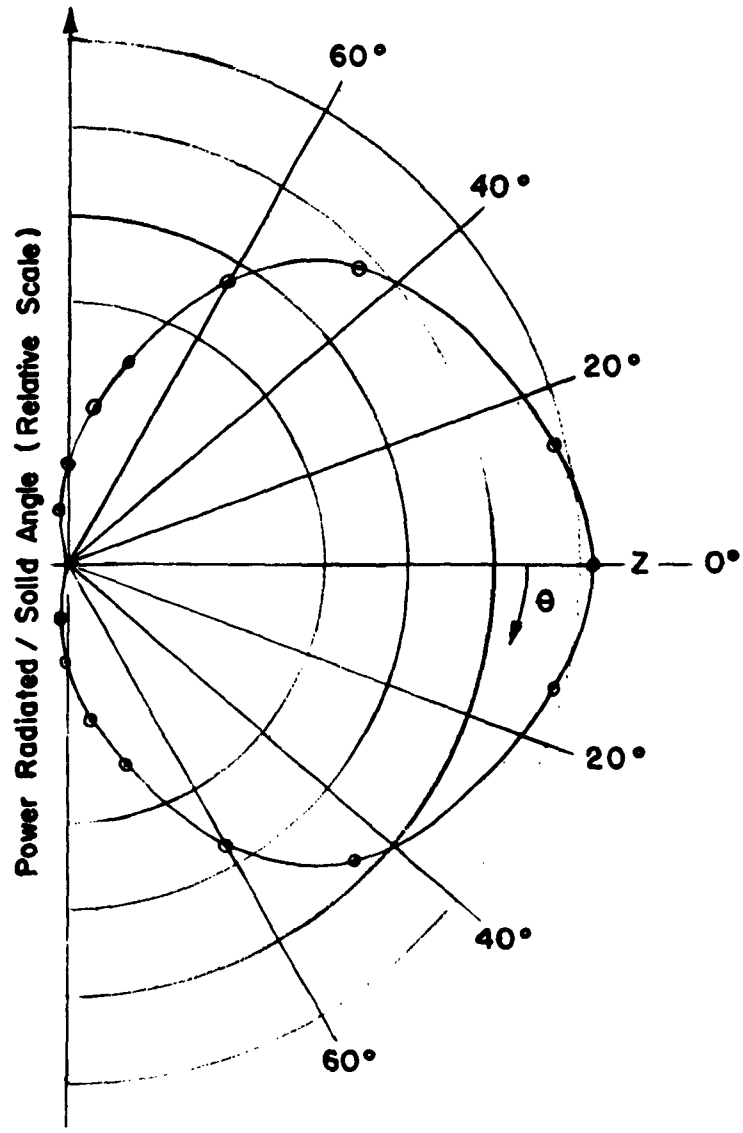

Fig. 23 Polar Diagram of 5.0-KW Argon Fluid-Transpiration Arc

The total power output per solid angle of the arc was computed from both the thermopile measurements and by integrating the spectrophotometer data. The calculated values from the data of the initial measurements showed a general lack of agreement between the two methods. These measurements are being continued and the general method is being checked to determine the causes for lack of agreement.

C. ADDITIONAL SOURCE POSSIBILITIES

1. New Source Concepts

In addition to the sources discussed in Technical Note No. 1 as possibly suitable for solar simulation, several other source concepts have been investigated briefly. Although some of these concepts may have potential, initial investigation indicates that long research and development programs would be required to substantiate their applicability to the facility.

a. Incandescent Nuclear Reactors

One unique concept for a radiation source is based on a hot incandescent nuclear reactor. In this particular case a critical size self-sustaining nuclear reaction is contained in a reactor which is allowed to operate at high temperatures, the body of the reactor at high temperature acting as the radiator. Obviously, to merit consideration for solar simulation, the operating temperature of the container should be in excess of 6000°K. Since the best high temperature materials are limited to temperatures well below 6000°K (4000°K and less) this concept is clearly limited by a materials problem.

Other concepts to circumvent the materials problem inherent in containing nuclear reactions, such as confinement of the reaction by magnetic fields, have not provided a practical solution to date. At best, such a concept would imply large, expensive, and cumbersome installations.

b. Gaseous Nuclear Reactor Source

In this particular concept the spherical reactor walls would be cooled to maintain structural integrity while the nuclear reaction would be viewed or projected through a viewport. Assuming a structurally sound, optically thin, viewport could be developed for such an installation, the theoretical minimum diameter for such a gaseous reactor would be in excess of 5 feet and operating

pressures would be 400 atmospheres. This would represent a permanent, bulky, and costly installation. In addition, a formidable thermal gradient would have to be established through the container of such a reactor to maintain structural integrity. Heat removal in the order of hundreds of megawatts would be required, further increasing the bulk of the installation.

c. Exploding Wires

Exploding conductors are also a means of obtaining intense thermal radiation. Extremely high temperatures can be produced for periods of a few microseconds. Although the intensity of radiation may warrant further investigation, the duration of this radiation, being as brief as it is, would imply extensive development work to develop rapid intermittent pulse techniques and feed mechanisms to supply new conductors to the point where the light is derived. The collection of vaporized material would also preclude the feasibility of this technique in the near future.

d. Chemical Reactions

Chemical bond energies released in exothermic reactions appear to be insufficient to produce the radiation required to simulate solar radiation. Chemical bonds are broken at fairly low temperatures.

e. Cathodoluminescence Sources

Radiation which is produced from luminescent materials by cathode-ray bombardment is known as cathodoluminescence. Phosphor materials of this type can produce luminances steadily up to several hundred candles per square millimeter. The radiation however is generally confined to narrow spectral limits. No one substance can luminesce in a continuous spectrum between 0.2μ and 3.0μ. Applicability of this phenomenon to produce a continuous radiation flux of the desired characteristics similar to solar radiation would depend on compounding several luminescent materials. It is not at all certain if such materials exist. Current work in this field is concentrated to a large measure on producing visible light. Development of long life phosphors and cooling techniques for the phosphors has not been completed as yet. Proof of feasibility of this technique is a long range research study and cannot be considered for the current requirements.

2. Developmental Sources

In addition to the short-arc gas lamps, another source receiving developmental attention is the carbon arc. The developmental objectives for this arc are primarily directed to improving or changing the spectral characteristics of the anode crater by changing the additives in the core of the carbon rods. High-powered reliable carbon arcs in the 20 kw range are also being developed. Some development is also being directed to increasing the continuous burning time of carbon arc devices with large magazine loading systems for the electrodes.

III. OPTICAL SYSTEMS

The second major element of a solar simulator is the optical system whose function is to collect and tailor the radiation to the desired properties of intensity, spectral distribution, collimation and uniformity. Several optical systems have been designed or proposed for other solar simulators, all having an area to be radiated much smaller than required for the chamber. In addition, none of these simulators have the high energy conversion efficiency or the close tolerances on the optical properties considered necessary for the chamber. It was therefore decided to design a reference system which would serve as a basis for preliminary assumptions of parameters and for comparison with existing and proposed systems.

The Reference Module* (Drawing F113749A) is shown as Exhibit I. Its design was based upon criteria considered most likely to be confirmed by the study and to fulfill the specified requirements. Design criteria were:

1. Use reflecting optics where possible, because they are generally less costly than refracting optics.
2. Collect virtually all of the lamp output, for efficiency.
3. Use a xenon compact-type arc lamp, because of efficiency, cleanliness and long unattended life.
4. Keep the number of optical surfaces to a minimum, for economy of construction and efficiency.
5. Locate the source outside the chamber for ease of cooling and replacement.
6. System to be suitable for use with double walls, 36" apart.
7. System to show promise of being amenable to simultaneous correction of uniformity and collimation.
8. Avoid concentration of lamp arrays, to reduce cooling problems.

* This design has been entitled "Chamber–Concept A". For the purpose of this report, it will be called simply "Reference Module".

The reference module used as a starting point in the present study has a minimum number of optical surfaces, collects the maximum possible lamp output, and can accept the largest available (10 kw) compact arc lamp. It was thus considered to be not only a reference standard for the comparison of other systems, but also a candidate, with them, for evaluation as an eventual choice for the chamber.

Final evaluation of the various systems and choice of the best for the purpose should not be made, however, until the other candidate systems have been adapted insofar as possible to the size, double-wall construction, configuration, collimation, uniformity, and other performance objectives of the proposed chamber.

A. SYSTEM FEASIBILITY

1. Spectral Distribution and Filtering

A major problem to be solved in this investigation is the feasibility of matching the solar energy, as found outside the Earth's atmosphere, within the limits specified. The region of interest lies between 2,000 and 30,000 angstroms and the standard to be matched is the Johnson curve, with latest revisions.

The starting point of this part of the study must of necessity be the spectral output of the selected lamp. This energy is selectively reduced by each element in the optical system, until it is finally projected, in a collimated beam, into the simulation chamber.

The problem of providing a good spectral match is approached by first choosing a lamp and assuming a suitable optical system. Then one must determine the spectral distribution of the useful lamp radiation, under practical operating conditions. Also, the spectrally distributed ratio of reflected to incident energy (reflectance) for each mirror and of transmitted to incident energy (transmittance) for each window or lens in the system must be established. The transmittance of air and of ozone, generated from atmospheric oxygen by the ultraviolet lamp radiation in the area between the lamp and the first window, must also be considered. The spectral product of these terms is the system output, which is then compared to the solar curve, using suitable scale factors to keep the system output above the minus tolerances of the solar standard. Any portion of the system output which exceeds the plus tolerances of the solar standard must then be filtered out. Suitable filters are chosen to accomplish this. The next step is to compare the spectral product of the system and filter characteristics to the solar curve, and to further refine the

filter designs if necessary, so that the final result falls within the specified limits. Any recommendations as to desirable or necessary changes to the solar match tolerance can then be made.

It is anticipated that the requirement that "any band" of listed width be within the limits (Table IV) might be changed to read "successive bands", particularly in the case of the 200-angstrom band, in order to handle the problem of spectral lines. Otherwise an unnecessarily large number of tests would be required to confirm this property.

In order to permit a preliminary study to proceed the use of a 10-kw xenon lamp was assumed, and as previously indicated a suitable reference module (Dwg. F113749A) was laid out. For preliminary calculation, omitting the center fill-in system, the module consists of three and one half reflectors (the spherical reflector near the lamp collects only the lower half of the lamp output) and two windows.

The spectral distribution of external (total) transmittance of suitable window materials (fused quartz and synthetic sapphire) is shown in Figures 24 and 25, and the reflectance of various numbers of high quality aluminized surfaces is shown in Figure 26.

The attenuation of energy due to Rayleigh scattering by the atmosphere is negligible, since at the ultraviolet end (2,000 angstroms) of the spectral range a one-meter path transmits 0.9991 of the incident energy. This factor approaches even closer to unity with increased wavelength.

Ozone has an absorption band at about 2500 angstroms, and will also modify the output spectrum. The ozone concentration surrounding a 2500-watt xenon lamp is approximately 89×10^{-6} grams per cubic meter. Fortunately, the lowest transmittance (at 2539 A) of a one-meter path of this concentration is 0.9993, which represents negligible absorption.

The spectral product of the window and reflector curves is shown in Figure 27, for each of the two window materials. This figure represents the transmittance of the reference module.

When the spectral distribution curves of the selected lamps are available the spectral product of each lamp curve and the appropriate curve of Figure 27 will represent the output, before filtering, for that combination of lamp and optical systems. It will then be possible to proceed with filter selection and with final calculations of efficiency and area to be covered by each unit.

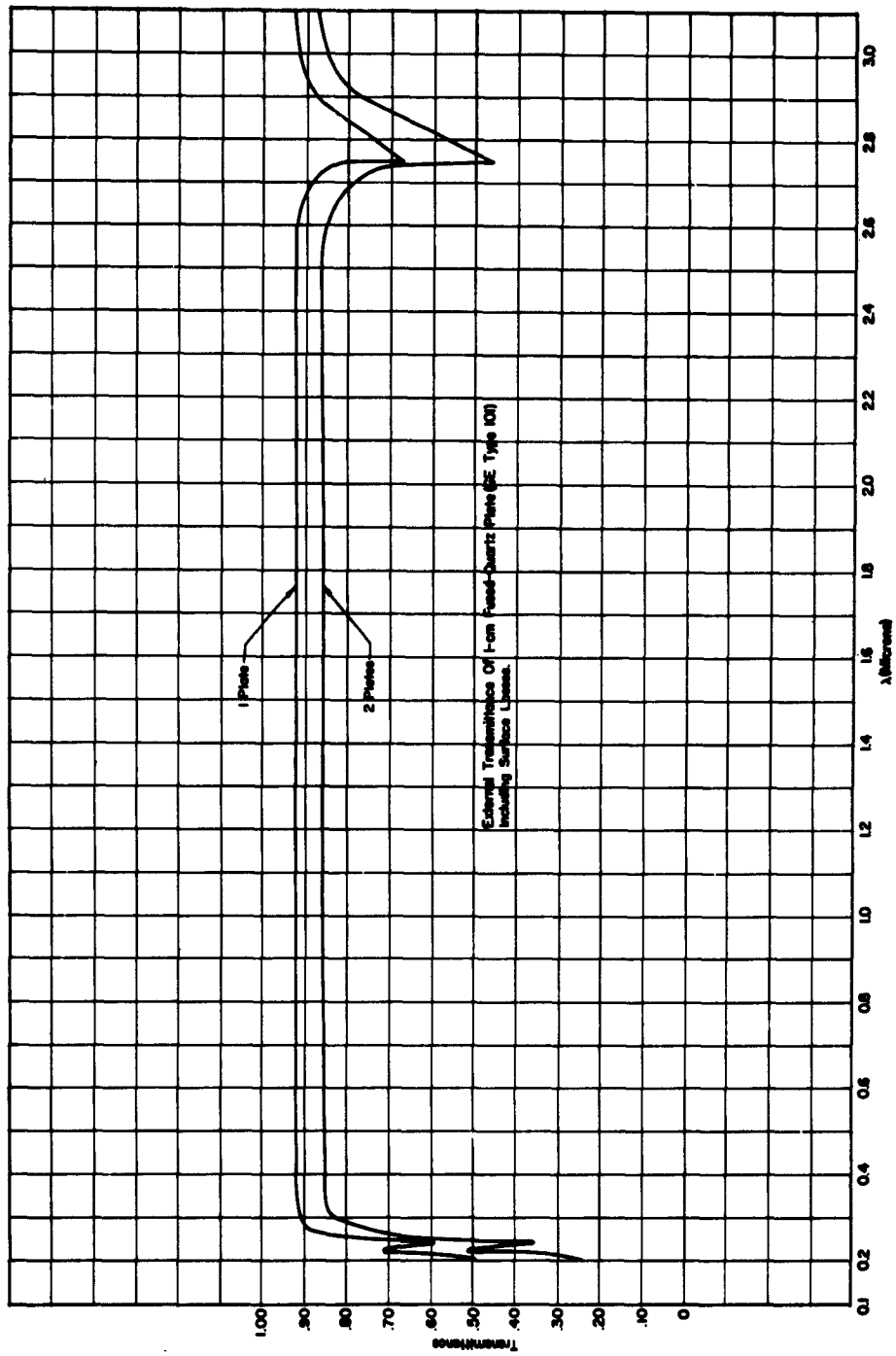

Fig. 24 External Transmittance – Fused Quartz Plates

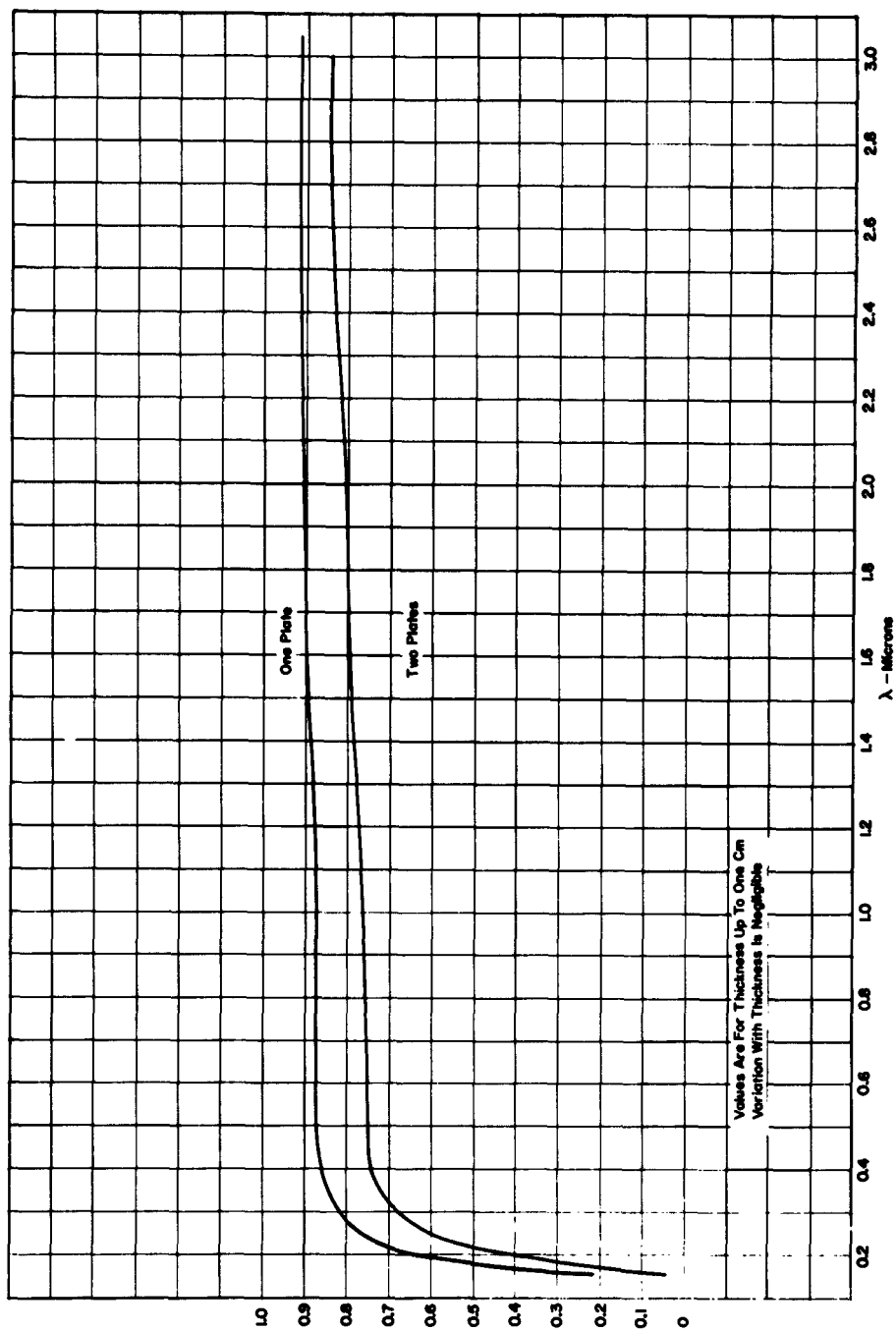

Fig. 25 External Transmittance – Synthetic Sapphire Plates

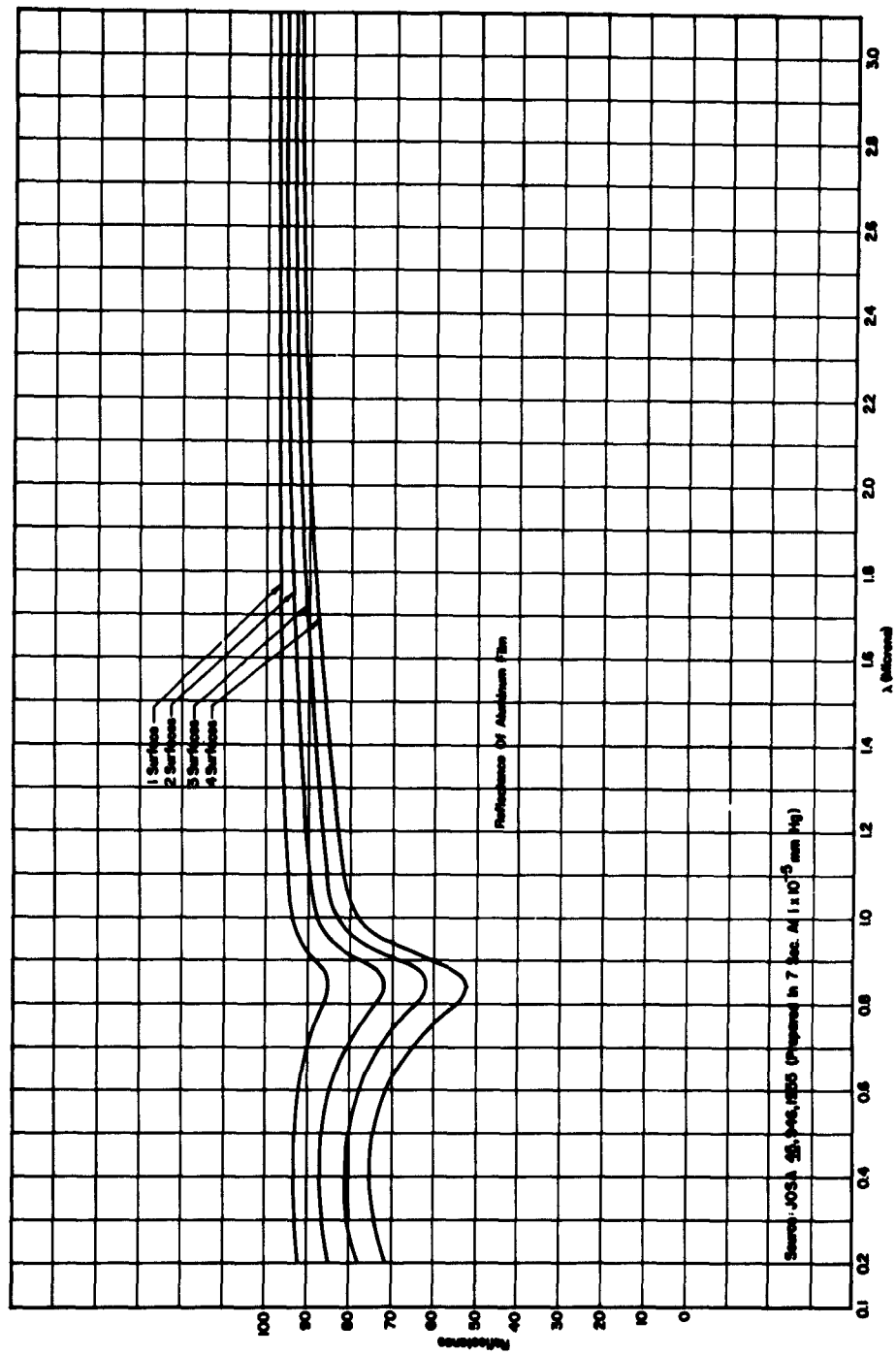

Fig. 26 Reflectance – Aluminum Films

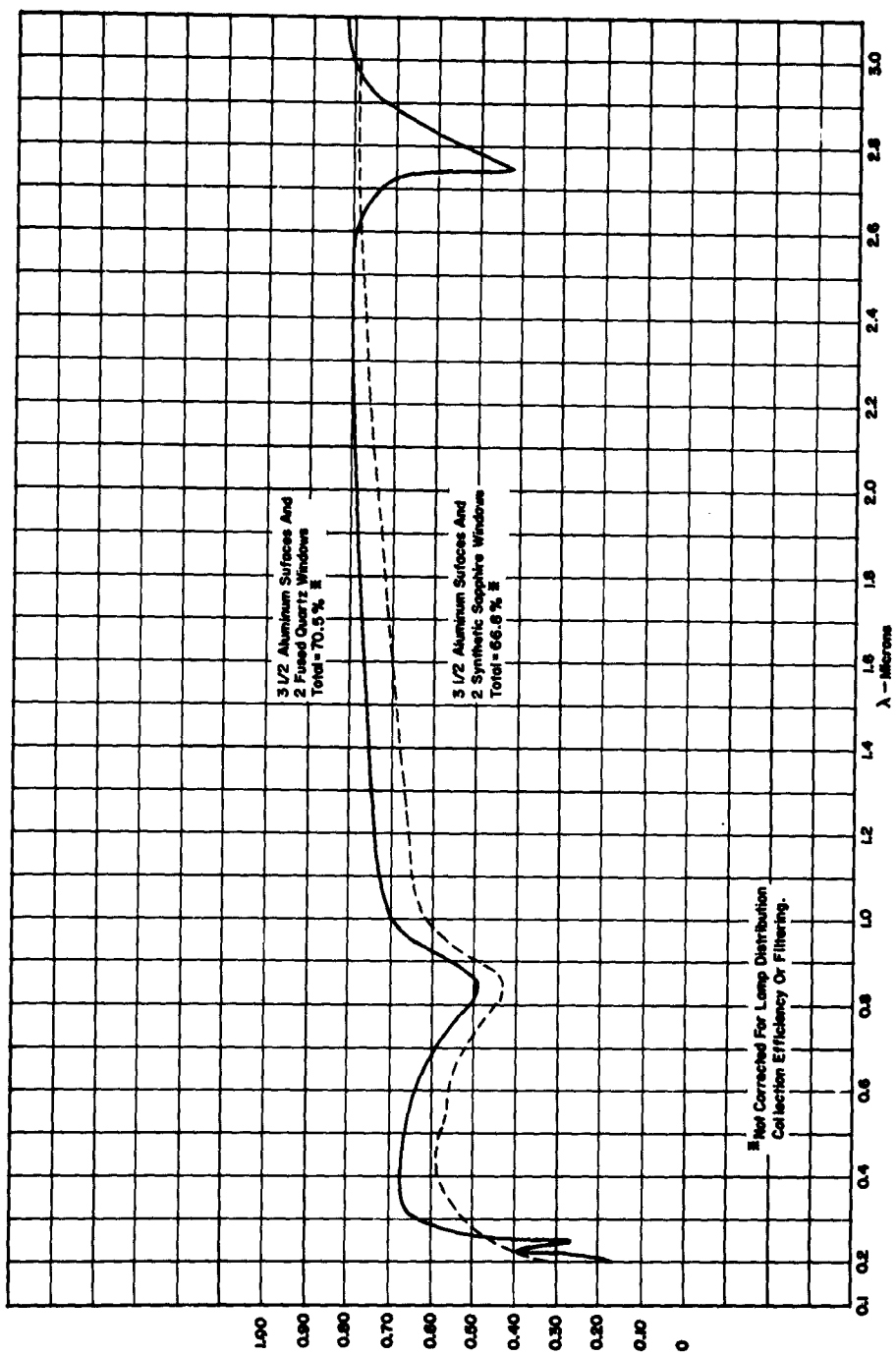

Fig. 27 Transmittance of Reference Module

2. Lamp Size

The lamp tentatively selected (10-kw Duro-Test, Figure 28) is of quite feasible mechanical size. For use in the reference module this lamp offers no physical interference, and is smaller in proportion to its wattage than similar 1,600, 2,500 and 5,000 watt lamps. Its configuration is also easily adaptable to the module as it provides a symmetrical arrangement in a module with a vertical axis, when operating, as it must, in a vertical position.

The wattage size (10 kw) is a distinct advantage over smaller lamps, in that a reasonable area can be covered by each lamp, and the number of modules is kept to a minimum.

The 8-mm arc length compares favorably with the 13.6-mm diameter crater of a 10-kw carbon arc and the 5.0-mm arc length of a 5,000-watt mercury-xenon lamp.

3. System Energy Conversion Efficiency

The efficiency of the solar simulation system will be equivalent to the efficiency of an individual module if the modular concept is adopted. Overall module efficiency is represented by the ratio W_0/W_i where W_0 is the useful radiant watts, within the specified wavelength limits, projected into the chamber and W_i is the electrical watts at the lamp connections. Power supply, ballast and line losses are not considered in this part of the study.

Overall module efficiency can be broken down into three parts: lamp efficiency, optical system efficiency, and filter efficiency and is the integrated spectral produce of the three.

Lamp efficiency is the ratio of useful radiant watts (from a small, finite source, and within the wavelength limits) to the electrical watts at the lamp connections.

Optical system efficiency consists of the product of collection efficiency (that fraction of the lamp output actually picked up by the mirror system), the reflectance and transmittance of the various elements of the optical system and the geometric efficiency (which considers losses incurred in shaping the naturally circular beam into the hexagonal shape required for the array of modules). The reflectance and transmittance of the module elements, including those used for geometric shaping and center fill-in, must be treated on a spectral distribution basis.

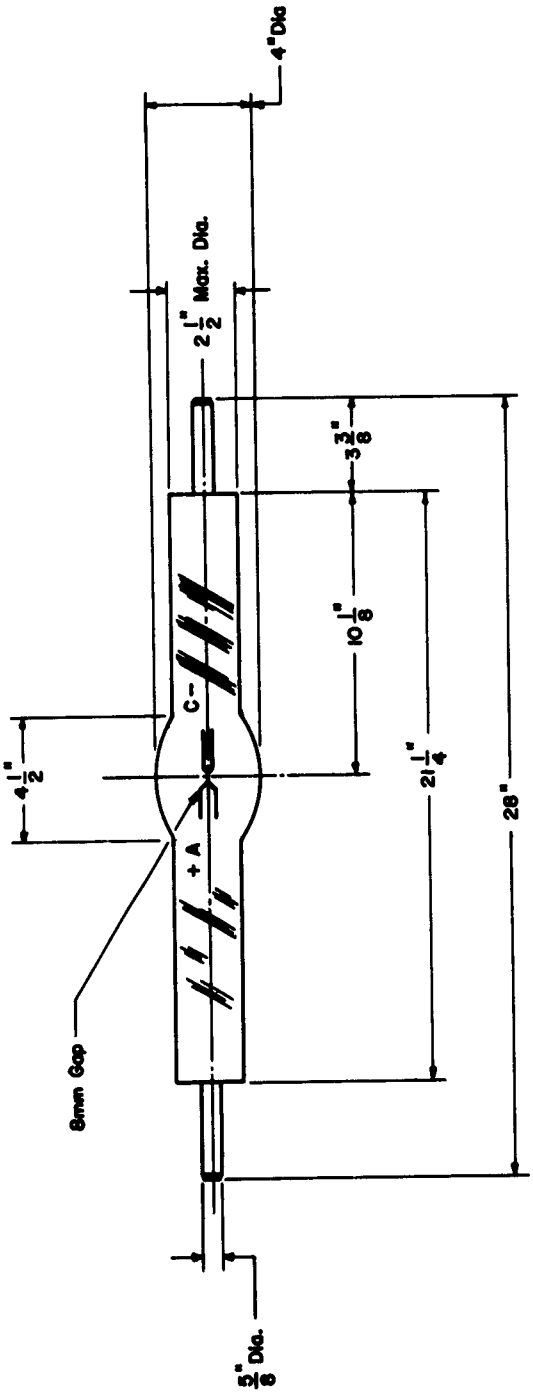

Est 7.5kw Starting Input

Fig. 28 10-KW Xenon Lamp

Filter efficiency will be determined after the filters have been selected and is, of course, highly selective as to spectral distribution.

The efficiency of the system of mirrors and windows shown in the reference module is given in Figure 27, and for a hypothetical lamp having uniform output at all wavelength between 2,000 and 30,000 angstroms, would be 70.5% for quartz windows, or 66.8% for sapphire windows. The efficiency under operating conditions would be weighed by the spectral distribution of the lamp energy.

Collection efficiency should be better than 90%, since a study of polar diagrams of the output of smaller but typical lamps of the compact type shows very little radiated energy beyond the acceptance of the mirrors (See Figure 29).

The area which can be covered by a module is a function of lamp power and module efficiency. In order to obtain an estimate of the area, the design of the reference module was based on the following parameters:

Assumed lamp: Duro-Test Xenon	10 kw
Input power to lamp at beginning of lamp life (to maintain constant output)	7.5 kw
Useful radiation (percent of input) estimated	48%
Collection efficiency estimated	90%
Module transmittance	68%
Filter efficiency estimated	70%

With a module conforming to the above values, there will be 1,540 watts available in the chamber. This is sufficient to cover a circle of 12.11 square feet at 127.16 watts per square foot, the value of the solar constant between 2,000 and 30,000 angstroms. Reducing the area to a hexagon inscribed within the circle results in 10.02 square feet of coverage. The hexagon would be 40.81 inches across flats, which is also the center-to-center spacing of the modules. The energy salvaged from the six circular segments outside the hexagon would be used for center fill-in, and it is doubted that any increase in hexagon area could be realized from use of this energy.

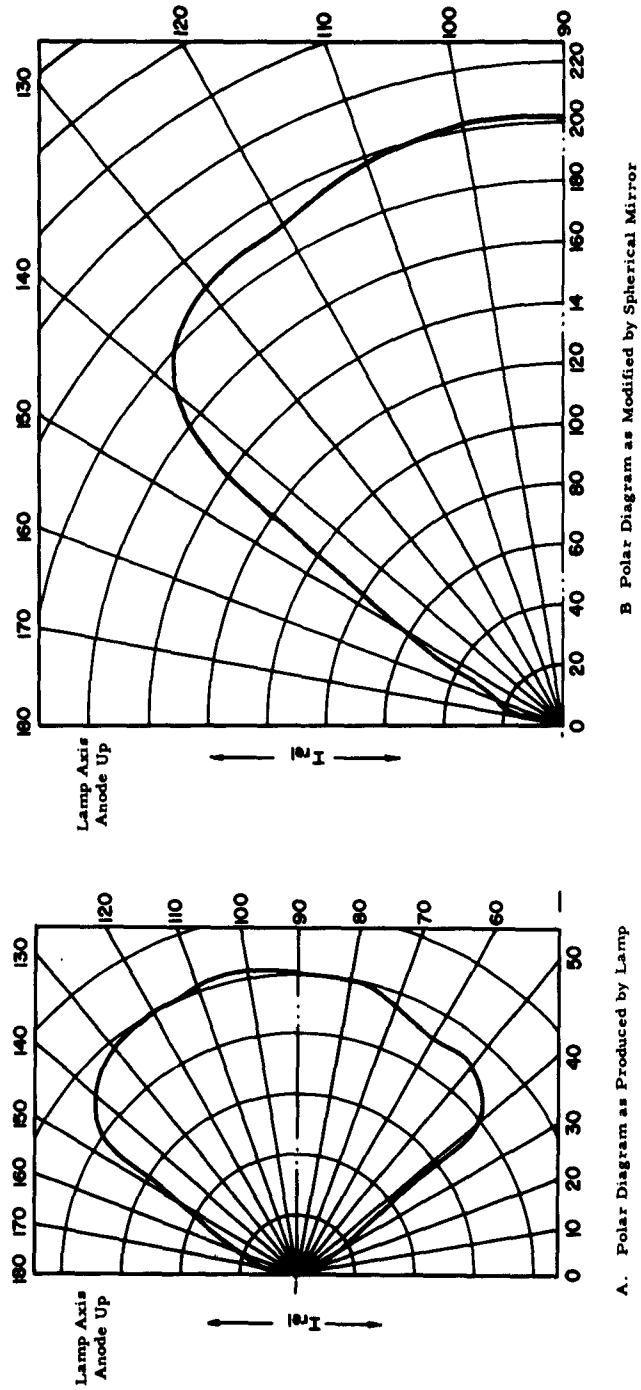

A. Polar Diagram as Produced by Lamp

B Polar Diagram as Modified by Spherical Mirror

Fig. 29 Polar Diagram of Xenon Lamp

The resulting overall module efficiency, W_0/W_i, is 127.16 x 10.02/7500 or 17.0% when the lamp is new. Assuming that the lamp input has increased to rated value (10 kw) at the end of lamp life, maintaining a constant output, the efficiency is then 12.7%.

In order to provide full illumination at the edges of the selected test area, the modules must cover an extra width, on each of the four sides. Thus the minimum area to be covered is slightly greater than the desired test area. Knowing the dimensions of the basic module, the number and arrangement of the modules can be obtained. A typical corner arrangement is shown in Figure 30. This however, is a tentative figure based on the assumptions previously indicated and will change when the overall efficiency of the system is calculated.

The maximum power consumption should be calculated on the power required by old lamps. Power losses ahead of the lamp terminals would be added to these figures.

4. Operational Life of Optics

The operational life of the various optical parts and their mountings should be practically without limit. With proper care in cleaning, and the use of filtered cooling air, the mirror and window surfaces should remain undamaged. Furthermore the window and lens materials are expected to recover, by heating, from any radiation-induced color centers. Radiation effects are discussed in Appendix B.

One cause of mirror and window damage would be exploding lamps. Lamps should be handed in protective screens during installation and removal. The probability of bursting can be reduced by limiting lamp power. When the gradually increasing lamp input reaches this limit, further increase should be prevented, and the lamp should be replaced as soon as possible. Although a bursting lamp might badly scratch a metal mirror, operation could be continued, in most cases, until a time convenient for replacement of the mirror.

If this modular design is selected, care must be taken not to drop objects on the windows during maintenance. The windows are protected by the ellipsoidal mirrors during operating periods.

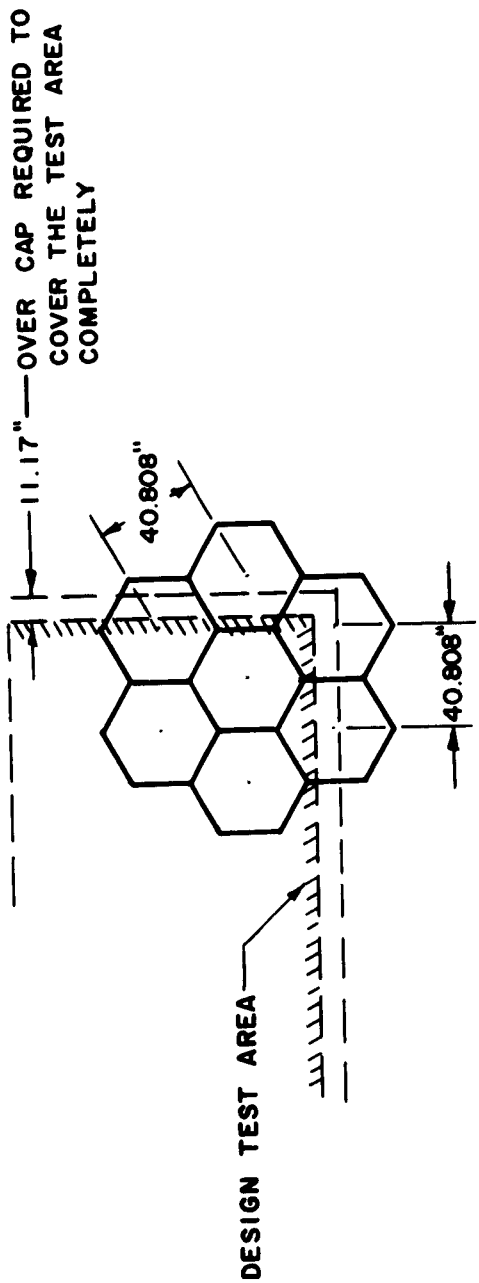

Fig. 30 Array of 10.02 Square-Foot Modules

5. Cooling Requirements

In order to study and evaluate the cooling requirements of the system, the heat to be dissipated by each element of the module must first be determined. Assuming a 10-kw lamp in the reference module, the heat loss, in watts, of each major element will be as shown in Figure 31.

The major heat loss is in the lamp itself. At 7500 watts starting input (new lamp), assuming 48% useful radiation, the loss to be carried away as heat is 3,900 watts. At the end of life, assuming that the input has been increased to 10,000 watts to compensate for blackening of the envelope, the loss would be 6,400 watts.

Depending upon the detail design of the lamp, part of this heat would be removed by liquid-cooled mountings or contact jaws and part by an air current provided by a vacuum exhaust connection. The air exhaust system would also remove the ozone generated from atmospheric oxygen by the ultraviolet lamp energy. The ozone could otherwise accumulate in the radiation shield and become a personnel hazard. A flow rate of 300 cubic feet of hot exhaust air per minute would remove waste lamp heat (estimated to be 6400 watts at the end of lamp life) with a 110°F air temperature rise.

Air for cooling the lower end of the lamp, if found to be necessary, could be carried by flattened tubes in line with the spokes supporting the spherical mirror, and introduced into the area surrounding the lower lamp support.

The spherical mirror loss is calculated to be 81 watts due to absorption. In addition, an estimated 180 watts of energy will not be collected due to obscuration such as edge chamfers and mountings, and due to lamp radiation at extreme angles below the arc. The actual value of the last effect will be calculated when the lamp data are available.

Due to the small radiating area of the mirror mounting, and to the proximity to the lamp, it is suggested that the mount be liquid-cooled. Coolant lines can be attached to or made a part of the support spokes.

Ellipsoidal mirror absorption loss is calculated to be 158 watts. Losses due to non-specular collection are estimated at 180 watts. Since this mirror is at the top of the module, where heated air will gather before being drawn off by the exhaust system, liquid cooling is recommended. Cooling fins on the back of the mirror would probably suffice as an alternate, but would greatly increase the heat inside the radiation shield above the module array, and would thus hamper maintenance operations.

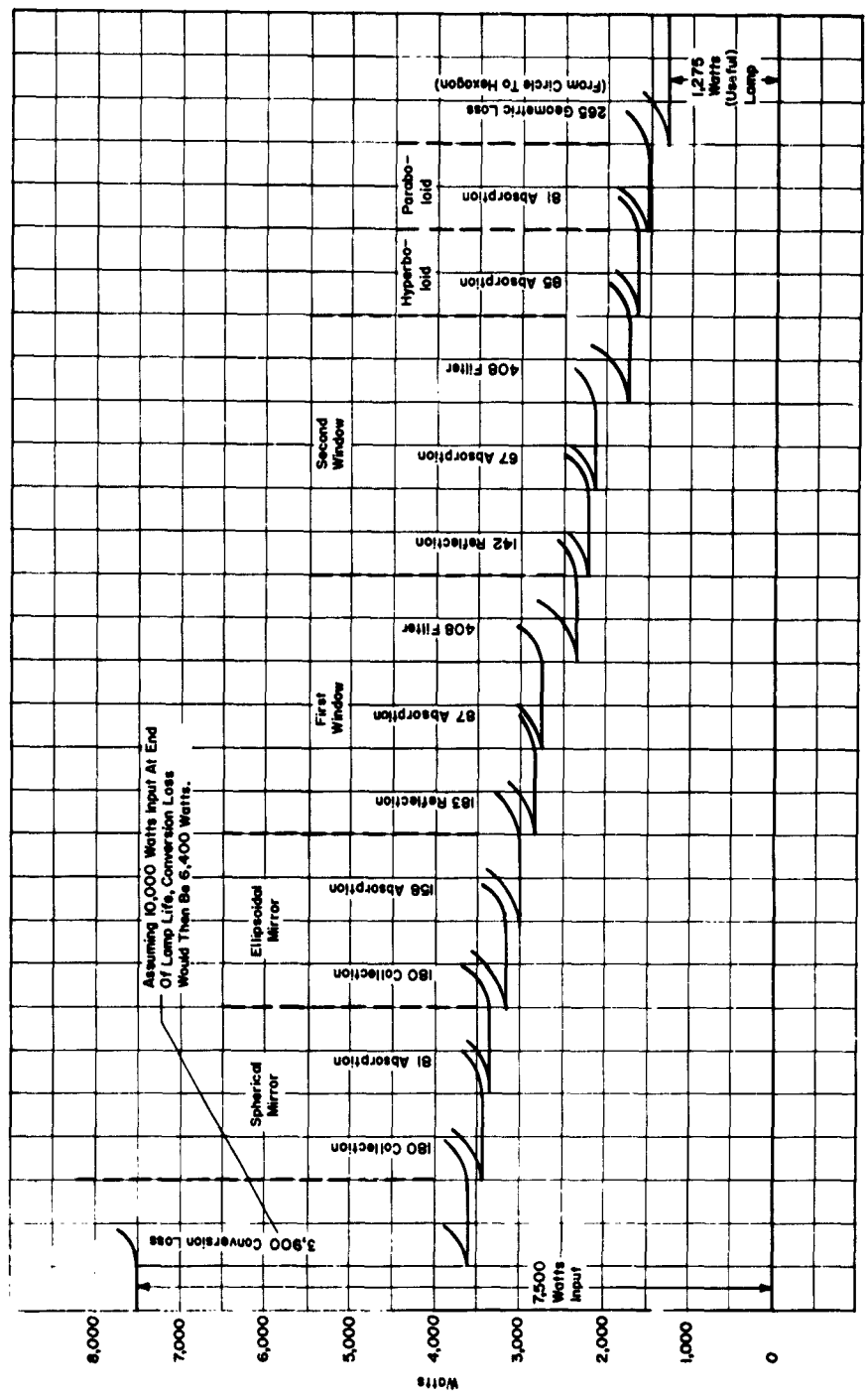

Fig. 31 Energy Losses in Reference Module

Two windows are required in order to provide for the guard vacuum between the atmosphere and the chamber vacuum. It is planned to incorporate the filters in the window surfaces in order to keep the number of optical surfaces to a minimum and thus maintain the best efficiency. The filter loss is estimated to be 816 watts and in order to prevent overheating, each window will provide half of the filter absorption. This design will also permit greater flexibility in filter design, in case it is found desirable to use several filters of different characteristics in order to provide a proper spectral match.

Liquid cooling of the window mounts would be required, in order to prevent excessive heat radiation into the chamber by the lower end of the module structure.

The hyperboloidal mirror-lens will absorb 85 watts due to the absorptivity of its partially reflecting coating and about ten watts due to absorption of the fill-in energy transmitted through it. Since this element can radiate to the cold walls of the chamber, no special cooling provisions will be required, unless its equilibrium temperature would adversely affect the test vehicle.

The paraboloidal mirror will absorb 81 watts due to its reflection loss. This can be dissipated easily to the cryogenic panels between the back of the mirror and the chamber wall.

The foregoing discussion of cooling requirements is based on the reference module. A final design might, of course, have somewhat different thermal values, and must be tested operationally to determine actual cooling requirements. This is especially necessary in the critical areas of the lamp and the filter-windows. If part or all of the filtering is of the interference type, the heat absorbed by the windows will be reduced, but the reflected energy must then be absorbed, and provision must be made to avoid reflected "ghost" images.

6. Maintenance

The principal maintenance operation will be lamp replacement. The design of mirrors, covers, etc., in the vicinity of the lamp should provide for easy lamp replacement. For example, the reference module shows a removable cover over the end of the lamp. Quick disconnects are shown in the electrical and air exhaust leads.

The possibility of a requirement for pre-focus adjustment of lamps before replacement is discussed below in connection with the adaptability of source to the reflector system.

Windows, mirrors and seals should be replaceable with a minimum of disassembly of surrounding parts.

The use of pilot fits and bench adjustment of sub-assemblies should be considered in the detail design of the system, so that a minimum amount of alignment and focussing will be necessary at installation and during maintenance operations.

7. Adaptability of Source to Reflector System

A short-arc type lamp is well suited for operation in a system such as the reference module for the following reasons:

The system is symmetrical when the lamp is operating in its required vertical position; practically all of the useful lamp radiation is collected and used (most important due to the overall power requirements and the cooling problem); the polar distribution of lamp energy, as modified by the spherical mirror (Figure 29) is so shaped as to help counteract the offense against the sine condition; excess energy from outside the hexagon is used to fill in the area vignetted by the lamp electrodes; the shape and orientation of the lamp permit replacement through a cover, without disturbing any of the optical parts.

The disadvantage lies in the 70° cone on the lamp axis that is obscured by the electrodes. The large amount of energy required to fill in this area necessitates a somewhat awkward arrangement of mirrors to collect and redirect energy from the periphery of the ellipsoid.

For reasons of maintenance, it is important that the lamps should be outside the vacuum chamber, in ambient atmosphere and temperature. Based on an estimated average lamp life of 1000 hours and a half-year test run (4400 hours), an appreciable number of the lamps can be assumed to fail, perhaps at the rate of one lamp every one or two hours. This replacement would be impractical to accomplish in the space environment.

Also, for cooling reasons, the lamps should be in the atmosphere. As shown above in the discussion of cooling requirements, the thermal energy to be removed ahead of the first window would be between 4,500 and 7,000 watts per module, depending upon the amount of lamp life expended. If the structure surrounding the lamp is operated at a high temperature, this heat can be removed more economically than would be the case if the structure had to be maintained at a low temperature acceptable to the interior of the chamber.

Further, air cooling of the lamp envelope could not be accomplished in the vacuum environment. It is doubtful that lamp life would be satisfactory without air cooling. However, this should be confirmed by a comparison test of lamp life in air and in vacuum.

Totally-refracting systems are not considered feasible due to the extreme cost of the optical materials that would be required. For instance, in a refracting module with efficiency equivalent to the reference module the final element would be approximately 47 inches in diameter across the corners of the hexagon. Extrapolation of the curve of price vs. size for optical grade fused silica indicates a price in the order of $45,000 for a single infinished blank of this size. Problems of availability in quantity, finishing, mounting, and losses due to absorption would further decrease the feasibility of a refracting system.

For ease and speed of lamp replacement, all lamps should have a pre-focussed arrangement of mounting surfaces, identical in size and in axial and radial relation to the arc center when hot. Likewise, each module's lamp mount should be of uniform size and location relative to the focus of its optical system.

The mount in the module should be aligned at assembly prior to installation in the chamber, and should require no further adjustment. Lamp mounting surfaces should be applied and inspected before the lamps are placed in storage for use. Gauges should be provided for both lamp and module adjustment.

Although the reference module is shown in diagrammetric form, several features should be noted.

The outer shell consists of two tubes and a connecting cone. These would be pre-fabricated. The inner and outer chamber walls would have concentric holes cut on a hexagonal spacing pattern as shown in Figure 30. The shells would then be inserted from the outside and welded to the inner and outer walls as shown, providing a suitable support structure between the walls.

The shells are so proportioned that the cylindrical portions will always be in contact with the chamber walls, whether at the corner of the array, as shown, or at the center where the walls will be normal to the module axis. Thus in the plan view the holes in the walls will be circular and concentric, simplifying the cutting operation.

The optical assembly is located and supported in the outer shell by a spherical joint in the region of the windows. The outer ring of this joint would be adjustable laterally to compensate for small errors in spacing during the wall-cutting and shell-welding operations. Aiming adjustments, to render the module axis vertical, are shown outside of the ellipsoidal mirror.

The spherical joint ring and aiming adjustments have no part in the structure or internal alignment of the module; therefore, the complete module can be assembled, adjusted and focussed as a unit by itself. It can then be disassembled at the region of the lower window for shipment. When the upper part is inserted into the outer shell and the lower part reattached, no further adjustment other than aiming should be necessary. This design provides for a continuous guard vacuum between the tank vacuum and the atmosphere.

B. ANALYTICAL STUDIES AND COMPUTATIONS

1. Optical Design of Reference Module

One purpose of this investigation is to determine the optimum optical system; one that will utilize a maximum of the lamp's energy, and that will redirect it into a uniform, collimated bundle.

From considerations listed in other sections of this report, it is indicated that the main collecting and collimating optics should be reflectors, rather than refractors, wherever possible.

It is well known in the art that reflectors of the conoid family (shapes generated by the revolution of conic sections) possess pairs of conjugates having the property that an object at one conjugate will produce a perfect image at the other. These conoids are:

1. Concave Sphere (positive power). Object and real image coincide at the center of curvature.
2. Concave Ellipsoid (positive power). Object at one focus and real image at the other.
3. Convex Hyperboloid (negative power). Object at one focus and virtual image at the other.
4. Concave paraboloid (positive power). Object at the focus and image at infinity (or vice-versa).

Most sources that produce a useful output over a solid angle greater than a hemisphere (2π steradians) can be equipped with a hemispherical mirror located concentric with the source. This serves to redirect some of the radiation back through the source so that the condensing system need not accept an included angle greater than 180°.

To evaluate the merit of an optical system in performing the task, rays were traced from an assumed point source having a radiation angle of one hemisphere.

A module concept showing promise is one consisting of the four conoids. The sphere is used to limit the source angle. An ellipsoid is placed with the source at its near focus and reimages the source at its far conjugate. This image is in turn picked up by a Cassegrain system, consisting of a hyperboloid and a paraboloid, and is focussed at infinity (perfectly collimated) by the latter.

However, when evaluated for uniformity of intensity across the aperture (diameter of the paraboloid), a tremendous variation is found, making the system unusable if not corrected. This variation of intensity is known to the optical designer as "offense against the sine-condition". The sine-condition requires that in a corrected optical system having one conjugate at infinity the ratio of the height (distance from the axis) of any ray in the collimated bundle to the sine of the angle between the same ray and the axis, at the image point, shall be a constant. Algebraically,

$$\frac{h_i}{\sin \theta_i} = \text{Constant} = \text{E.F.L. (Effective Focal Length) of the system.}$$

As one evaluates this ratio from the paraxial or central ray out to the marginal ray, the variation in E.F.L. is found. The square of this variation, or $\left(\frac{\text{E.F.L. paraxial}}{\text{E.F.L. marginal}}\right)$ is the ratio of flux in the marginal zone of the aperture to that at the axis.

Study of a typical system (similar to the reference module Dwg. F113749A) shows the following relative values for the contribution of each of three image-forming elements to this defect:

Ellipsoid:	1.424 negative
Hyperboloid:	0.1674 positive
Paraboloid:	0.1814 negative

Values of these contributions can be changed by detail variation of the elements of the system. Six possible variables are:

1. Magnification at which the condenser (ellipsoid) is working. It was generally found that the smaller the magnification, the smaller the defect. Mechanical considerations of diameter and wall thickness limit the magnification to approximately 6X. Once having ascertained this value, it was used throughout the reference module computations.

2. Use of Fresnel-type mirrors. Replacement of the ellipsoid by a Fresnel-type mirror was investigated. Figure 32 shows such a mirror, corrected for spherical aberration and sine-condition, and is designed to make the expression $\left(\frac{\text{sine of the angle at source}}{\text{sine of the angle at image}}\right)$ equal a constant, and to permit all of the reflected rays to pass through the image point.

   It can be seen, however, that with such a mirror a considerable amount of the illumination is lost in the blank spaces between the reflecting facets.

3. Use of a concave secondary (Gregorian) in place of the indicated convex (Cassegrain) system. This leads to very similar final results in terms of sine-condition variation for the total system. However, in general, the elliptical secondary of the Gregorian system is larger than the hyperbolic secondary of the Cassegrain system, and is less

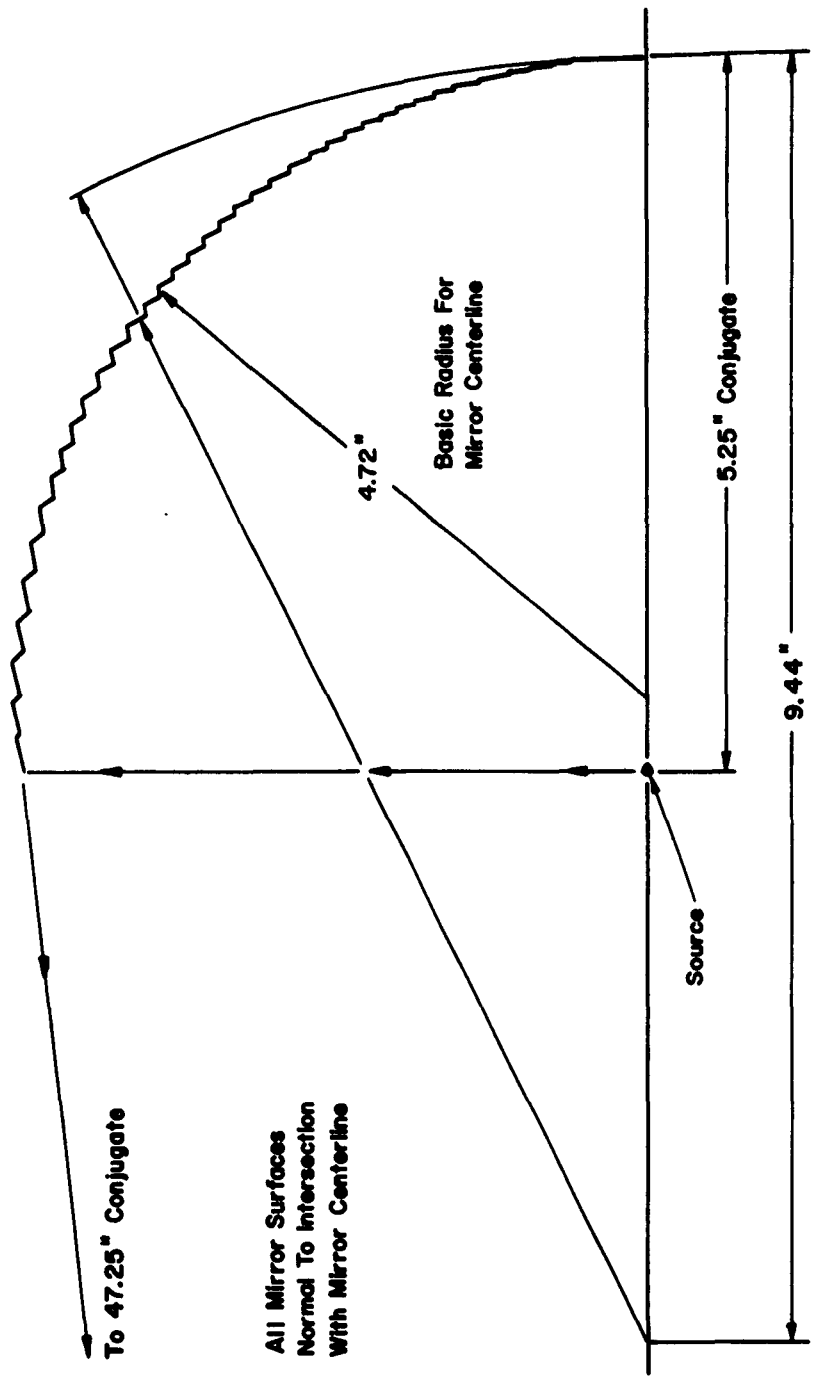

Fig. 32 Geometrically Derived Fresnel Mirror

desirable because it requires more fill-in energy to compensate for its shadow. This leads to large refracting fill-in optics.

4. f/number of the individual components of the projection system (primary and secondary). The characteristic of this variable is such that the higher the f/number (slower system), the less the contribution to the offense. However, higher f/numbers lead to larger - diameter secondaries, and increased fill-in requirements.

5. A conic departure of surfaces from their theoretical conic sections. Properly designed combinations of departure for two or more surfaces will maintain collimation while improving the sine-condition. This possibility has not been evaluated as yet.

6. Insertion of refracting elements (lenses) in place of the two windows which are required for vacuum sealing. By utilizing very special lenses, a considerable control over the sine-condition has been achieved.

The basic system, No. 1311, with plane windows, (Drawing F113749A) has the following characteristics:

Element	Radius (inches)	Eccentricity	Separation (inches)
Source			9.0
Ellipsoid	+15.42853	0.7143	54.0
Image Plane			37.2
Hyperboloid	+28.87170	1.7761	28.6
Paraboloid	+78.00000		

Rays were traced from a point source at the short focus of the ellipsoid, and at angles from zero to 1.5 radians to the axis, at intervale of 0.1 radian. The heights and exit angles of the rays at the exit pupil (leaving the paraboloid) were tabulated. Decollimation angles are plotted (Curve 1311) on the graph of decollimation at exit aperture (Figure 33), and variations in the E.F.L. (Effective Focal Length) are plotted (Curve 1311) on the graph of offense against the sine condition (Figure 34). It is to be noted that these curves are for a point source at the focus of the ellipsoid.

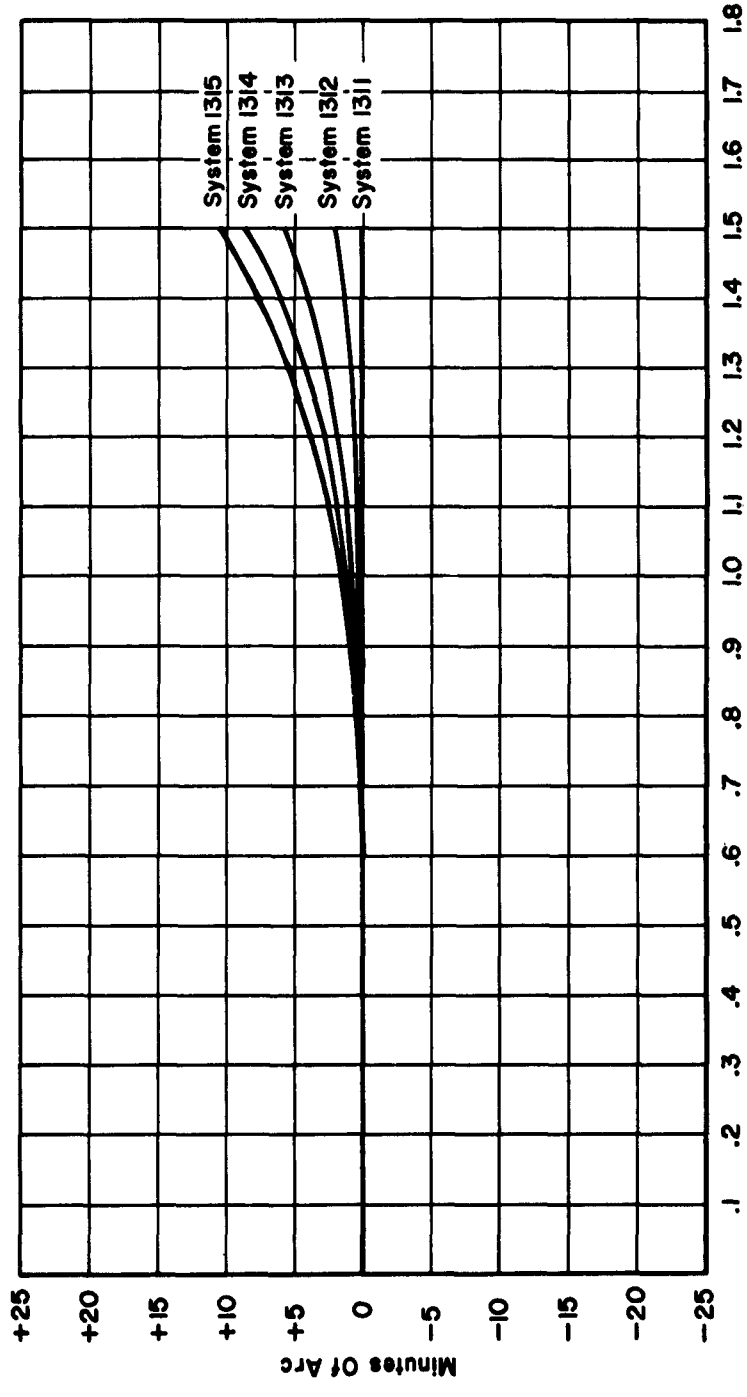

Fig. 33 Decollimation of Exit Aperture

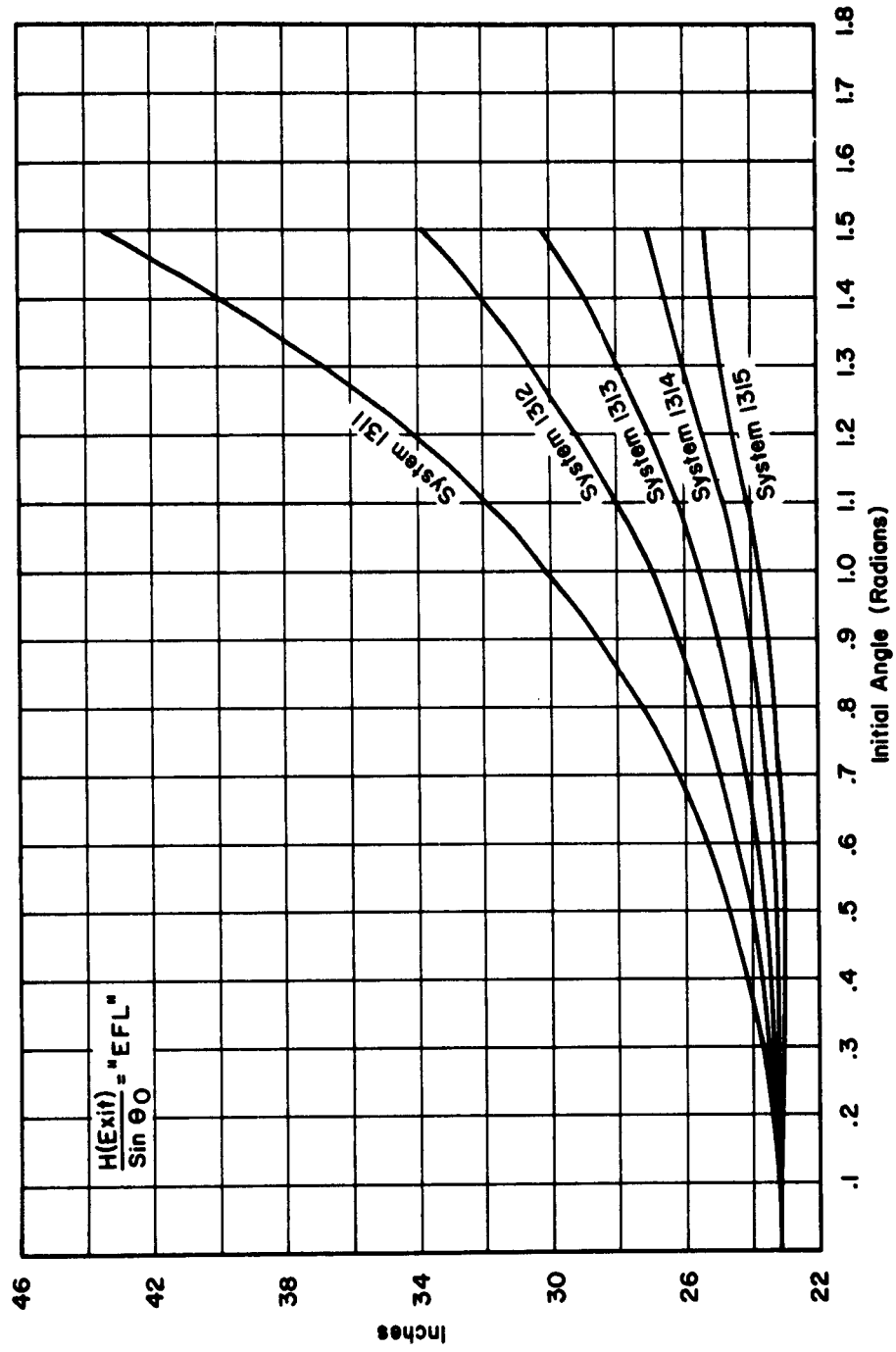

Fig. 34 Offense Against the Sine-Condition

In theoretical investigation of corrective lens elements, a form convenient for analysis, known as the "Invisible Null Lens" was used. This is a lens made up of two surfaces having identical radii of curvature and zero thickness. Thus when both surfaces are spherical the net effect of the lens is zero. However, when one surface is changed to aspheric form, the paraxial power is zero, but the power is variable with respect to spherical aberrations and sine-condition. We can have two such types of lens, as shown in Figure 35, in which the left-hand diagrams show the theoretical forms used in computations to study the effects of aspherizing.

In the computations we have used two of these lenses, equidistant from and on opposite sides of the long focal point of the ellipsoid. The lens on the side toward the ellipsoid has parabolized positive and spherical negative surfaces, causing overcorrected spherical aberration and overcorrected sine-condition. On the other side of the focus, the negative surface of the lens is parabolized and the positive surface is spherical, causing undercorrected spherical aberration and overcorrected sine-condition.

The net effect of the two lenses is to leave the spherical aberration unchanged and to contribute a large amount of overcorrected sine-condition, thus leaving the collimation unchanged but greatly improving the sine-condition.

Four systems (numbers 1312 through 1315) utilizing correctors of two different curvatures and consisting of fused quartz and synthetic sapphire were studied. They had the characteristics shown in Table VI.

For comparison, the decollimation angles and variation in E.F.L. of these systems are also plotted in Figures 33 and 34. It can be seen that in System 1311, the collimation is perfect, but there is an 89% increase in E.F.L. from the center to the edge of the aperture. It is also shown that this defect can be significantly reduced by use of the lenses, and has been cut to 10% in System 1315. Since error remains monotonic, further development of the lenses can reduce the error practically to zero.

The collimation has drifted to about 10 minutes of angle, but this is also monotonic and amenable to correction.

However, in the systems under study it is not sufficient to confine the computations to a point source, since even the most compact of sources has finite size. Therefore, further computations have been carried out for these five systems to investigate their performance with an assumed source one quarter of an inch long, oriented along the axis and extending one eighth of an inch

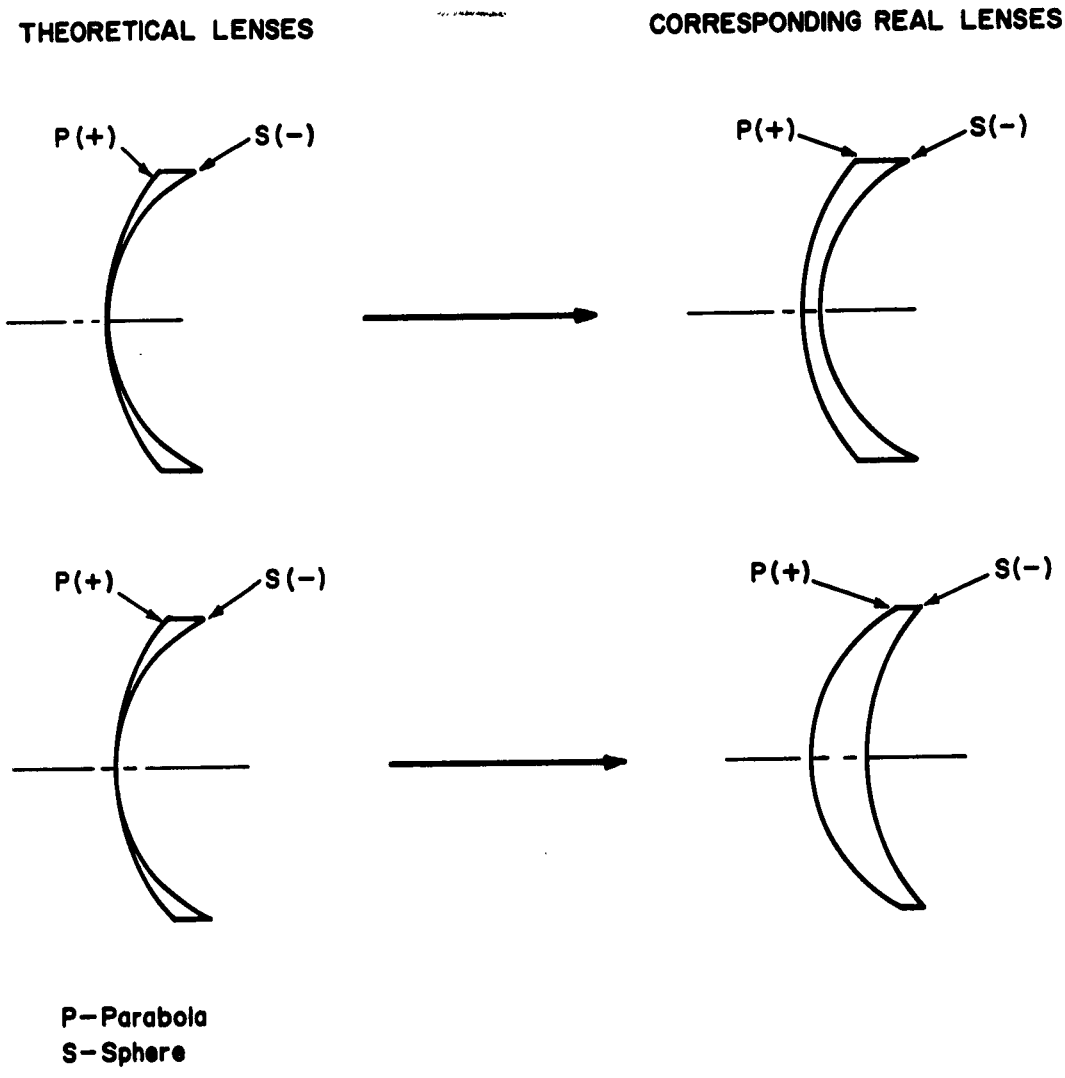

Fig. 35 Corrector Lenses

TABLE VI

SUMMARY OF CHARACTERISTICS FOR FOUR OPTICAL SYSTEMS

Element	Radius (inches)	Eccentricity	Separation (inches)
System 1312			
Source			
			9.0
Ellipsoid	+15.42853	0.7143	
			50.0
First Corrector (Fused Quartz)	R_1 + 2.00000	Paraboloid	
			0.0
	R_2 + 2.00000	Sphere	
			4.0
Focal Plane			
			4.0
Second Corrector (Fused Quartz)	R_1 - 2.00000	Paraboloid	
			0.0
	R_2 - 2.00000	Sphere	
			33.2
Hyperboloid	+28.87170	1.7761	
			28.6
Paraboloid	+78.00000		
System 1313			
Source			
			9.0
Ellipsoid	+15.42853	0.7143	
			50.0
First Corrector (Synthetic Sapphire)	R_1 + 2.00000	Paraboloid	
			0.0
	R_2 + 2.00000	Sphere	
			4.0
Focal Plane			
			4.0

TABLE VI - (CONT'D.)

Element	Radius (inches)	Eccentricity	Separation (inches)
System 1313 (cont'd.)			
Second Corrector (Synthetic Sapphire)	R_1 - 2.00000	Paraboloid	0.0
	R_2 - 2.00000	Sphere	33.2
Hyperboloid	+28.87170	1.7761	28.6
Paraboloid	+78.00000		
System 1314			
Source			9.0
Ellipsoid	+15.42853	0.7143	50.0
First Corrector (Fused Quartz)	R_1 + 1.55040	Paraboloid	0.0
	R_2 + 1.55040	Sphere	4.0
Focal Plane			4.0
Second Corrector (Fised Quartz)	R_1 - 1.55040		0.0
	R_2 - 1.55040		33.2
Hyperboloid	+28.87170	1.7761	28.6
Paraboloid	+78.00000		

TABLE VI - (CONT'D.)

Element	Radius (inches)	Eccentricity	Separation (inches)
System 1315			
Source			9.0
Ellipsoid	+15.42853	0.7143	50.0
First Corrector (Synthetic Sapphire)	R_1 + 1.73160	Paraboloid	0.0
	R_2 + 1.73160	Sphere	4.0
Focal Plane			4.0
Second Corrector (Synthetic Sapphire)	R_1 - 1.73160	Paraboloid	0.0
	R_2 - 1.73160	Sphere	33.2
Hyperboloid	+28.87170	1.7761	28.6
Paraboloid	+78.00000		

inside and outside of the focal point of the ellipsoid. Curves of the decollimation and offense against the sine-condition for three points on the source are plotted in Figures 36 through 45 inclusive. The curve of Point B in each case represents the center of the source, at focus, and is the same as shown on Figures 33 and 34. Curves A and C represent the end points of the source. The area between points A and B is the envelope of the outside half of the source, and that between B and C is the envelope of the half inside the focal point.

It can be seen that for System 1315 (Figure 45) in which the sine-condition correction for the center of the source is approaching perfection, the values at the outer ends are varying quite rapidly.

2. Multiple Sources Feeding a Single Collimator

The use of multiple sources and condensers to feed a single large collimator will invariably result in a compromise between collimation and the advantage of having "local blackout" protection through the concept of each source illuminating the total area.

If perfect collimation is desired, a system such as shown in Figure 46 can be used, in which the condensers 1, 2, 3, 4 are oriented parallel to each other, and each source illuminates only its corresponding area in the chamber. Failure of a source would cause a corresponding dark area in the chamber.

If each source is to illuminate the total chamber area, then the condensers must be set at converging angles as shown in Figure 47. The images of the sources will then fall in the same image plane but will be displaced laterally from each other, and will form a large combination image, which will be larger in proportion to the number of sources and condensers employed. Through the use of proper field lenses the images of the individual apertures of the condensers may be made to superimpose at the exit pupil of the large collimator, thus reinforcing each other at this plane. However, along with this advantage there must be a significant increase in angular spread or decollimation. This increase in decollimation is essentially equal to

$$\theta \times \frac{A}{B}$$

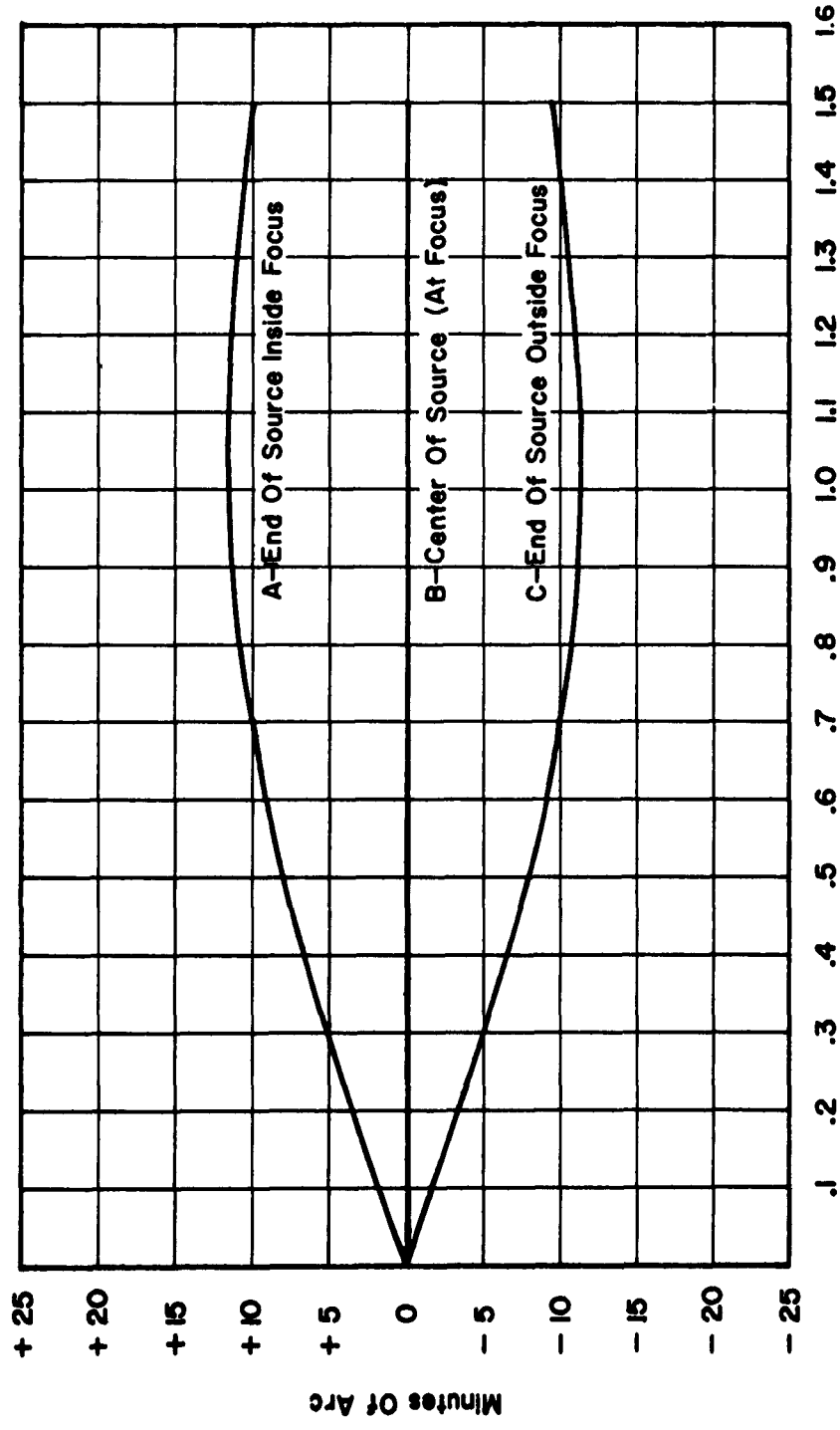

Fig. 36 Decollimation at Exit Aperture, System 1311

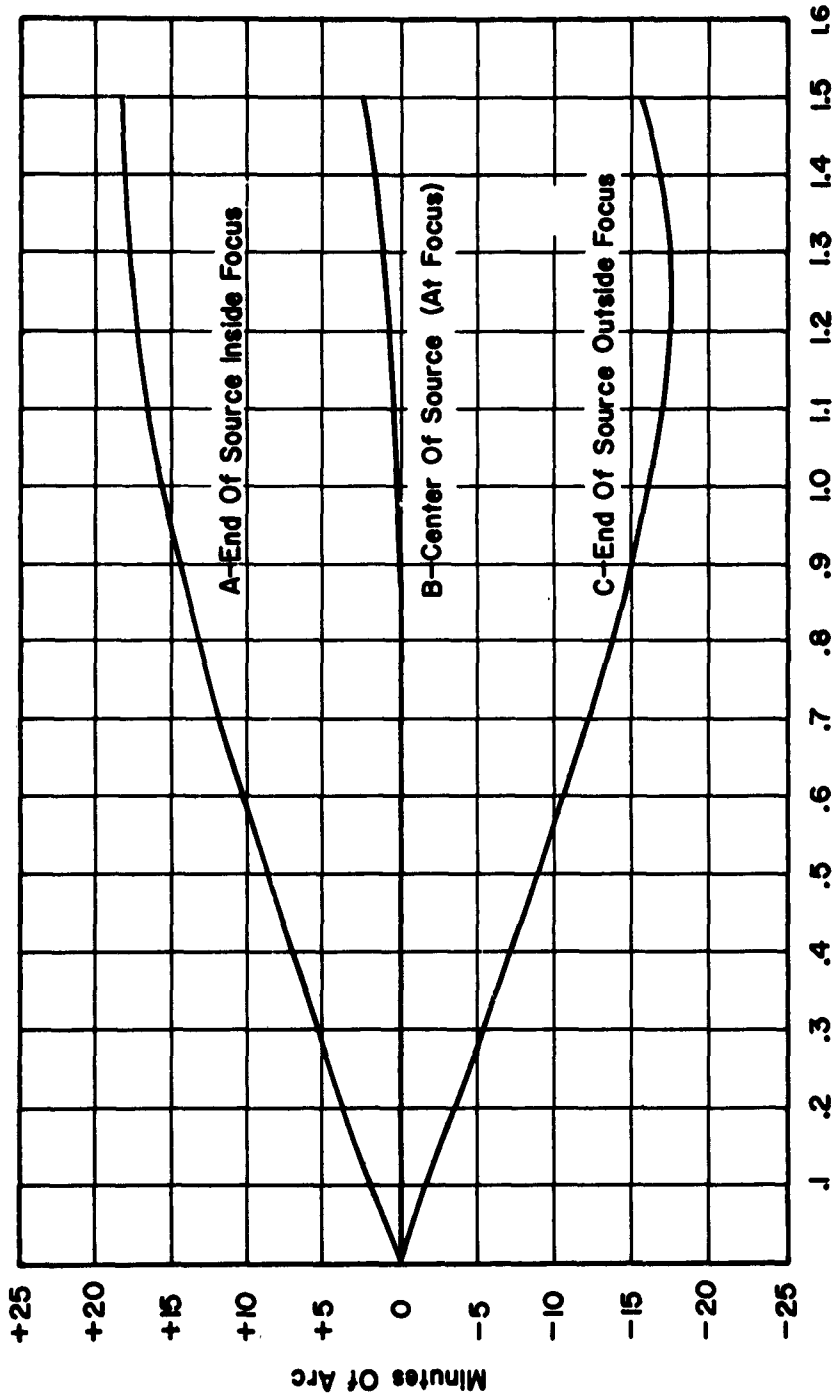

Fig. 37 Decollimation at Exit Aperture, System 1312

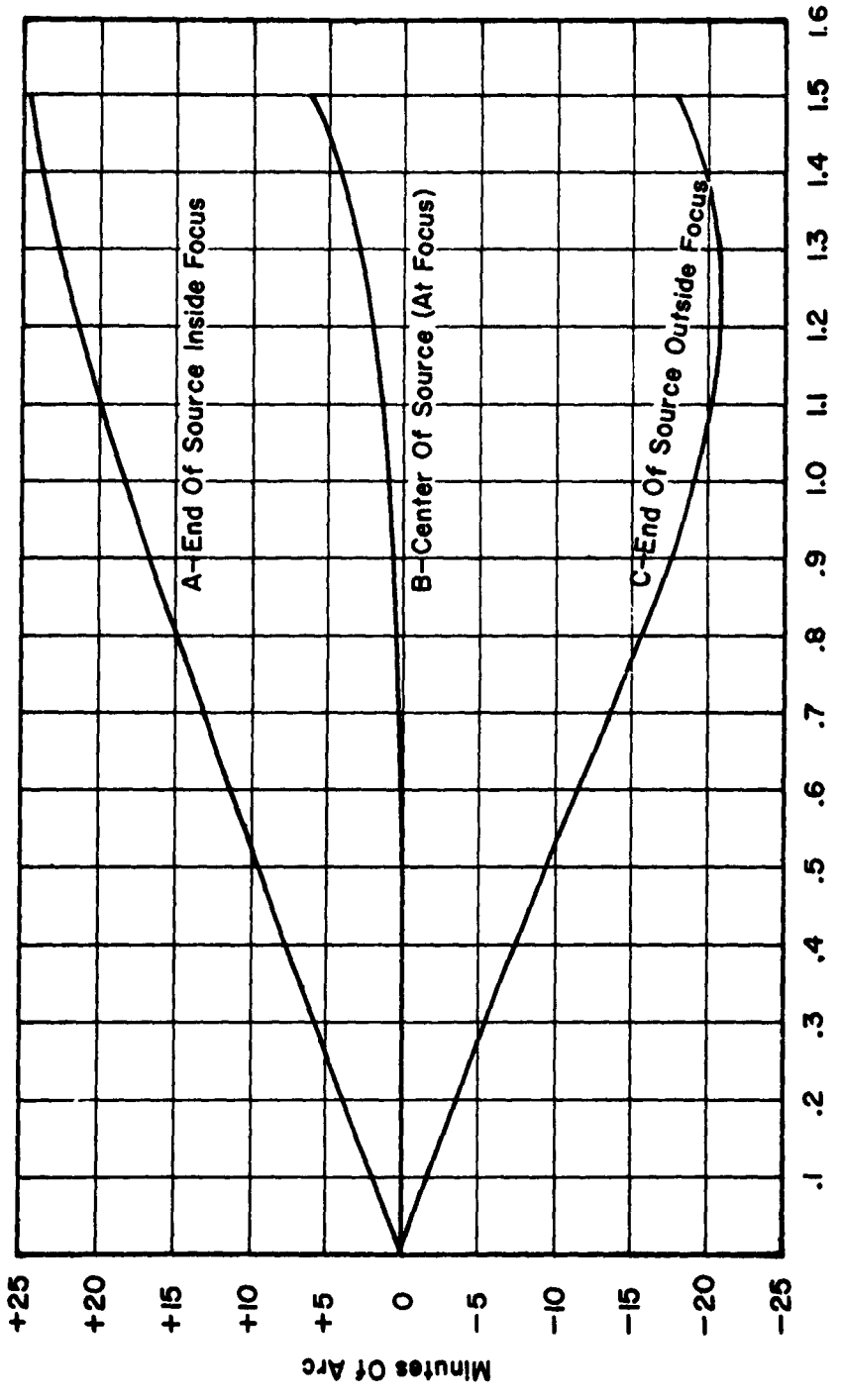

Fig. 38 Decollimation at Exit Aperture, System 1313

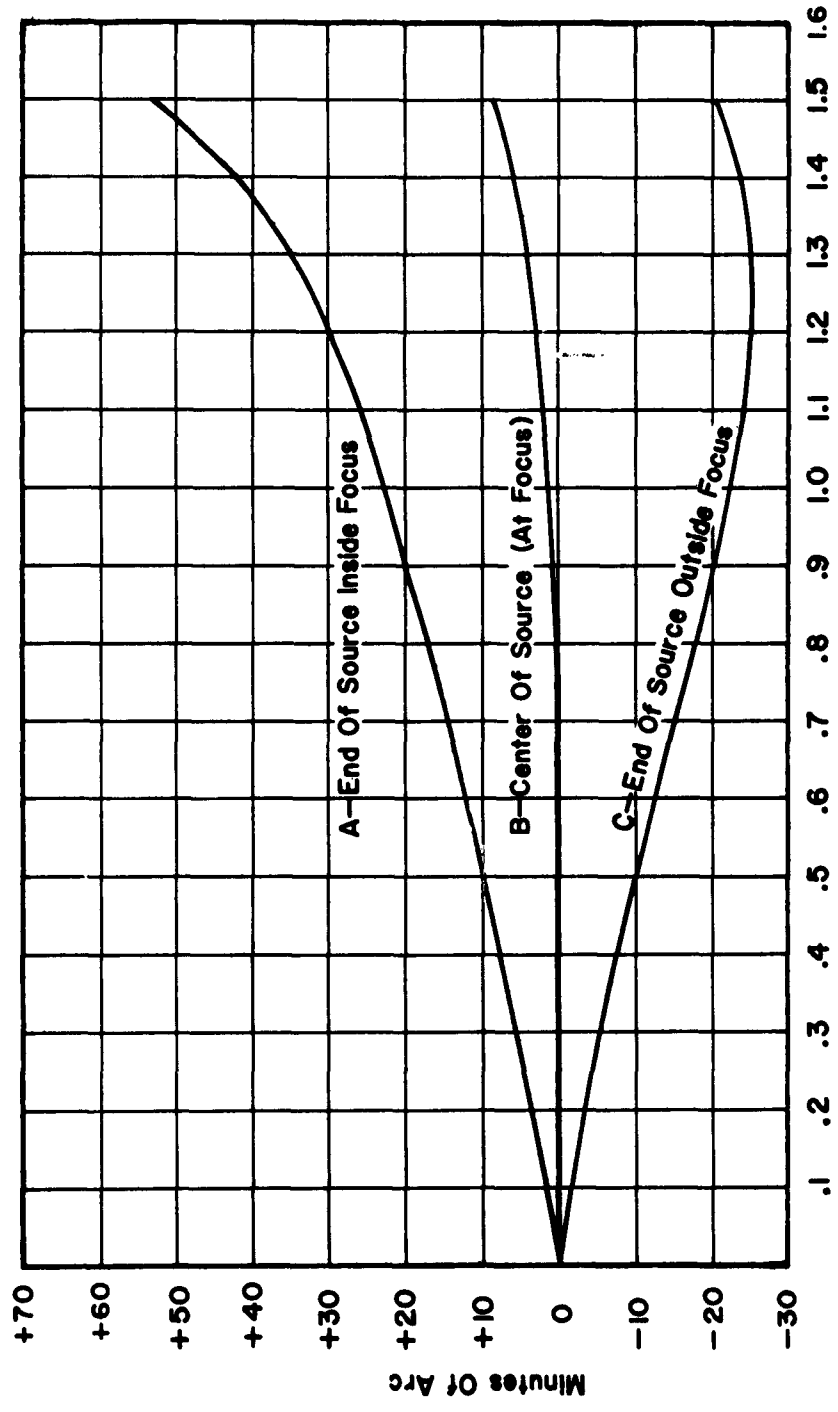

Fig. 39 Decollimation at Exit Aperture, System 1314

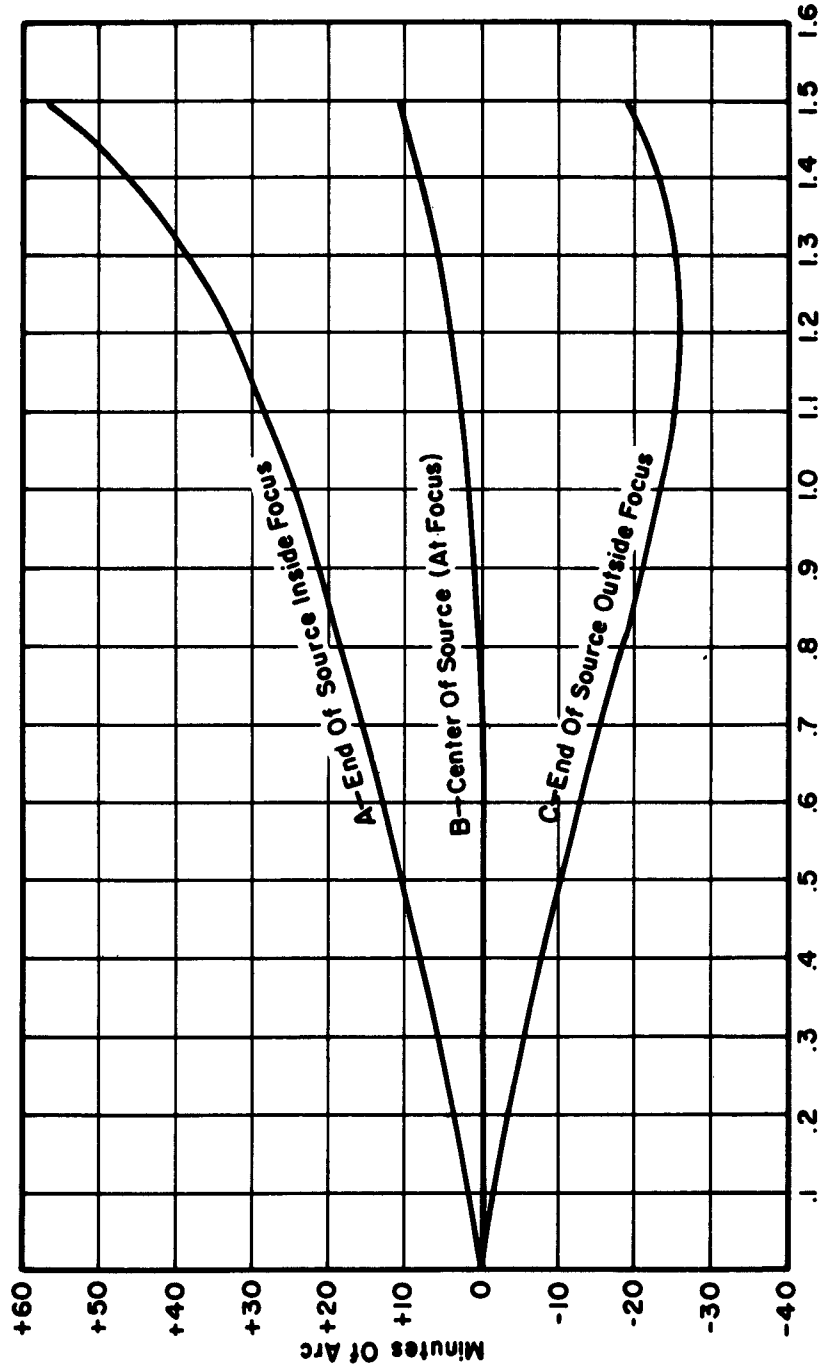

Fig. 40 Decollimation at Exit Aperture, System 1315

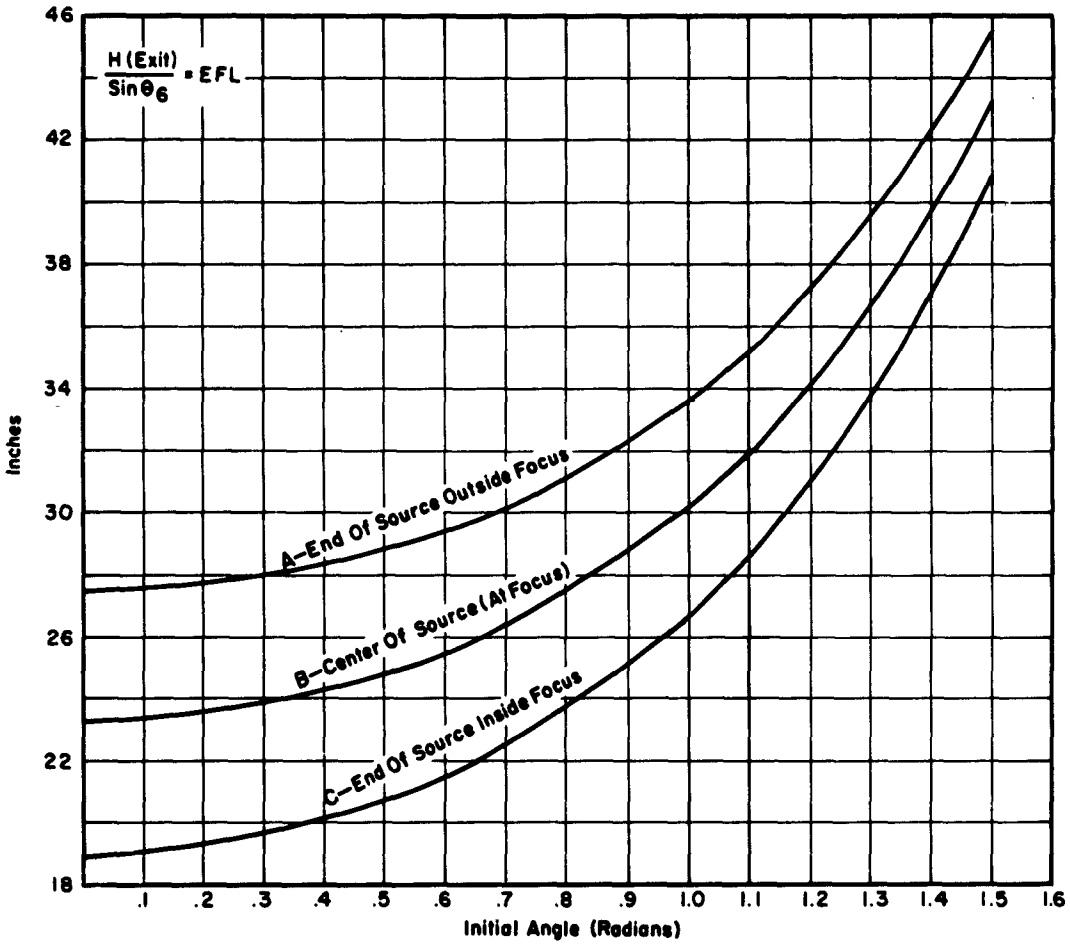

Fig. 41 Offense Against the Sine Condition – System 1311

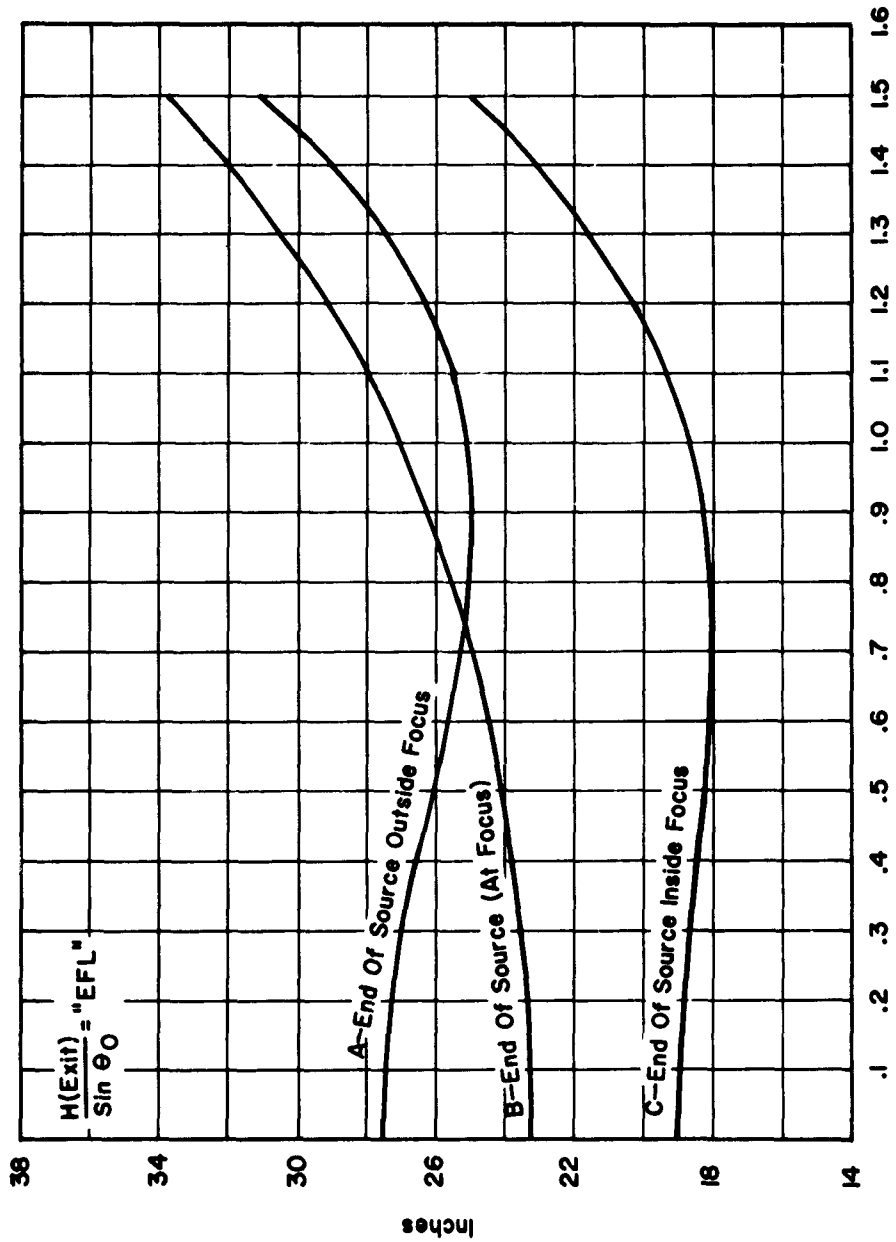

Fig. 42 Offense Against the Sine Condition – System 1312

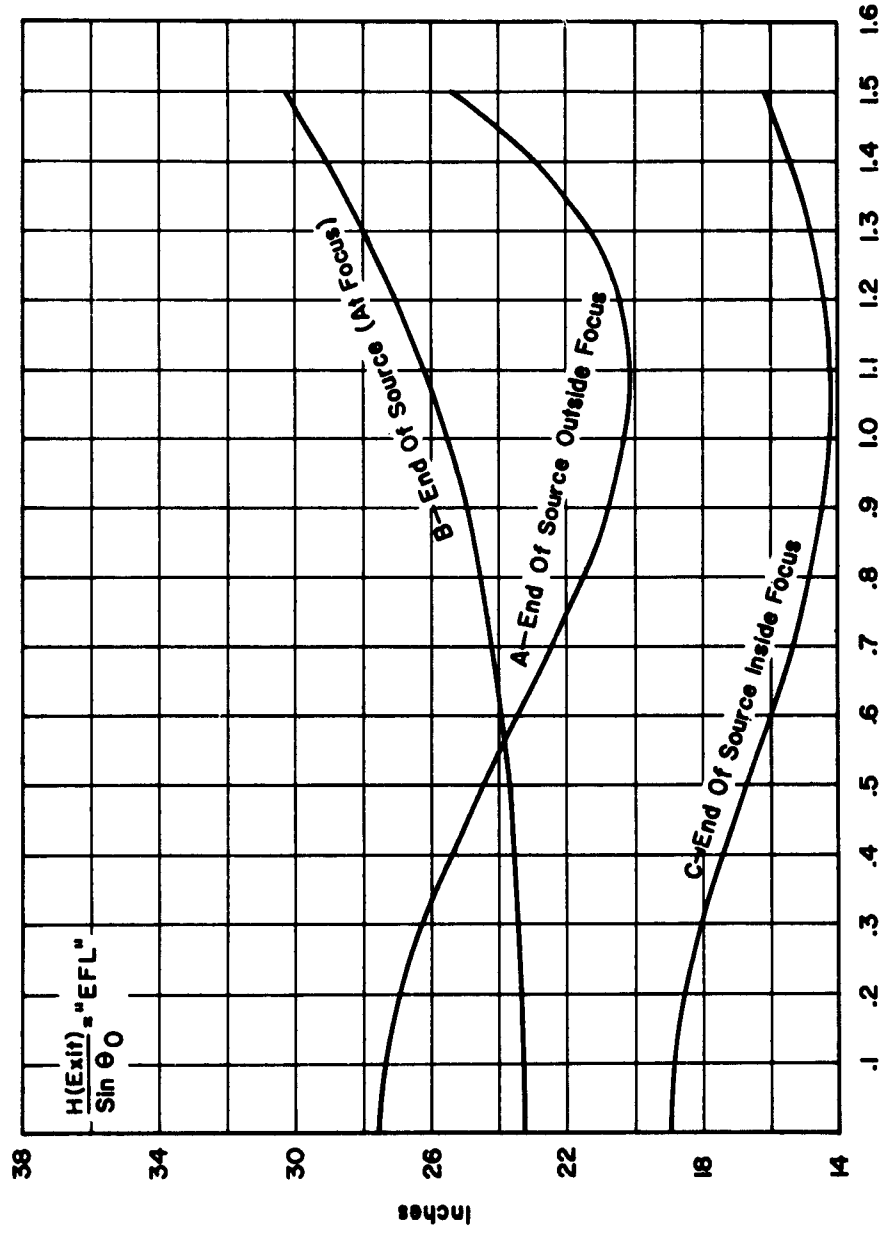

Fig. 43 Offense Against the Sine Condition – System 1313

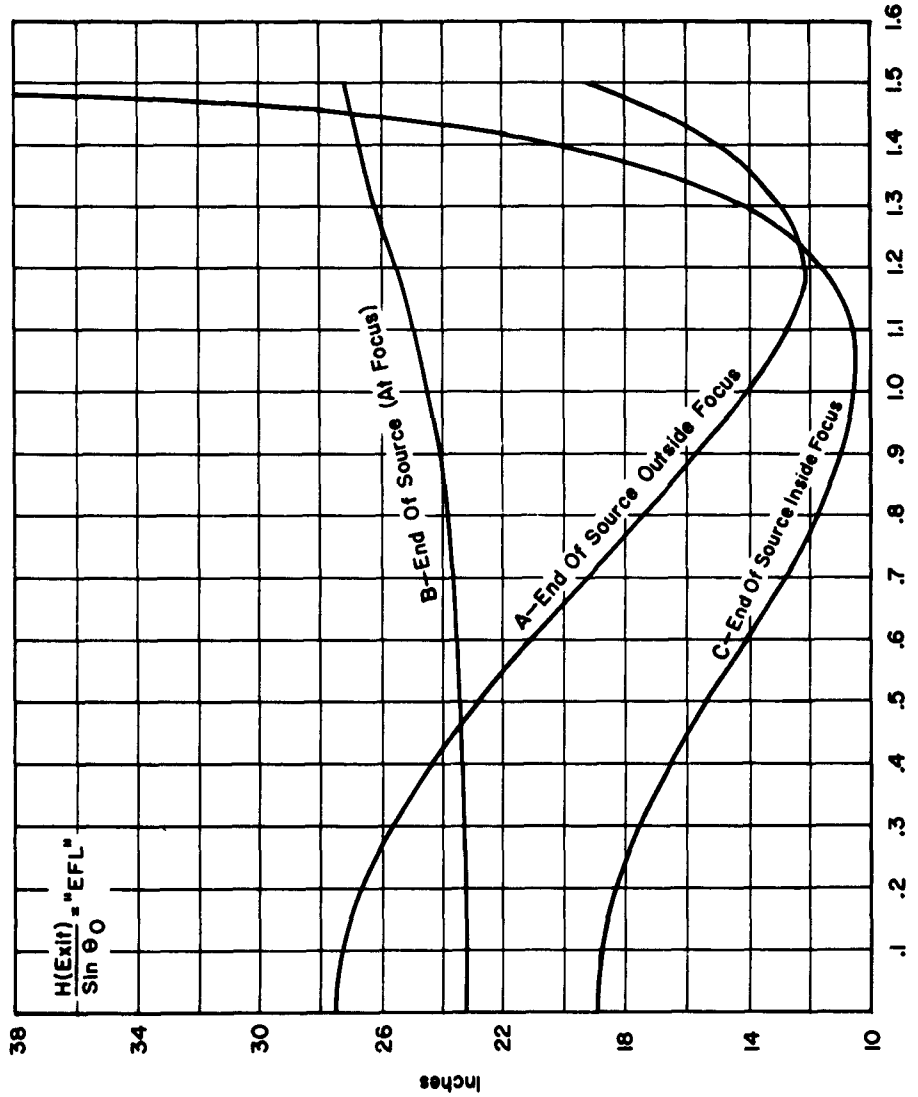

Fig. 44 Offense Against the Sine Condition – System 1314

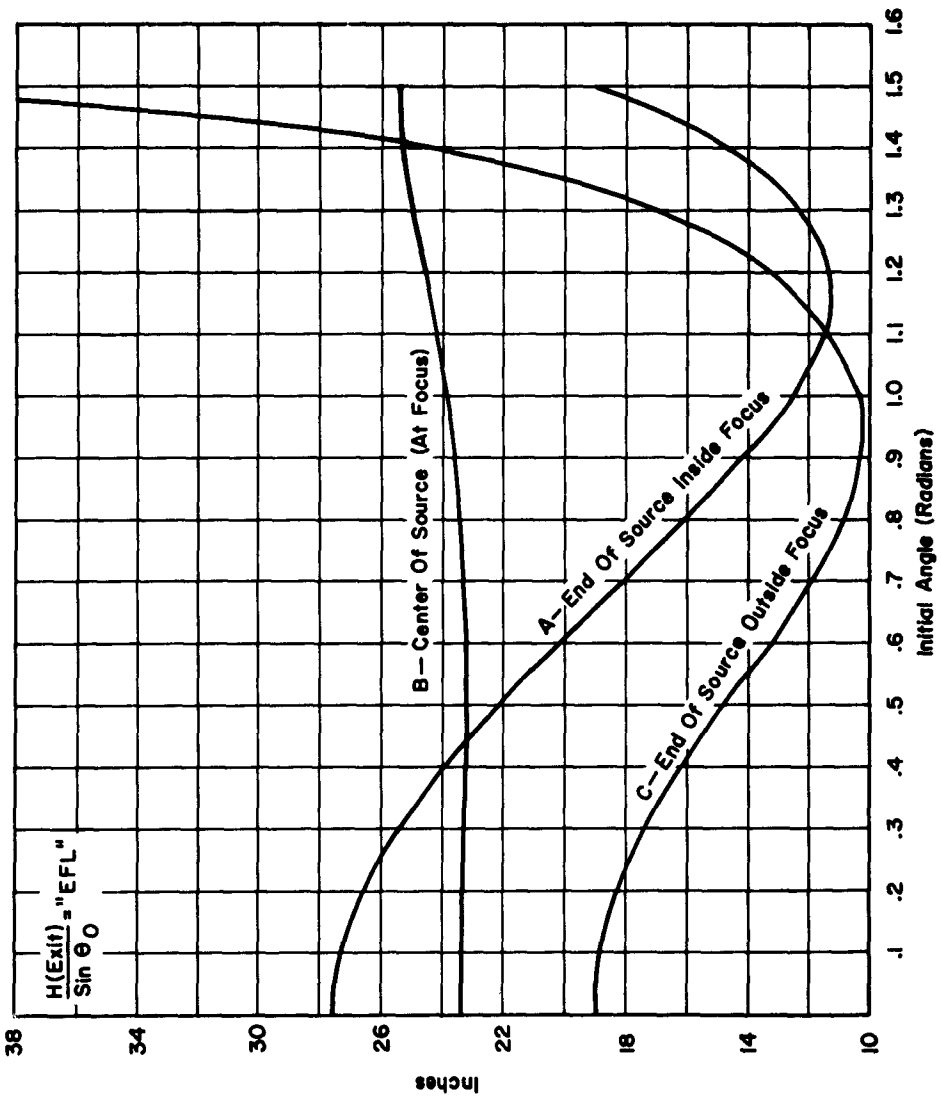

Fig. 45 Offense Against the Sine Condition – System 1315

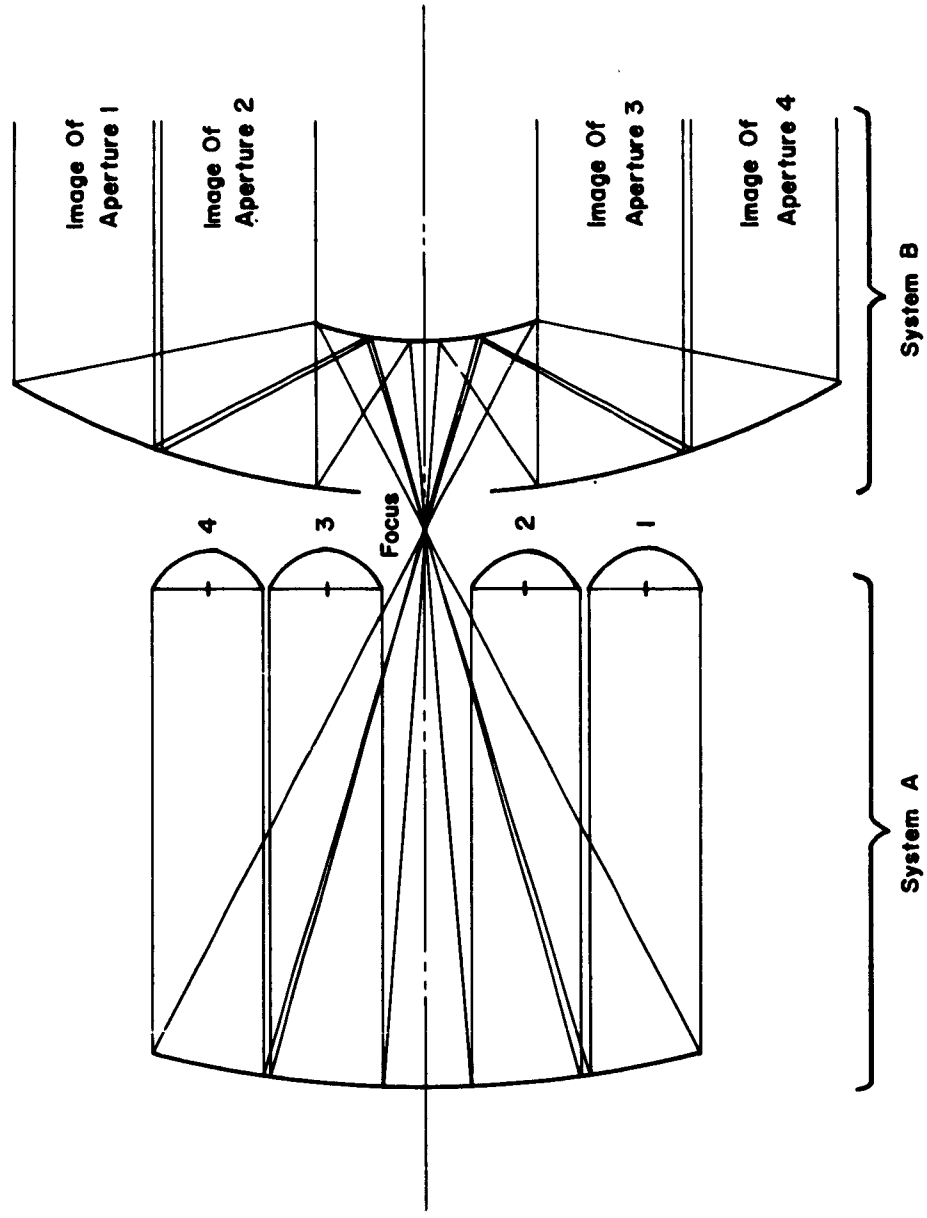

Fig. 46 Parallel Condensers With Large Collimator

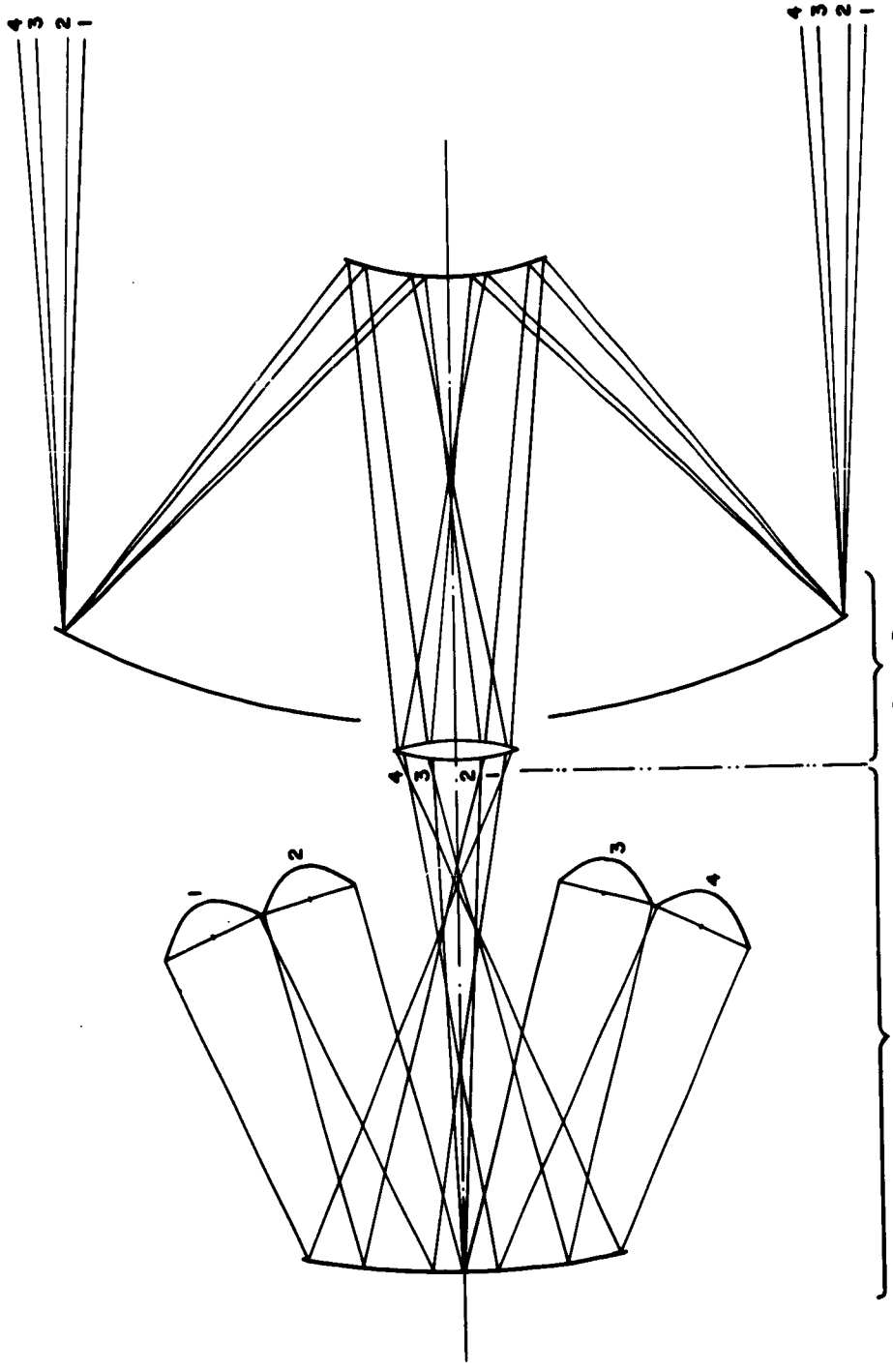

Fig. 47 Converging Condensers With Large Collimator

where

θ = Angular convergence of condenser axis

A = Focal length of System A

B = Focal length of System B

Figure 47 shows the decollimation to be expected from such an arrangement.

Hybrid combinations of such arrangements can be designed, in which the rays from parallel-oriented condensers are sent through a main focus and then impinge upon multiple mirrors forming the secondary of the collimator. Each of these multiple mirrors then forms a virtual image of the single main focus image, thus giving the desired superposition of pupils. The multiple sources thus seen by the collimator, however, lead to the same decollimation that would be caused by converging condensers.

3. Reflecting versus Refracting Elements

A study of refracting elements as the main image-forming components of a system equivalent to the reference module (Dwg. F113749A) presents the limitation of materials suitable for optical transmission in the 0.2 to 3.0 micron region. Requirements of transmittance, insolubility, availability and strength, among others, narrow the possibilities to synthetic sapphire and fused quartz. In sizes above about seven inches in diameter, only fused quartz remains available.

The practical difficulties and cost of achromatizing such a system are aggravated by the near-parallel dispersion of the two materials. For instance, the dispersion numbers, ν, between the limits of 0.4 and 1.45 microns is 20.08 for synthetic sapphire and 18.20 for fused quartz. In using these materials to achieve an achromatized system having a total positive power ϕ (= 1/E.F.L.) we would go through the following computations:

$$\phi_+ + \phi_- = \phi$$

$$\frac{\phi_+}{\nu_+} + \frac{\phi_-}{\nu_-} = 0$$

where

ϕ_+ = power of positive (sapphire) lens

ϕ_- = power of negative (quartz) lens

ν_+ = dispersion number of sapphire = 20.08

ν_- = dispersion number of quartz = 18.20

in the pair of simultaneous linear algebraic equations. Substituting the numbers for ν_+ and ν_- and solving the equations,

$$\phi_+ + \phi_- = \phi$$

$$\frac{\phi_+}{20.08} + \frac{\phi_-}{18.20} = 0$$

we obtain

$$\phi_+ = +10.68\,\phi$$

$$\phi_- = -9.68\,\phi$$

It is thus evident that to achromatize the system we would need positive and negative elements of +10.68 and -9.68 times the power of a single non-achromatized element, leading to very thick and perhaps even to multiple sets of lenses to achieve the necessary power.

In addition, the sphero-chromatic aberration (variation of spherical aberration with wavelength) that would be introduced by these extremely powerful lenses would probably be even worse than the original chromatic aberration.

If in the non-achromatized system we consider the refracting element to be of Fresnel form, that is, a series of wedge-prisms increasing in power in a radial direction, the angular dispersion or decollimation for any wavelength region is a function of the f/number that the refracting element must collimate. For instance, if the element is made of synthetic sapphire and must collimate an f/1.0 bundle, then this would produce an angular spread of approximately eight degrees for the wavelength region between 0.2 and 3.0 microns.

4. Orientation of Source

While no final decision as to lamp type has been reached, it is here assumed that a compact xenon arc will be used, and that this arc unit operates with its long axis in a vertical or near-vertical position.

With the condensing system and source oriented as in Figure 48A, reference to the polar diagram, Figure 29 shows that there is very little illumination in the central 70° cone. This is due to the shadow of the upper electrode.

If one assumes a system corrected for offense against the sine-condition and accepting 2π steradians (a hemisphere) of radiation from the source, then the 70° cone represents a loss of energy in the central 57% of the collimated output diameter, or 32% of the area.

This must be filled in by energy taken from the outer portion of the hemisphere, by a system somewhat as shown in the reference module.

Using a condenser oriented as shown in Figure 48B, the solid cone of illumination seen by the condenser is approximately 110° in one plane and 180° in the other meridian. There would be blockage by the electrodes and the spherical mirror, and a diagonal mirror would have to be added to direct the energy downward. The module would no longer be symmetrical, and the area illuminated would be rectangular, but the fill-in requirements would be greatly reduced. Further study of this scheme is indicated.

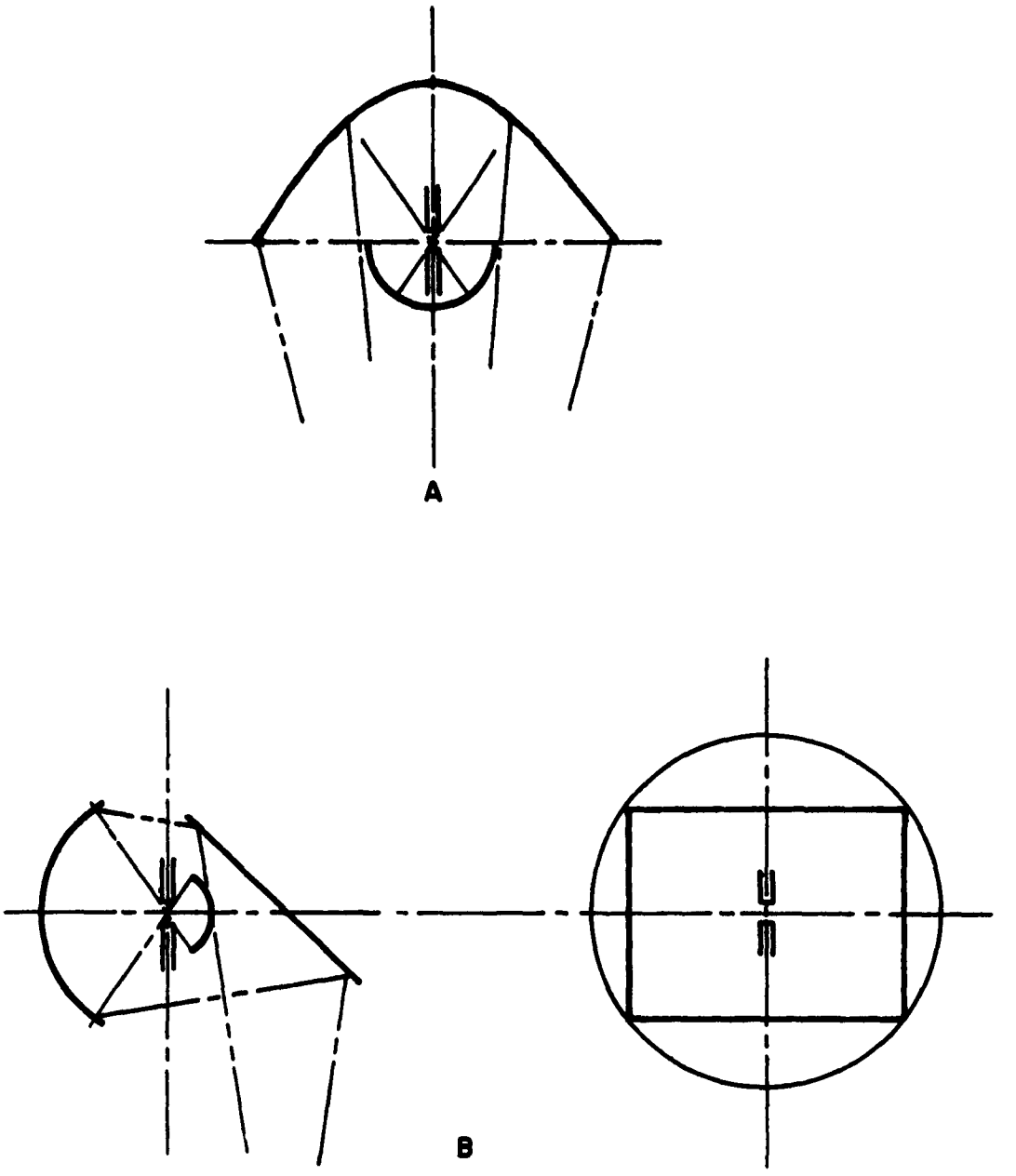

Fig. 48 Orientation of Source

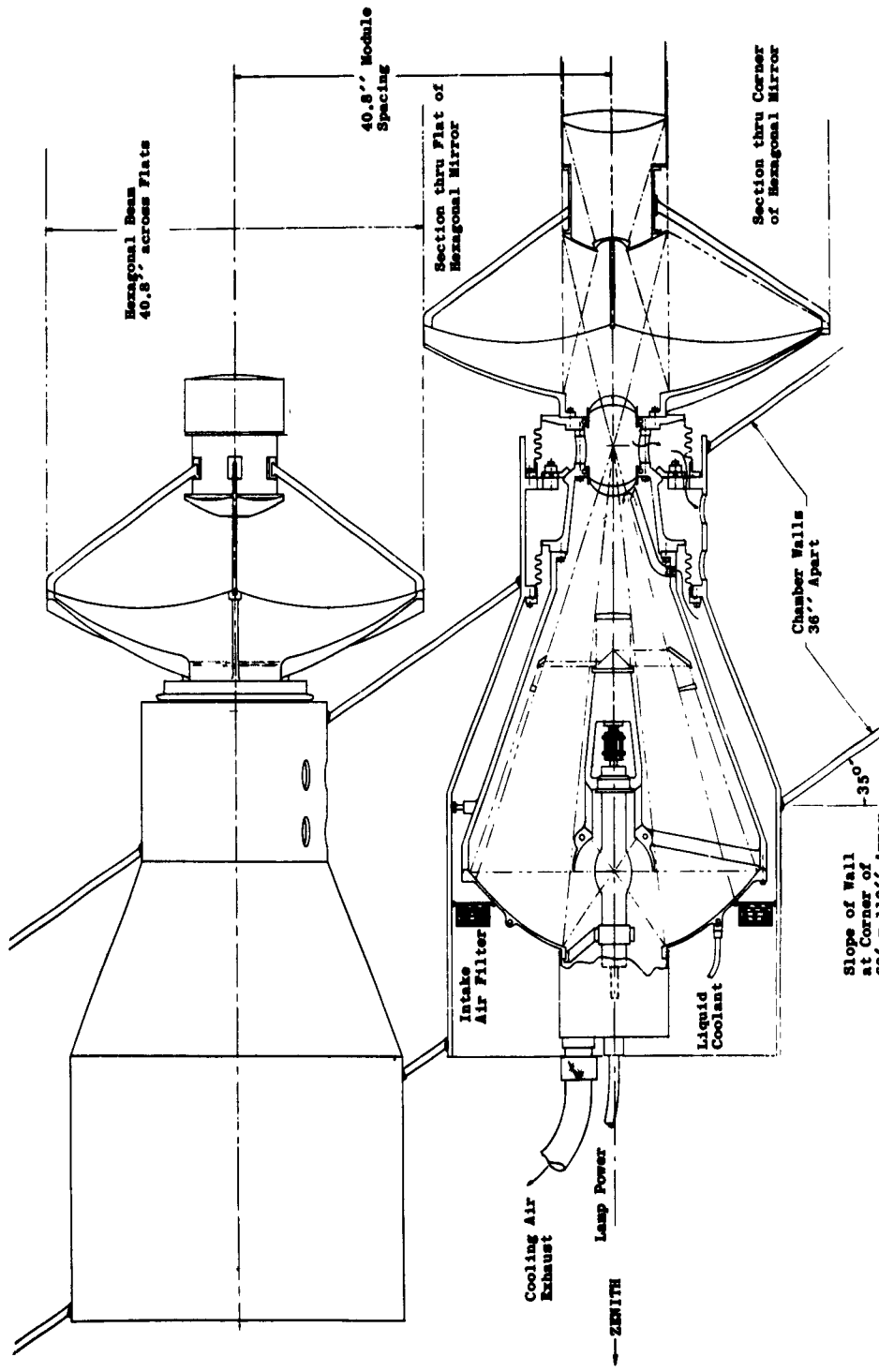

Exhibit I

Reference Module, Concept A, Drawing F-113749A

APPENDIX A

DOUBLE-BEAM RECORDING SPECTROPHOTOMETER

A schematic diagram of the apparatus for measuring the spectral energy distribution with a double beam recording spectrophotometer is given in Figure A-1.

As shown in Figure A-1, the test source and the reference lamp are imaged on the reference field slit and the source field slit by spherical mirrors "A" and "D". Both the reference and source field slits are placed at the focal length of the monochromator mirrors "B" and "C". Thus, mirrors "B" and "C" collimate the light coming from the images at the reference and source field slits. The collimated light beams from both the reference and test source are then alternately superimposed on the monochromator entrance slit by means of the flip-flop mirror. The beam entering the slit is then collimated and reflected by the monochromator mirror to the quartz prism where it is dispersed. The back of the prism is silvered and the dispersed light is then reflected back to the monochromator mirror which in turn focuses the dispersed light on the exit slit. The flat mirror then reflects the image to the energy detector. The energy detector alternately sees the reference lamp and test source spectrum as the flip-flop mirror continuously swings back and forth. The reference lamp and test source signals from the energy detector are separated into two channels by a switch driven by the flip-flop mirror.

The entrance and exit slits of the monochromator are mechanically linked together in parallel and are both opened and closed by a single servo-motor. That is, at any given instant, both slits are open to the same width. The servo-motor is part of a servo-loop which responds to the output of the reference lamp part of the detector signal. The servo-motor adjusts the widths of the slits so that the reference lamp output signal is a constant. The two signals from the detector are then put through a mixing circuit, the output signal of which is proportional to the ratio of the test source signal to the reference lamp signal. This ratio is then recorded as a function of wavelength.

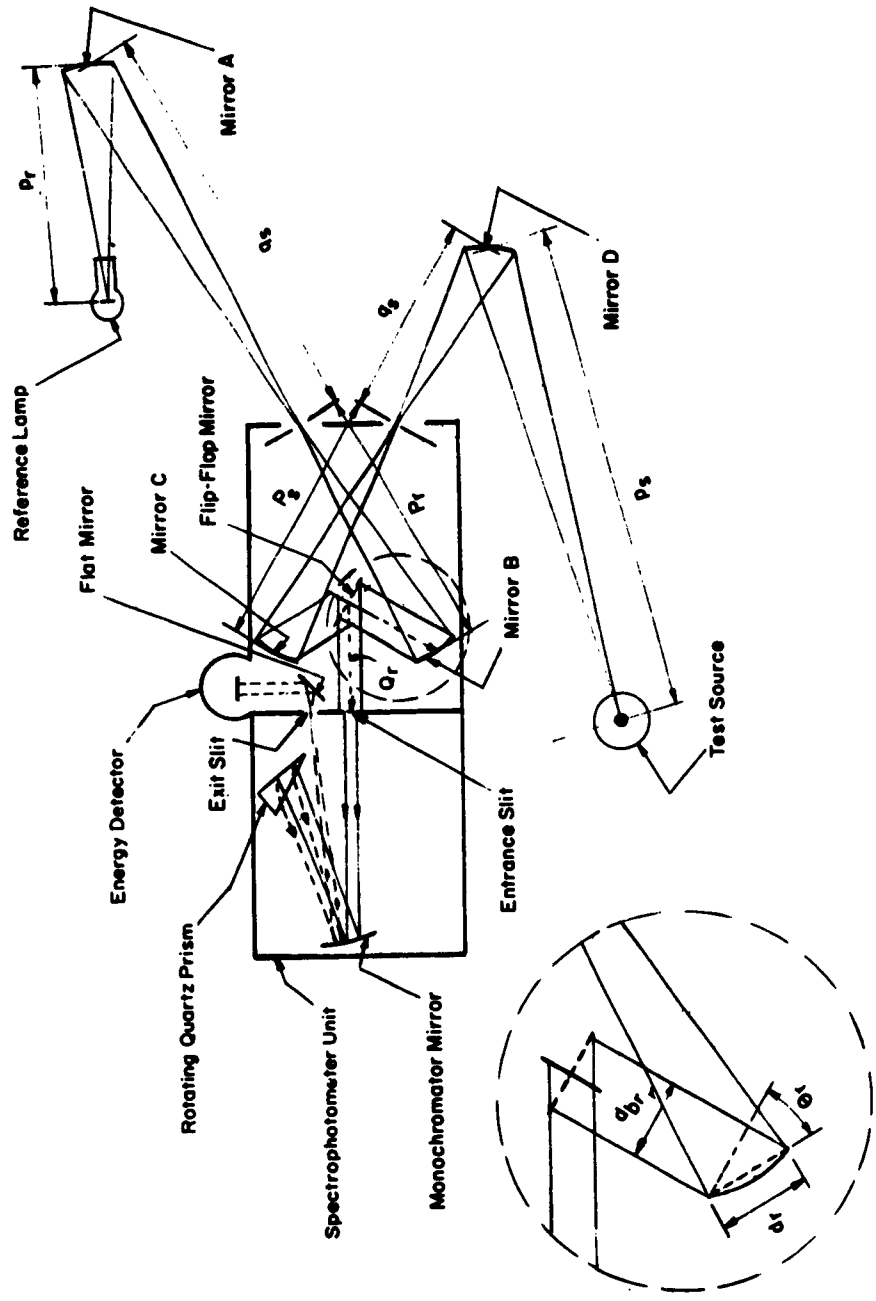

Fig. A-1 Schematic of Apparatus for Measuring Spectral Energy Distribution

To calculate the intensity of the test source from the ratio of intensities measured by the spectrophotometer, a photometric analysis of the light beams of both the reference lamp and test source channels was made. The recorded ratio is proportional to the ratio of the power-density per unit-of-wavelength-interval in the collimated light beams that are alternately superimposed on the entrance slits to the monochromator.

The radiant power density per unit wavelength interval of the collimated beam, T_r, entering from mirror "B" (reference lamp channel) is:

$$T_r = \frac{R_B (B_r)_i (A_r)_i (\Omega_r)_i}{A_{br}}$$

where, in accordance with Figure A-1:

R_B = Spectral reflectivity of mirror B (dimensionless).

R_A = Spectral reflectivity of mirror A.

λ = Wavelength of the radiation.

$(B_r)_i$ = Brightness of the reference lamp image at the reference field slits (microwatts/(mm² of image)(solid angle) (millimicron of wavelength interval).

(B_r) = Brightness of the reference lamp source (microwatts/(solid angle) (mm² area of reference lamp) (millimicron of wavelength interval).

$(A_r)_i$ = Area of the reference lamp image passed by the reference field slits (mm²).

A_s = Area of the test source (mm²).

$(A_s)_i$ = Area of the image of the test source passed by the test source field slits (mm²).

$(\Omega_r)_i$ = Solid angle of the reference lamp image subtended by mirror "B" (steradians).

(A_{br}) = Cross-sectional area of the collimated beam from reference channel.

d_b = Diameter of collimated beam leaving mirror "B".

$d\Omega$ = Diameter of pencil rays from reference source image at reference mirror "B".

θ_r, θ_s = Angles as drawn on Figure A-1.

P_s, q_s, P_r, Q_r, etc. = Dimensions as given on Figure A-1.

The area of the collimated beam is then:

$$A_{br} = \frac{\pi d_b^2}{4}$$

The brightness ratio, r_B, actually determined by the spectrophotometer can be derived as follows;

$$d_b = d\Omega \cos \theta_r$$

$$(\Omega_r)_i = \frac{\pi d\Omega}{4 P_r^2}$$

It can be shown from the principles of photometry* that:

$$(B_r)_i = R_A B_r$$

Making the above substitutions in the power density equation we obtain:

$$T_r = \frac{R_A B_r (A_r)_i}{(\cos \theta_r)^2 P_r^2}$$

* Borne, M., and Wolf, E., "Principles of Optics," Pergamon Press, New York, 1959, pg. 18, equation (22).

The same analysis can be applied to the test source channel, the result of which is:

$$T_s = \frac{R_D (B_s) (A_s)_i}{P_s^2 (\cos \theta_s)^2}$$

The ratio recorded by the spectrophotometer, r_B, is:

$$r_B = \frac{T_s}{T_r} = \frac{R_D B_s (A_s)_i / P_s^2 (\cos \theta_s)^2}{R_A B_r (A_r)_i / P_r^2 (\cos \theta_r)^2}$$

The geometry and physical properties of the optics are such that:

$$R_D = R_A$$
$$\theta_r = \theta_s$$
$$P_r = P_s$$

Therefore:

$$r_B = \frac{B_s (A_s)_i}{B_r (A_r)_i}$$

From the definition of the magnification of an image it can be shown that

$$(A_s)_i = A_s \left(\frac{q_s}{p_s}\right)^2$$

This relates the image of the source of the field slits to the actual test source area. If this equation is substituted in the above equation for r_B we obtain:

$$r_B = \frac{B_s A_s (q_s/p_s)^2}{(B^2)(A_r)_i}$$

then:

$$(B_s A_s) = r_B B_r (A_r)_i \left(\frac{p_s}{q_s}\right)^2$$

The area A_s of the test source is difficult to measure exactly since A_s is not sharply defined. In any circumstance, in order to calculate the output of an optical system using this spectral data, the B_s has to be multiplied by A_s.

Comparison of the product term B_sA_s with the term, I, the intensity as defined by Borne and Wolf*, shows that they are the same. The term B_sA_s thus represents the power radiated per solid angle of source per unit wavelength interval for the entire source area.

* Ibid: page 181, equation (6).

APPENDIX B
RADIATION STABILITY

The materials chosen for use in the simulator must be stable under the conditions of radiation existing during reactor tests. Radiation is a widely diverse category which includes, among others, neutrons, gamma rays, electrons, protons, alpha particles and deuterons. The energy of these particles covers a wide spectrum of values. It will be necessary to evaluate each problem individually; however, it is first desirable to indicate the differences and similarities of different bombardment particles.

The following is a brief description of the mechanism by which radiation causes optical defects. There are two general means of introducing atomically dispersed, chemically different atoms into a crystalline solid by irradiation; first, the bombarding particle itself becomes lodged in the lattice and, second, the bombarding particle causes atomic transmutations by introducing nuclear reactions. When a fast particle traverses the lattice of a crystalline solid it may lose energy by several processes depending on the nature of the particle and its energy. Electrons or holes released during ionization may become trapped at defects initially present in a crystal, or by atomic defects produced during the bombardment. This can lead to optical absorption in the normally transparent region. Alternatively the displaced atom may itself give rise to an observable absorption spectrum. For the displacement of atoms, the most important means of energy loss is by elastic collisions with atoms of the crystal. If in an elastic collision the lattice atom receives an energy E_p in excess of E_d (the displacement energy or Wigner energy), it is displaced from its normal lattice site. This process is called the primary process, i.e., the interaction between the incident energetic particle and the lattice atom is the primary collision. If $E_p >> E_d$, multiple collisions occur and a displacement cascade will result. The number of displacements that result from a single primary event is a function of the primary energy and is denoted by $V(E_p)$. If $E_p >> E_d$ then approximately*

$$V(E_p) = \frac{E_p}{2E_d}$$

* Kinchin, G. H. and Pease, R. S., "The Displacement of Atoms in Solids by Radiation," Reports Prog. Phys., 18, 1-51 (1955).

For a given flux $\phi(E)$ of incident radiation with energy, E, the number of events producing primaries of energy between E_p and $E_p + dE_p$ per unit volume is

$$N(E_p)\, dE_p = N_a\, \phi(E)\, K(E, E_p)\, dE_p$$

where $K(E, E_p)$ is the cross-section per unit energy and N_a is the number of lattice atoms per unit volume.

If the incident radiation is distributed in energy, integration over this energy spectrum gives

$$N(E_p) = N_a \int \phi(E)\, K(E, E_p)\, dE$$

where $\phi(E)$ is the integrated flux per unit energy of the spectrum.

To complete this simplified picture the displacement cross-section, σ_d, should be considered.

$$\sigma_d = \int_{E_d}^{E_d(\text{max.})} K(E, E_p)\, dE_p$$

or

$$d\sigma_d = \sigma_d\, W_d(E, E_p)\, dE_p = K(E, E_p)\, dE_p$$

where $W_d(E, E_p)$ is the probability per unit energy that, given a collision, the primary energy will be E_p.

The number of primaries per unit volume per unit energy is

$$N_p(E_p) = N_a\, \phi \sigma_d\, W_d(E_p)$$

for a bombarding particle of single energy, and

$$N_p(E_p) = N_a \int \phi(E) \sigma_d\, W_d(E, E_p) dE$$

for the case of incident flux distributed in energy.

The atomic displacement for various radiations will be considered in terms of the primary process.

a. Fission Neutrons

The neutrons emitted on fissioning of a U^{235} atom are distributed in energy from approximately 0.5 Mev to approximately 10 Mev, with an average at 1.5 Mev. The scattering cross-section σ_s for fission neutrons* is only slightly energy dependent and has a value in the range 2 to 4 x 10^{-24} cm^2 for most nuclei. Hence,

$$\sigma_d = \sigma_s \left[1 - \frac{E_d}{E_{p(max)}}\right] = \sigma_s \left(1 - \frac{AE_d}{4E_n}\right)$$

where A is the atomic weight and E_n is 1.5 Mev.

Since N_a is in the range of 0.5 to 1 x 10^{23} atoms per cubic cm, the mean free path is approximately 1 cm; thus, it is seen that primary displacements due to a single neutron are produced very far apart.

b. Reactor-Supplied Neutrons

The energy spectrum of neutrons obtained from a reactor is highly dependent upon the type of reactor used. In a solid (graphite) moderator reactor the neutron spectrum can be approximated by a $1/E_n$ distribution extending up to fission energies. The situation is different in a liquid or hydrogenous moderator reactor. Here, the spectrum is $1/E_n$ with an appreciable fission "bump" in the fission energy range, the magnitude of the bump amounting to as much as 10% of the total flux. The neutron energy distribution from a graphite reactor decreases the average primary energy, and neutrons considerably below fission energy contribute appreciably to the damage process.

c. Heavy Charged Particles (Protons, Deuterons, Alpha Particles, etc.)

In the investigation of radiation damage caused by heavy charged particles, the usual energy range is from 2 to 20 Mev. In this energy range interactions occur

* Hughes, D. J. and Schwartz, R. B., "Neutron Cross Sections," Brookhaven National Labs., Upton, N. Y., 2nd Ed., BNL-325.

between the particle and a nucleus of the target atom by Coulombic repulsion. The displacement cross-section is

$$\sigma_d = \int_{E_d}^{E_d(Max)} K(E, E_p)\, dE_p = \frac{\pi b^2}{4} \frac{E_p(max)}{E_d}$$

where $E_p(max)$ = maximum energy transferred in an elastic collision, and b is the closest distance of approach between the charged particle and the nucleus.

For example, 10 Mev deuterons incident on copper have $\sigma_d \simeq 10^{-20}$ cm^2 and a mean free path of $\sim 10^3$ cm, which is much greater than the range of a primary. Therefore, to a good approximation, the lattice damage along the track of a 10 Mev neutron may be visualized as small clumps of disorders resulting from primary collisions separated by a distance of approximately 10 microns.

d. Electrons (Relativistic Range)

The simple Rutherford scattering law used above does not apply to electrons with energy in the Mev range. Because of the very small mass relative to the other charged particles the energy needed for producing displacements corresponds to relativistic velocities and the equations governing energy transfer need modification to include this fact.

The modification is in the value $E_p(max)$ which for electron energies is $E_e << Mc^2$ (M is the mass of the target atom):

$$E_p(max) = \frac{2(E_e + 2M_e c^2)}{Mc^2} E_e$$

where M_e is the rest mass of the electron and c is the velocity of light.

For high electron energies ($E_e >> M_e c^2$) it may be shown* that the displacement cross-section σ_d is approximately

* Seitz, F. and Koehler, J. S., "Displacement of Atoms During Irradiation," Solid State Physics, 2, N. Y.: Academic Press, 1945, pp. 305-448.

$$\sigma_d \simeq \frac{\pi I^2}{4} \frac{E_p(max)}{E_d}$$

where $I = b\sqrt{1 - \frac{v^2}{c^2}}$ and v is the relative velocity of the incident electron and the target atom.

e. Photons (Gamma Rays)

Photons (in the Mev range) are capable of displacing atoms in solids.* There are several ways by which a photon may transfer energy to a lattice:

1. A direct Compton event on the nucleus.
2. A photonuclear reaction.
3. Indirect interaction via an energetic photoelectron.
4. Indirect interaction via the components of pairs (electron-position).
5. Indirect interaction via energetic Compton electrons.

The indirect processes are potentially more important than the first two items for energies of readily available gamma rays. For a given gamma ray energy E_γ the pair production cross-section σ_{pp} is proportional to Z^2 of the absorbing material (Z = atomic number), rising from zero at $E_\gamma = 1.02$ Mev to appreciable values ($\sigma_{pp} \simeq 10^{-24}$ cm^2) for atoms of intermediate Z at $E_\gamma \simeq 5$ Mev.

In contrast to the pair production process, low energy photons favor photoelectric production. The cross-section for K-electron ejection starts at a maximum of $E_\gamma = I_K$, the K-electron binding energy, and decreases monatomically according to $E_\gamma^{7/2}$ for increasing E_γ. For a given E_γ, σ_k is proportional to Z^5 for the atom in question. Hence, for high Z atoms, σ_k may have appreciable values for $E_\gamma \cong 1$ Mev.

Situated between the pair production range and the photoelectric range is the domain of Compton scattering. For gamma rays in the range of 1 to 2 Mev and for $Z < 40$ this is the much more important process.

* McKinley, W. A. and Feshbach, H., "The Coulomb Scattering of Relativistic Electrons by Nuclei," Phys. Rev., 74, No. 12, 1759-63 (1948).

The displacement cascade following the primary process is extremely important to the determination of the total number of lattice defects by neutrons, protons, deuterons and alpha particles. This cascade is initiated by the primary recoil through secondary collision with the lattice atoms. The distance of closest approach, b, is the factor that determines the scattering event. When $b << a$ (a is the Bohr radius of a hydrogen atom), as is the case for energetic light particle collisions in which $E_p \geq E_d$, there is virtually no screening and the Rutherford scattering law holds. When $b >> a$, the screening is almost complete and scattering is essentially of the hard sphere type, with $b(E_p)$ acting as the hard sphere radius. In the intermediate range where $b \simeq a$, the scattering law leads to a distribution of transferred energies which lie intermediately between the $1/E^2$ distribution of the Rutherford law and the uniform distribution of the hard sphere scattering.

f. Effect of Lattice Defects on Properties of Solids

The term "radiation damage" implies damage to the crystalline lattice of a solid; the physical evidence of such a process must manifest itself in those properties which are more sensitive to lattice perfection. Defects or imperfections in solids are usually defined with respect to the ideal of a perfect infinite array of lattice points, i.e., a crystal whose structure is perfectly periodic. On this basis any transient interruption of periodicity such as lattice vibrations, the potential field of a conduction electron in a polar crystal, etc., may be considered a lattice imperfection.

The basic structural defects are point defects and dislocations. The point defects include lattice vacancies, interstitial atoms and impurity atoms (taking the place of an atom in the solids, or situated interstitially). Around such a defect the ideal structure of the lattice is perturbed for several lattice distances. A dislocation is essentially a linear defect around which the lattice is disturbed only a few lattice distances radial to the dislocation line. This linear imperfection may either follow a closed path within the crystal or extend to an end at the surface.

Point defects give rise to density changes and also affect the plastic behavior of the crystal. These defects scatter lattice waves (phonons) thereby causing a decrease in thermal conductivity and have a measurable influence on the specific heat. Because the electric potential of the crystal is altered in their vicinity, point defects act as electron-scattering centers and therefore increase resistivity in metal. The alteration of crystal potential at the site of the defect usually results in the introduction of localized electronic states which, though of little importance in most metals, have extensive consequences in insulating

crystals and most semiconductors. Optical absorption bands, luminescence, photoconductivity, and acceptor and donar states are all manifestations of the role that point imperfections play in influencing the electronic behavior in non-metals.

Line defects or a dislocation may be described as a line irregularity which is able to move under stress far below the yield stress of the perfect crystal and whose motion leads to plastic deformation. The yield stress in the vicinity of a dislocation line is drastically reduced.

g. Neutron-Induced Optical Defects in Sapphire (Al_2O_3)

Sapphire contains color bands which exist before irradiation. These bands peak at 5.45 ev and at 4.85 ev, and have full widths, U, and half maximum intensity, of 0.6 ev and 0.54 ev respectively. Since wavelength, in angstroms, = 12,395/ev, these bands are located at:

Peak(A)	Half-Power Points(A)
2274	2156, 2407
2556	2421, 2706

Additional color centers are created by neutron and gamma ray flux. If sapphire is irradiated by gamma rays on the order of 3×10^4r, additional bands appear at 5.45 ev, U = 1.25 ev; 3.08 ev, U = 1.5 ev; 4.28 ev, U = 0.70 ev. These are located at:

Peak(A)	Half-Power Points(A)
2274	2040, 2569
4024	3236, 5320
2896	2677, 3154

These defects may be removed by annealing; the amount of color removed is proportional to the total annealing time. Roughly 90% of the color centers produced anneal out immediately at room temperature.

The color centers created by neutrons are located at:

Peak		Half-Power Points			
ev	A	ev		A	
6.02	2059	6.32	5.72	1961	2167
5.35	2317	5.55	5.15	2233	2407
4.85	2556	5.12	4.58	2421	2706
4.21	2944	4.61	3.81	2689	3253
3.74	3314	4.18	3.30	2965	3756
2.64	4695	2.96	2.32	4188	5343
2.00	6198	2.22	1.78	5583	6963

To quantitatively indicate the change in external transmittance that will result from a specified neutron and gamma flux for a given time, the following analysis is made:

Table III defines the nuclear radiation flux impingent on the chamber wall, emanating from the epithermal, fast,and advanced fast reactors which may be present in the test vehicles.

All the neutrons above 0.1 Mev can be considered to produce damage and an average value of 1 Mev is appropriate. Those neutrons below 0.1 Mev will be discarded since the damage they contribute is less than 1%. Hence for each reactor the pertinent resultant flux is:

Epithermal:

$$\begin{array}{r} 40 \times (10^6 \text{ n/cm}^2\text{-sec}) \\ 130 \\ 68 \\ 99 \\ \underline{120} \\ 457 \text{ or } 4.57 \times 10^8 \text{ n/cm}^2\text{-sec} \end{array}$$

Fast:

$$\begin{array}{r} 79 \times (10^6 \text{ n/cm}^2\text{-sec}) \\ 230 \\ 93 \\ 190 \\ 240 \\ \hline 832 \end{array} \text{ or } 8.32 \times 10^8 \text{ n/cm}^2\text{-sec}$$

Advanced Fast:

$$\begin{array}{r} 39 \times (10^6 \text{ n/cm}^2\text{-sec}) \\ 140 \\ 50 \\ 110 \\ 180 \\ \hline 519 \end{array} \text{ or } 5.19 \times 10^8 \text{ n/cm}^2\text{-sec}$$

Employing Smakula's equation, we are able to relate the number of color centers created by neutron irradiation to observed optical absorption. Thus it is possible to quantitatively indicate the magnitude of absorption peaks produced by a given flux in a given time.

The data used are obtained from a paper* by Paul W. Levy of Brookhaven National Laboratory and apply at room temperature. The procedure described here was suggested by Dr. Levy.

As an example, consider the epithermal reactor whose flux is 4.57×10^8 n/cm^2-sec for a maximum time of 20 hrs. The number of color centers as given by Smakula's equation is:

$$N_i = (N_{oi} - K_i/f_i)(1 - e^{-f_i\tau}) + K_i\tau$$

* Levy, P. W., "Color Centers and Radiation-Induced Defects in Al_2O_3," Phys. Rev., 123, No. 4, 1226-33 (1961).

where

N_{oi} is in units of color centers/cm^3

f_i is in units of fraction of uncolored centers colored/hr.

K_i is in units of uncolored centers/cm^3 formed per sec.

τ is time in hours

To determine how the band at 6.02 ev (2059 A) varies with flux and time we have:

$$N_i = (5.39 \times 10^{16} - \frac{1.33 \times 10^{12} \times 3600)}{.267} (1 - e^{-(.267)(20)}) + (1.33 \times 10^{12} \times 72000)$$

therefore $N_i = 1.315 \times 10^{17}$.

Since the above data were measured at a flux level of 10^{12} n/cm^2-sec, the N_i must be corrected by a factor of $10^{12}/4.57 \times 10^8 = 2.2 \times 10^3$. Therefore the new N_i is

$$\frac{1.315 \times 10^{17}}{2.2 \times 10_3} = 6.03 \times 10^{13}$$

The relationship between the number of color centers and the peak absorption point (expressed in cm^{-1}) is

$$N_i = 0.87 \times 10^{17} \quad \frac{n}{(n^2 + 2)^2} \quad U a_m$$

where

n = index of refraction

U = full width of band at half max. (ev)

a_m = absorption at peak of band (cm^{-1})

If we assume n = 1.7, then $N_i = 6.2 \times 10^{15} U a_m$. Hence for the 6.02 ev band, U = 0.6 ev. Solving for a_m, we have

$$a_m = \frac{6.03 \times 10^{13}}{(6.2 \times 10^{15})} \quad (.6) = 5.84 \times 10^{-3} \text{ cm}^{-1}.$$

The a_m is related to the external transmittance (t) by the relationship:

$$t = \frac{I}{I_0} = e^{-a_m I}$$

where $\frac{I}{I_0}$ is the ratio of transmitted to incident radiation

h. Gamma-Ray Induced Optical Defects in Sapphire (Al_2O_3)

Color centers are also created by gamma-rays (γ). Irradiation of 3×10^4 r produces saturation (in Al_2O_3) of the gamma-ray induced bands which occur at Eo = 5.45 ev, U = 1.25 ev; Eo = 3.08 ev, U = 1.50 ev. In each reactor the photon flux is sufficient to reach this saturation level of 3×10^4r, if we consider 20 hours as the time of exposure. The conversion of gamma-ray quanta to roetgens is given by:

$$\frac{2 \times 10^9 \ \gamma \text{ quanta}}{E(\text{Mev})} = 1\text{r}$$

therefore for the epithermal reactor we have

$.2 \times 10^4$r at 10 Mev

$.4 \times 10^4$r at 8 Mev

$.54 \times 10^4$r at 5.5 Mev

9.2×10^4r at 3.5 Mev

or a total of

1.03×10^5r

From the curves* of gamma-ray induced coloring, the changes in optical density (D), at the peaks, for the two bands are 0.1 at 5.45 ev and 0.08 at 3.05 ev. This corresponds to a change in external transmittance of 26.6% at 5.45 ev (2274 A) and 21% at 3.08 ev (4024 A). The relationship used to arrive at the above figures is $D = \log_{10}(\frac{1}{t})$ where t is the external transmittance.

Fortunately, the color bands may be removed by thermal bleaching. The color removed is proportional to the total annealing time. However, after annealing, color bands may be reintroduced by additional radiation.

Bleaching at 1800°C for five hours will remove the color bands. Since neither the equilibrium temperature of the windows nor the minimum annealing temperature are known, it is recommended that these factors be the subject of investigation when a breadboard module is constructed.

i. Radiation - Induced Optical Defects in Fused Silica

In the spectral range of 2000 A to 8000 A various absorption bands are created by irradiation. There are two broad overlapping visible bands, A_1 and A_2, at 6200 A (2 ev) and 4500 A (2.75 ev), respectively. Another two absorption bands appear at 3023 A (4.1 ev) and at 2430 A (5.1 ev) and are denoted as B_1 and B_2, respectively. A single absorption band (C) also appears at 2140 A (5.8 ev). Studies of the visible bands reveal that the A and B absorption regions are variable from specimen to specimen and are completely bleached out by prolonged neutron bombardment > 10^{19} n/cm^2. The A band is attributed to an aluminum impurity in the quartz since Brown and Thomas**found no A band discoloration in high purity synthetic alpha quartz crystals. The C band is found to increase linearly with increasing neutron exposure and is therefore attributed to radiation-produced lattice defects. Optical bleaching (which removes electrons and holes from lattice defects) of the C band is possible if the material is illuminated with the wavelength absorbed, even in the purest substances. A preferential optical and thermal bleaching (which removes the

* Levy, P. W., "Color Centers and Radiation-Induced Defects in Al_2O_3," Phys. Rev., 123, No. 4, 1226-33 (1961).

** Brown, C. S. and Thomas, L. A., "Response of Synthetic Quartz to X-Ray Irradiation," Nature, 169, 35-6 (1952).

defects themselves) is observed at 2300 A (5.4 ev) during the early stages of the bleaching of neutron-irradiated specimens. The time required for thermal bleaching depends on the temperature, bleaching being completed at 500°C.

It has been shown that in neutron irradiated alpha quartz the index of refraction decreased from 1.550 to 1.470 at saturation. The flux for this case was 10^{19} n/cm^2.

Whittles*, et al, showed that prolonged neutron exposure of approximately 5×10^{20} n/cm^2 caused the density to approach a limiting value of 2.26 grams per cubic centimeter, while at 3×10^{19} n/cm^2 a 1% change in density was observed.

Further investigation of the thermal bleaching of fused silica is continuing at Brookhaven National Laboratory, and reports are expected early in 1962. Dr. Levy at Brookhaven has stated that the radiation and bleaching data for fused silica are basically similar to those for sapphire.

* Whittles, M. and Sherrill, F. A., "Radiation Damage in SiO_2 Structures," Phys. Rev., 93, No. 5, 1117-8 (1954).

Arnold Engineering Development Center
Arnold Air Force Station, Tennessee
Rpt. No. AEDC-TDR-63-91. SOLAR RADIATION SIMULATION STUDIES, PART 2. May 1963, 123 p. incl illus., tables.

Unclassified Report

Studies and tests performed to establish the feasibility of solar simulation systems for an environmental chamber are reported. Performance objectives for the chamber and other solar simulator systems have been delineated and compared. The earlier survey of radiation sources had shown that short-arc lamps have sufficient feasibility for this application to warrant further critical testing. Tests were initiated on several sources of this type including the 10-kw xenon lamp, the 2.5-kw xenon-mercury lamp and the fluid-transpiration arc source. The spectral energy distribution, radiant efficiency, polar diagram, intensity and uniformity as well as size and shape of the radiating medium under several conditions for each radiant source are being examined. More energy in line spectra was detected than had previously been reported. The 10-kw lamp had excessive radiant energy relative to the solar spectrum in the near infrared range. This energy must be reduced by filters. A deficiency of energy also relative to the solar requirement was noted in the range below 0.6 microns. The influence of quartz envelope adsorption, envelope blackening, optical system reflectivities, detector fatig e, and standard source calibration on this deficiency is under evaluation. A reference module optical system concept based upon three and one half on-axis reflectors is examined. Ray tracing techniques are applied to determine the collimation and uniformity obtainable with an ideal short-arc source, and optical efficiencies of the several components are examined. After determination of the module efficiency, the number of molecules required to illuminate the chosen test area and the amount of power required for operation can be simply determined. Preliminary studies of the stability of simulator materials in the nuclear radiation environment of the chamber are also reported, In addition, the multiple source concept supplying a single collimator and the problems associated with refracting vs reflecting elements are analyzed.

1. Solar radiation
2. Simulation
3. Space environmental conditions

I. AFSC Program Area 850E, Project 7778, Task 777801
II. Contract AF 40(600)-951
III Vitro Labs, Div. of Vitro Corp of America, West Orange, N. J. and Farrand Optical Co., Inc., N. Y., N. Y.
IV. W. A. Jaatinen, D. L. Rothacker, C. D. Fitz, et al.
V. Secondary Report No. VL-2244-6-0
VI. Available from OTS
VII. In ASTIA Collection

Arnold Engineering Development Center
Arnold Air Force Station, Tennessee
Rpt. No. AEDC-TDR-63-91. SOLAR RADIATION SIMULATION STUDIES, PART 2. May 1963, 123 p. incl illus., tables.

Unclassified Report

Studies and tests performed to establish the feasibility of solar simulation systems for an environmental chamber are reported. Performance objectives for the chamber and other solar simulator systems have been delineated and compared. The earlier survey of radiation sources had shown that short-arc lamps have sufficient feasibility for this application to warrant further critical testing. Tests were initiated on several sources of this type including the 10-kw xenon lamp, the 2.5-kw xenon-mercury lamp and the fluid-transpiration arc source. The spectral energy distribution, radiant efficiency, polar diagram, intensity and uniformity as well as size and shape of the radiating medium under several conditions for each radiant source are being examined. More energy in line spectra was detected than had previously been reported. The 10-kw lamp had excessive radiant energy relative to the solar spectrum in the near infrared range. This energy must be reduced by filters. A deficiency of energy also relative to the solar requirement was noted in the range below 0.6 microns. The influence of quartz envelope adsorption, envelope blackening, optical system reflectivities, detector fatigue, and standard source calibration on this deficiency is under evaluation. A reference module optical system concept based upon three and one half on-axis reflectors is examined. Ray tracing techniques are applied to determine the collimation and uniformity obtainable with an ideal short-arc source, and optical efficiencies of the several components are examined. After determination of the module efficiency, the number of molecules required to illuminate the chosen test area and the amount of power required for operation can be simply determined. Preliminary studies of the stability of simulator materials in the nuclear radiation environment of the chamber are also reported, In addition, the multiple source concept supplying a single collimator and the problems associated with refracting vs reflecting elements are analyzed.

1. Solar radiation
2. Simulation
3. Space environmental conditions

I. AFSC Program Area 850E, Project 7778, Task 777801
II. Contract AF 40(600)-951
III. Vitro Labs, Div. of Vitro Corp of America, West Orange, N. J. and Farrand Optical Co., Inc., N. Y., N. Y.
IV. W. A. Jaatinen, D. L. Rothacker, C. D. Fitz, et al.
V. Secondary Report No. VL-2244-6-0
VI. Available from OTS
VII. In ASTIA Collection